

NCHRP

REPORT 465

**NATIONAL
COOPERATIVE
HIGHWAY
RESEARCH
PROGRAM**

Simple Performance Test for Superpave Mix Design

TRANSPORTATION RESEARCH BOARD

NATIONAL RESEARCH COUNCIL

TRANSPORTATION RESEARCH BOARD EXECUTIVE COMMITTEE 2001 (Membership as of December 2001)

OFFICERS

Chair: John M. Samuels, Senior Vice President-Operations Planning & Support, Norfolk Southern Corporation, Norfolk, VA

Vice Chair: E. Dean Carlson, Secretary of Transportation, Kansas DOT

Executive Director: Robert E. Skinner, Jr., Transportation Research Board

MEMBERS

WILLIAM D. ANKNER, Director, Rhode Island DOT

THOMAS F. BARRY, JR., Secretary of Transportation, Florida DOT

JACK E. BUFFINGTON, Associate Director and Research Professor, Mack-Blackwell National Rural Transportation Study Center, University of Arkansas

SARAH C. CAMPBELL, President, TransManagement, Inc., Washington, DC

JOANNE F. CASEY, President, Intermodal Association of North America

JAMES C. CODELL III, Secretary, Kentucky Transportation Cabinet

JOHN L. CRAIG, Director, Nebraska Department of Roads

ROBERT A. FROSCH, Senior Research Fellow, John F. Kennedy School of Government, Harvard University

GORMAN GILBERT, Director, Oklahoma Transportation Center, Oklahoma State University

GENEVIEVE GIULIANO, Professor, School of Policy, Planning, and Development, University of Southern California, Los Angeles

LESTER A. HOEL, L. A. Lacy Distinguished Professor, Department of Civil Engineering, University of Virginia

H. THOMAS KORNEGAY, Executive Director, Port of Houston Authority

BRADLEY L. MALLORY, Secretary of Transportation, Pennsylvania DOT

MICHAEL D. MEYER, Professor, School of Civil and Environmental Engineering, Georgia Institute of Technology

JEFF P. MORALES, Director of Transportation, California DOT

JEFFREY R. MORELAND, Executive Vice President-Law and Chief of Staff, Burlington Northern Santa Fe Corporation, Fort Worth, TX

JOHN P. POORMAN, Staff Director, Capital District Transportation Committee, Albany, NY

CATHERINE L. ROSS, Executive Director, Georgia Regional Transportation Agency

WAYNE SHACKELFORD, Senior Vice President, Gresham Smith & Partners, Alpharetta, GA

PAUL P. SKOUTELAS, CEO, Port Authority of Allegheny County, Pittsburgh, PA

MICHAEL S. TOWNES, Executive Director, Transportation District Commission of Hampton Roads, Hampton, VA

MARTIN WACHS, Director, Institute of Transportation Studies, University of California at Berkeley

MICHAEL W. WICKHAM, Chairman and CEO, Roadway Express, Inc., Akron, OH

JAMES A. WILDING, President and CEO, Metropolitan Washington Airports Authority

M. GORDON WOLMAN, Professor of Geography and Environmental Engineering, The Johns Hopkins University

MIKE ACOTT, President, National Asphalt Pavement Association (ex officio)

BRUCE J. CARLTON, Acting Deputy Administrator, Maritime Administration, U.S.DOT (ex officio)

JOSEPH M. CLAPP, Federal Motor Carrier Safety Administrator, U.S.DOT (ex officio)

SUSAN M. COUGHLIN, Director and COO, The American Trucking Associations Foundation, Inc. (ex officio)

JENNIFER L. DORN, Federal Transit Administrator, U.S.DOT (ex officio)

ELLEN G. ENGLEMAN, Research and Special Programs Administrator, U.S.DOT (ex officio)

ROBERT B. FLOWERS (Lt. Gen., U.S. Army), Chief of Engineers and Commander, U.S. Army Corps of Engineers (ex officio)

HAROLD K. FORSEN, Foreign Secretary, National Academy of Engineering (ex officio)

JANE F. GARVEY, Federal Aviation Administrator, U.S.DOT (ex officio)

THOMAS J. GROSS, Deputy Assistant Secretary, Office of Transportation Technologies, U.S. Department of Energy (ex officio)

EDWARD R. HAMBERGER, President and CEO, Association of American Railroads (ex officio)

JOHN C. HORSLEY, Executive Director, American Association of State Highway and Transportation Officials (ex officio)

MICHAEL P. JACKSON, Deputy Secretary of Transportation, U.S.DOT (ex officio)

JAMES M. LOY (Adm., U.S. Coast Guard), Commandant, U.S. Coast Guard (ex officio)

WILLIAM W. MILLAR, President, American Public Transportation Association (ex officio)

MARGO T. OGE, Director, Office of Transportation and Air Quality, U.S. Environmental Protection Agency (ex officio)

MARY E. PETERS, Federal Highway Administrator, U.S.DOT (ex officio)

VALENTIN J. RIVA, President and CEO, American Concrete Pavement Association (ex officio)

JEFFREY W. RUNGE, National Highway Traffic Safety Administrator, U.S.DOT (ex officio)

JON A. RUTTER, Federal Railroad Administrator, U.S.DOT (ex officio)

ASHISH K. SEN, Director, Bureau of Transportation Statistics, U.S.DOT (ex officio)

ROBERT A. VENEZIA, Earth Sciences Applications Specialist, National Aeronautics and Space Administration (ex officio)

NATIONAL COOPERATIVE HIGHWAY RESEARCH PROGRAM

Transportation Research Board Executive Committee Subcommittee for NCHRP

JOHN M. SAMUELS, Norfolk Southern Corporation, Norfolk, VA (Chair)

E. DEAN CARLSON, Kansas DOT

LESTER A. HOEL, University of Virginia

JOHN C. HORSLEY, American Association of State Highway and Transportation Officials

MARY E. PETERS, Federal Highway Administration

ROBERT E. SKINNER, JR., Transportation Research Board

MARTIN WACHS, Institute of Transportation Studies, University of California at Berkeley

Project Panel 9-19 Field of Materials and Construction Area of Bituminous Materials

LARRY A. SCOFIELD, Arizona DOT (Chair)

HUSSAIN BAHIA, University of Wisconsin-Madison

LUIS JULIAN BENDAÑA, New York State DOT

E. RAY BROWN, National Center for Asphalt Technology

ERIC E. HARM, Illinois DOT

DALLAS N. LITTLE, Texas Transportation Institute

CARL L. MONISMITH, University of California-Berkeley

JAMES A. MUSSELMAN, Florida DOT

LINDA M. PIERCE, Washington State DOT

RAYMOND S. ROLLINGS, U.S. Army Cold Regions Research and Engineering Laboratory

JOHN BUKOWSKI, FHWA Liaison Representative

THOMAS HARMAN, FHWA Liaison Representative

DALE S. DECKER, Industry Liaison Representative

KURT JOHNSON, AASHTO Liaison Representative

LARRY L. MICHAEL, Maryland State Highway Administration Liaison Representative

FREDERICK HEJL, TRB Liaison Representative

JON A. EPPS, Industry Observer

KATHERINE A. PETROS, FHWA Staff

Program Staff

ROBERT J. REILLY, Director, Cooperative Research Program

CRAWFORD F. JENCKS, Manager, NCHRP

DAVID B. BEAL, Senior Program Officer

B. RAY DERR, Senior Program Officer

AMIR N. HANNA, Senior Program Officer

EDWARD T. HARRIGAN, Senior Program Officer

CHRISTOPHER HEDGES, Senior Program Officer

TIMOTHY G. HESS, Senior Program Officer

RONALD D. McCREADY, Senior Program Officer

CHARLES W. NIESSNER, Senior Program Officer

EILEEN P. DELANEY, Managing Editor

HILARY FREER, Associate Editor II

ANDREA BRIERE, Associate Editor

ELLEN M. CHAFEE, Assistant Editor

BETH HATCH, Assistant Editor

NCHRP REPORT 465

**Simple Performance Test for
Superpave Mix Design**

M. W. WITCZAK

K. KALOUSH

T. PELLINEN

M. EL-BASYOUNY

Arizona State University

Tempe, AZ

AND

H. VON QUINTUS

Fugro-BRE, Inc.

Austin, TX

SUBJECT AREAS

Materials and Construction

Research Sponsored by the American Association of State Highway and Transportation Officials
in Cooperation with the Federal Highway Administration

TRANSPORTATION RESEARCH BOARD — NATIONAL RESEARCH COUNCIL

NATIONAL ACADEMY PRESS
WASHINGTON, D.C. — 2002

NATIONAL COOPERATIVE HIGHWAY RESEARCH PROGRAM

Systematic, well-designed research provides the most effective approach to the solution of many problems facing highway administrators and engineers. Often, highway problems are of local interest and can best be studied by highway departments individually or in cooperation with their state universities and others. However, the accelerating growth of highway transportation develops increasingly complex problems of wide interest to highway authorities. These problems are best studied through a coordinated program of cooperative research.

In recognition of these needs, the highway administrators of the American Association of State Highway and Transportation Officials initiated in 1962 an objective national highway research program employing modern scientific techniques. This program is supported on a continuing basis by funds from participating member states of the Association and it receives the full cooperation and support of the Federal Highway Administration, United States Department of Transportation.

The Transportation Research Board of the National Research Council was requested by the Association to administer the research program because of the Board's recognized objectivity and understanding of modern research practices. The Board is uniquely suited for this purpose as it maintains an extensive committee structure from which authorities on any highway transportation subject may be drawn; it possesses avenues of communications and cooperation with federal, state and local governmental agencies, universities, and industry; its relationship to the National Research Council is an insurance of objectivity; it maintains a full-time research correlation staff of specialists in highway transportation matters to bring the findings of research directly to those who are in a position to use them.

The program is developed on the basis of research needs identified by chief administrators of the highway and transportation departments and by committees of AASHTO. Each year, specific areas of research needs to be included in the program are proposed to the National Research Council and the Board by the American Association of State Highway and Transportation Officials. Research projects to fulfill these needs are defined by the Board, and qualified research agencies are selected from those that have submitted proposals. Administration and surveillance of research contracts are the responsibilities of the National Research Council and the Transportation Research Board.

The needs for highway research are many, and the National Cooperative Highway Research Program can make significant contributions to the solution of highway transportation problems of mutual concern to many responsible groups. The program, however, is intended to complement rather than to substitute for or duplicate other highway research programs.

Note: The Transportation Research Board, the National Research Council, the Federal Highway Administration, the American Association of State Highway and Transportation Officials, and the individual states participating in the National Cooperative Highway Research Program do not endorse products or manufacturers. Trade or manufacturers' names appear herein solely because they are considered essential to the object of this report.

NCHRP REPORT 465

Project 9-19 FY'98

ISSN 0077-5614

ISBN 0-309-06715-4

Library of Congress Control Number 2001134114

© 2002 Transportation Research Board

Price \$17.00

NOTICE

The project that is the subject of this report was a part of the National Cooperative Highway Research Program conducted by the Transportation Research Board with the approval of the Governing Board of the National Research Council. Such approval reflects the Governing Board's judgment that the program concerned is of national importance and appropriate with respect to both the purposes and resources of the National Research Council.

The members of the technical committee selected to monitor this project and to review this report were chosen for recognized scholarly competence and with due consideration for the balance of disciplines appropriate to the project. The opinions and conclusions expressed or implied are those of the research agency that performed the research, and, while they have been accepted as appropriate by the technical committee, they are not necessarily those of the Transportation Research Board, the National Research Council, the American Association of State Highway and Transportation Officials, or the Federal Highway Administration, U.S. Department of Transportation.

Each report is reviewed and accepted for publication by the technical committee according to procedures established and monitored by the Transportation Research Board Executive Committee and the Governing Board of the National Research Council.

Published reports of the

NATIONAL COOPERATIVE HIGHWAY RESEARCH PROGRAM

are available from:

Transportation Research Board
National Research Council
2101 Constitution Avenue, N.W.
Washington, D.C. 20418

and can be ordered through the Internet at:

<http://www.trb.org/trb/bookstore>

Printed in the United States of America

FOREWORD

*By Staff
Transportation Research
Board*

This report presents the findings of a research task to identify a simple test for confirming key performance characteristics of Superpave volumetric mix designs. In this initial phase of the work, candidate tests for permanent deformation, fatigue cracking, and low-temperature cracking were identified and recommended for field validation in the next phase of work. The report will be of particular interest to materials engineers in state highway agencies, as well as to materials suppliers and paving contractor personnel responsible for design and production of hot mix asphalt.

The Superpave volumetric mix design procedure (AASHTO MP2 and PP28) developed in the Asphalt Research Program (1987–1993) of the Strategic Highway Research Program (SHRP) does not include a simple, mechanical “proof” test analogous to the Marshall stability and flow tests or the Hveem stabilometer method. Instead, the original Superpave method relied on strict conformance to the material specifications and volumetric mix criteria to ensure satisfactory performance of mix designs intended for low-traffic-volume situations (defined as no more than 10^6 equivalent single axle loads [ESALs] applied over the service life of the pavement). For higher trafficked projects, the original SHRP Superpave mix analysis procedures¹ required a check for tertiary creep behavior with the repeated shear at constant stress ratio test (AASHTO TP7) and a rigorous evaluation of the mix design’s potential for permanent deformation, fatigue cracking, and low-temperature cracking using several other complex test methods in AASHTO TP7 and TP9.

User experience with the Superpave mix design and analysis method, combined with the long-standing problems associated with the original SHRP Superpave performance models supporting what was then termed “Level 2 and 3” analyses, demonstrated the need for such simple performance tests (SPTs). In 1996, work sponsored by FHWA (Contract DTFH61-95-C-00100) began at the University of Maryland at College Park (UMCP) to identify and validate SPTs for permanent deformation, fatigue cracking, and low-temperature cracking to complement and support the Superpave volumetric mix design method. In 1999, this effort was transferred to Task C of NCHRP Project 9-19, “Superpave Support and Performance Models Management,” with the major portion of the task conducted by a research team headed by UMCP subcontractor Arizona State University (ASU).

The research team was directed to evaluate as potential SPTs only existing test methods measuring hot mix asphalt (HMA) response characteristics. The principal evaluation criteria were (1) accuracy (i.e., good correlation of the HMA-response characteristic to actual field performance); (2) reliability (i.e., a minimum number of false negatives and positives); (3) ease of use; and (4) reasonable equipment cost.

¹ *The Superpave Mix Design Manual for New Construction and Overlays*, Report SHRP-A-407, Strategic Highway Research Program, National Research Council, Washington DC (1994).

The research team conducted a comprehensive laboratory testing program to statistically correlate the actual performance of HMA materials from the MnRoad, West-Track, and FHWA Accelerated Loading Facility (ALF) experiments with the measured responses of specimens prepared from original materials for 33 promising test method–test parameter combinations.

Based on the results of this testing program, the research team recommends three test-parameter combinations for further field validation as an SPT for permanent deformation: (1) the dynamic modulus term, $E^*/\sin\phi$, (determined from the triaxial dynamic modulus test; (2) the flow time, F_t , determined from the triaxial static creep test; and (3) the flow number, F_n , determined from the triaxial repeated load test. All combinations exhibit a coefficient of determination, R^2 , of 0.9 or greater for the combined correlation of the laboratory test results with performance in the MnRoad, West-Track, and FHWA ALF experiments.

For fatigue cracking, the experimental results are far less conclusive. The research team recommends the dynamic modulus, E^* , measured at low test temperatures; the modulus offers a fair correlation with field performance data and provides some consistency with one of the tests recommended for permanent deformation. For low-temperature cracking, the team recommends the creep compliance measured by the indirect tensile creep test at long loading times and low temperatures; this recommendation is based solely on work carried out for SHRP and C-SHRP and recently confirmed in NCHRP Project 1-37A, “Development of the 2002 Guide for the Design of New and Rehabilitated Pavement Structures.”

This report includes a detailed description of the experimental program, a discussion of the research results and the basis for selection of the candidate SPTs, a description of the future field validation effort, and five supporting appendixes presenting test methods for the candidate SPTs:

- Appendix A: Test Method for Dynamic Modulus of Asphalt Concrete Mixtures for Permanent Deformation;
- Appendix B: Test Method for Repeated Load Testing of Asphalt Concrete Mixtures in Uniaxial Compression;
- Appendix C: Test Method for Static Creep/Flow Time of Asphalt Concrete Mixtures in Compression;
- Appendix D: Test Method for Dynamic Modulus of Asphalt Concrete Mixtures for Fatigue Cracking; and
- Appendix E: Test Method for Indirect Tensile Creep Testing of Asphalt Mixtures for Thermal Cracking.

The entire report will also be distributed as a CD-ROM (*CRP-CD-10*) along with the final reports for NCHRP Projects 9-10 and 9-14.

CONTENTS

1	CHAPTER 1 Introduction
	1.1 Background, 1
	1.2 Definition of Simple Performance Test, 1
	1.3 Ranking of Applicable Test Methods, 1
	1.4 Scope of Report, 3
6	CHAPTER 2 Candidate Tests and Response Parameters
	2.1 Permanent Deformation Tests, 6
	2.1.1 Triaxial Dynamic Modulus Tests, 6
	2.1.2 Shear Dynamic Modulus—Superpave Shear Tester, 6
	2.1.3 Quasi-Direct Shear Dynamic Modulus—Field Shear Tester, 7
	2.1.4 Elastic Modulus—Ultrasonic Wave Propagation Tests, 8
	2.1.5 Dynamic Modulus Calculated from Regression Equations, 8
	2.1.6 Triaxial Shear Strength Tests, 9
	2.1.7 Static Triaxial Creep Tests, 10
	2.1.8 Triaxial Repeated Load Permanent Deformation Tests, 11
	2.1.9 SST Repeated Shear Permanent Deformation Tests, 13
	2.2 Fracture Tests, 14
	2.2.1 Triaxial Dynamic Modulus Tests, 14
	2.2.2 Indirect Tensile Tests, 14
	2.2.3 Indirect Tensile Strength Tests, 14
	2.2.4 Indirect Tensile Resilient Modulus Tests, 15
	2.2.5 Indirect Tensile Fatigue Tests, 15
	2.2.6 Indirect Tensile Creep Tests, 16
18	CHAPTER 3 Experimental Factorial and Testing Plan
	3.1 Experimental Plan, 18
	3.1.1 Experimental Goal, 18
	3.1.2 Tiered Factorial Approach, 18
	3.1.3 Experimental Analysis Plan, 18
	3.1.4 Evaluation Criteria, 19
	3.2 Test Sites and Mixtures, 20
	3.2.1 MnRoad, 20
	3.2.2 Accelerated Loading Facility—Turner Fairbanks, 20
	3.2.3 WesTrack, 20
	3.3 Test Specimen Preparation and Conditioning, 22
	3.3.1 Triaxial Dynamic Modulus Specimens, 22
	3.3.2 SST Specimens, 23
	3.3.3 FST Specimens, 24
	3.3.4 Ultrasonic Wave Propagation Specimens, 24
	3.3.5 Triaxial Shear Strength Specimens, 25
	3.3.6 Static Creep and Repeated Load Specimens, 25
	3.3.7 Repeated Shear Permanent Deformation Specimens, 26
	3.3.8 Indirect Tensile Specimens, 27
29	CHAPTER 4 Analyses and Comparisons of Mixture Response to Permanent Deformation
	4.1 Modulus Parameters Versus Rutting, 29
	4.1.1 Triaxial Dynamic Modulus, 29
	4.1.2 Ultrasonic Wave Propagation Elastic Modulus, 29
	4.1.3 SST and FST Dynamic Shear Modulus, 29
	4.1.4 Predictive Equations for Dynamic Modulus, 30
	4.2 Static Creep Parameters Versus Rutting, 34
	4.2.1 Unconfined Static Creep Test Parameters, 36
	4.2.2 Confined Static Creep Test Parameters, 38
	4.3 Triaxial Repeated Load Permanent Deformation Parameters Versus Rutting, 39
	4.4 SST Repeated Load Permanent Deformation Parameters Versus Rutting, 40
	4.5 Triaxial Shear Strength Parameters Versus Rutting, 43
48	CHAPTER 5 Analyses and Comparisons of Mixture Response to Fracture
	5.1 Modulus Parameters Versus Cracking, 48
	5.2 Indirect Tensile Test Parameters Versus Cracking—General, 48

	5.3 Indirect Tensile Creep Parameters Versus Cracking, 48
	5.3.1 MnRoad, 50
	5.3.2 ALF, 50
	5.3.3 WesTrack, 50
	5.4 Indirect Tensile Strength Parameters Versus Cracking, 50
	5.5 Indirect Tensile Fatigue Parameters Versus Cracking, 52
53	CHAPTER 6 Summary of Findings
	6.1 Test Methods Applicable for the SPT, 53
	6.1.1 SPT for Permanent Deformation—Rutting, 53
	6.1.2 SPT for Fracture—Fatigue and Thermal Cracking, 54
	6.1.3 SPT Protocols, 55
	6.1.4 Time Estimates for SPT Test Methods, 55
	6.2 Development of SPT Criteria, 55
	6.3 Field Validation of the SPT, 57
58	CHAPTER 7 Recommendations and Future Activities
	7.1 Summary and Recommendations, 58
	7.2 Future Activities, 58
	7.2.1 Specimen Diameter Study: 4-in. (100-mm) Versus 6-in. (150-mm), 58
	7.2.2 Dynamic Complex Modulus Study: Flexural Versus Compressive Testing, 59
	7.2.3 Sensitivity Study: SPT Response Parameter and Magnitude, 59
	7.2.4 Tertiary Flow Measurement Methods Study, 59
60	REFERENCES
62	GLOSSARY
64	APPENDIX A Test Method for Dynamic Modulus of Asphalt Concrete Mixtures for Permanent Deformation
73	APPENDIX B Test Method for Repeated Load Testing of Asphalt Concrete Mixtures in Uniaxial Compression
83	APPENDIX C Test Method for Static Creep/Flow Time of Asphalt Concrete Mixtures in Compression
93	APPENDIX D Test Method for Dynamic Modulus of Asphalt Concrete Mixtures for Fatigue Cracking
101	APPENDIX E Test Method for Indirect Tensile Creep Testing of Asphalt Mixtures for Thermal Cracking

AUTHOR ACKNOWLEDGMENTS

The research reported herein was performed under Task C of NCHRP Project 9-19, “Superpave Support and Performance Models Management.” This report represents the test results from the Task C experimental plan that was used to select a simple performance test and response parameter to complement the Superpave volumetric mixture design procedure.

Dr. Matthew W. Witczak of Arizona State University (previously of the University of Maryland) was the principal investigator for NCHRP Project 9-19; Mr. Harold Von Quintus of Fugro-BRE, Inc., and Dr. Charles W. Schwartz of the University of Maryland were the co-principal investigators. Ms. Kathy Petros was the FHWA contract-

ing officer’s technical representative, and Dr. Edward Harrigan was the NCHRP program manager.

The report was prepared by Mr. Von Quintus and by Dr. Kamil Kaloush, Dr. Tehri Pellinen, and Mr. Mohammed El-Basyouny of Arizona State University. The general overview of the work, as well as review and revision of the report, was provided by Dr. Witczak. Special thanks are given to FHWA, the Superpave Mixtures and Aggregate Expert Task Group, the National Asphalt Pavement Association, the NCHRP panel, and numerous other individuals who provided valuable feedback information to a series of questions concerning the characteristics and attributes of an “ideal simple performance test.”

CHAPTER 1

INTRODUCTION

1.1 BACKGROUND

The Superpave® mix design and analysis method was developed more than a decade ago under the Strategic Highway Research Program (SHRP) (1). Many agencies in North America have adopted different parts of that method, including the performance-grade (PG) binder specification and the volumetric mixture design method.

The Superpave design method for hot mix asphalt (HMA) mixtures consists of three phases: (1) materials selection for the asphalt binder and aggregate, (2) aggregate blending, and (3) volumetric analysis on specimens compacted using the Superpave gyratory compactor (SGC) (2). However, other than a final check for tertiary flow, there is no general strength or “push–pull” test to complement the volumetric mixture design method as there is for the more traditional Marshall and Hveem mixture design methods.

Results from WesTrack, NCHRP Project 9-7 (“Field Procedures and Equipment to Implement SHRP Asphalt Specifications”), and other experimental construction projects have raised the question of whether the Superpave volumetric mix design method alone is sufficient to ensure reliable mixture performance over a wide range of traffic and climatic conditions. Industry has expressed the need for a simple “push–pull” type of test to complement the Superpave volumetric mix design method, especially for use on design–build or warranty projects.

In response to this need, FHWA committed funding in 1996 to identify and evaluate a simplified test method. FHWA referred to this test as a “simple strength test” that should provide reliable information on the probable performance of the HMA design during the volumetric mixture design process using the SGC. The focus of the test was to measure a fundamental engineering property that can be linked back to the advanced material characterization methods needed for detailed distress-prediction models. This measurement would enable the use of a simple performance model in the development of criteria for HMA mixture design. It was envisioned that this simple strength or performance test would play a key role in the quality control and acceptance of HMA mixtures.

As a commitment to this effort, FHWA authorized the University of Maryland Superpave Models Team (under

Phase II of FHWA Contract No. DTFH61-95-C-00100) to develop all necessary test protocols, criteria, and guidelines for the simple performance test (SPT) to support the Superpave volumetric mix design procedure. NCHRP Project 9-19 (“Superpave Support and Performance Models Management”) continues that commitment.

1.2 DEFINITION OF SIMPLE PERFORMANCE TEST

The definition for the SPT, as used in this report, is as follows:

A test method(s) that accurately and reliably measures a mixture response characteristic or parameter that is highly correlated to the occurrence of pavement distress (e.g., cracking and rutting) over a diverse range of traffic and climatic conditions.

Given this definition, it is not necessary for the SPT to predict the entire distress or performance history of the HMA mixture, but the test results must allow a determination of a mixture’s ability to resist fracture and permanent deformation under defined conditions.

1.3 RANKING OF APPLICABLE TEST METHODS

As stated above, a consensus has been building among materials and construction engineers, as well as among consultants and researchers, that an SPT should be included as a final stage in the Superpave volumetric mix design method. That final stage is a diagnostic evaluation—the measurement and determination of properties related to performance—of the HMA mixture. The test methods that accurately and precisely measure those properties and that are highly correlated to pavement distress should be considered as candidates for more detailed laboratory studies.

Many tests have been proposed for use as an SPT, including dynamic modulus, repeated shear at constant height, shear

dynamic modulus, creep compliance, and other test methods. Under Phase II of the FHWA contract with the University of Maryland, the Superpave Models Team evaluated a variety of possible tests that would be applicable to the definition of an SPT.

Table 1 summarizes the different test categories that were used for the SPT in the Phase II work of the FHWA contract. Results from the initial evaluation of these test methods clearly demonstrated that there is no “perfect” test method for all types of HMA mixtures placed under varying traffic and climatic conditions. Thus, the different test methods were compared using a series of factors that were believed to be consistent with the definitions of the SPT. This work was completed under Phase II of the FHWA contract and documented in an Interim Task C Report entitled “Preliminary Recommendations for the Simple Performance Test” (3).

A utility analysis was initially used to rank each of the test methods that were considered candidates for use as an SPT. The information needed for this analysis was obtained from literature reviews, results from previous and ongoing test programs, and the experience of the research team. Table 2 shows the different combinations of material properties and test methods that were considered in the initial evaluation for different types of distress.

In completing the utility analysis, a relative weight (or importance) of each factor was needed. The project team prepared a questionnaire to obtain that information directly from industry. Input from industry or the potential users of the SPT was considered very important to the future acceptance of this test. The questionnaire was sent to industry representatives across North America.

The questionnaire was divided into three parts. The first part was used to estimate the importance of the distress types that should be correlated to the SPT. Three distresses were listed on the questionnaire: rutting, fatigue cracking, and thermal cracking. On a scale of 1 to 3, the average relative impor-

tance of the SPT’s ability to measure the responses correlated to three distresses are as follows:

- Rutting—1.1,
- Fatigue cracking—1.8, and
- Thermal cracking—2.2.

A “1” indicates the distress must be considered by the performance test, a “2” that the distress is moderately important to consider, and a “3” that the distress is relatively unimportant to consider. Thus, industry rates rutting as the most important distress for consideration by the SPT, followed by fatigue cracking and then by thermal cracking. These responses are consistent with the results from other surveys (4).

The second part of the questionnaire obtained industry’s perspective on a reasonable initial investment cost for the equipment and on how much time should it take to perform the SPT. Results from this part of the questionnaire are listed below:

- Initial investment cost = \$36,800, and
- Testing time = 8.6 h.

The third and final part of the questionnaire obtained industry’s opinion on the relative importance of each factor included in the utility analysis. These factors were subdivided into two categories: those related to the reliability of the test method and those related to fundamental factors of the test method. The responses were provided on a scale of 0 to 10, in which “10” represented a very important factor and “0” represented an unimportant factor. Table 3 summarizes the mean values for each factor included in the questionnaire.

The review of test methods by the project team, the industry questionnaire, and the utility analysis resulted in a set of preliminary recommendations for the SPT. Those tests judged

TABLE 1 Test categories for SPT

Type of Test or Test Geometry	Type of Load Application	Type of Load Pulse
<ul style="list-style-type: none"> ▪ Uniaxial or triaxial compression testing ▪ Indirect tensile testing ▪ Direct tensile testing ▪ Simple shear testing ▪ Direct shear testing ▪ Hydrostatic testing ▪ Torsional or rotational testing ▪ Flexural beam testing 	<ul style="list-style-type: none"> ▪ Static (or creep) loading ▪ Constant deformation rate ▪ Repeated loading ▪ Cyclic or dynamic loading 	<ul style="list-style-type: none"> ▪ None ▪ Square ▪ Haversine ▪ Sinusoidal ▪ Triangular

TABLE 2 Combinations of material properties and test methods considered in the initial evaluation (3)

Test Method	Materials Properties											
	Modulus Dynamic/Resilient	Secant or Tangent Modulus	Bulk Modulus	Strength	Work or Energy	Creep Compliance	Flow Time	Poisson's Ratio	Fatigue Parameters	Rutting Parameters	Excess Fluids Content, Plasticity, Flushing	Refusal Density, Traffic Densif.
<i>Superpave Shear Tests</i>	F, R					F, R	R			R		
<i>Quasi / Direct Shear Tests</i>	F, R	R		R	R	F, R	R			R		
<i>Plane Shear Tests</i>		R									R	R
<i>Torsional or Rotational Shear Tests</i>	F, R					F, R	R			R		
<i>Triaxial Tests (with Constant Confining Pressures)</i>	F, R	R	F, R	R	R	F, R	R	F, R		R		
<i>Uniaxial Unconfined Compression Tests</i>	F, R	R		R	R	F, R	R	F, R		R		
<i>Indirect Tensile Tests</i>	F, R	F		F, T	F, T	F, T	F, T	F, T	F			
<i>Direct Tension Tests</i>	F, R	F			F, T	F, T	F, T	F, T	F			
<i>Hydrostatic Pressure Tests</i>			F, R			F, R		F, R				
<i>Lateral Pressure Testers</i>	F, R		F, R			F, R		F, R				
<i>Flexural Beam Tests</i>	F	F		F	F	F			F			
<i>Rut-Depth Testers</i>										R	R	

* Distresses considered in each cell: F = fatigue cracking; R = rutting; T = thermal cracking.

to have the greatest potential for meeting the definition of the SPT are listed in Table 4. Table 4 identifies the test methods and the responses from each test that were evaluated for their correlation to performance (i.e., rut depth, fatigue cracking, and thermal cracking). Other candidate test methods and responses listed in Table 4 are being evaluated in other studies sponsored by FHWA and NCHRP.

1.4 SCOPE OF REPORT

This report summarizes the work completed under NCHRP Project 9-19 to select those test methods and HMA mixture responses that are highly correlated to pavement distress (i.e., permanent deformation and fracture). The report is divided into six chapters, including this introduction (Chapter 1).

TABLE 3 Results from industry questionnaire on importance of the different factors considered in the utility analysis

Utility Factor Categories	Relative Importance of Category, %	Utility Factor	Mean Rating Value
A	62	Reliability to Identify Inferior Mixes	9.3
		Reliability for Distress Predictions	8.4
		Test Parameter Sensitivity	8.1
B	38	Variability of the Responses	8.0
		Applicability to Test Cores	7.3
		Sample Preparation Time	7.2
		Testing Time	7.1
		Maintenance and Repair Costs	6.9
		Size of Test Specimen	6.8
		Initial Investment Cost	6.8
		Calibration Requirements	6.3
		Sophistication of Data Reduction	5.8
		Mobility of the Equipment	5.6

TABLE 4 Candidate test methods and responses for the SPT

Test Method	Mixture Response Parameter	Experimental Plan
Dynamic Modulus Test	Dynamic modulus	Permanent deformation and fatigue
	Phase angle	Permanent deformation
SST Shear Modulus Test	Dynamic modulus	Permanent deformation
	Phase angle	Permanent deformation
Quasi-Direct Shear (Field Shear Test)	Dynamic modulus	Permanent deformation
	Phase angle	Permanent deformation
Triaxial Repeated Load Test	Slope and intercept of accumulated permanent and total strain	Permanent deformation
	Plastic to resilient strain ratio	Permanent deformation
	Resilient modulus, total and instantaneous	Permanent deformation
	Plastic and resilient strains	Permanent deformation
SST Repeated Shear, Constant-Height	Slope and intercept of accumulated permanent and total shear strains	Permanent deformation
	Plastic to resilient strain ratio	Permanent deformation
	Resilient shear modulus, total and instantaneous	Permanent deformation
	Plastic and resilient shear strains	Permanent deformation
Triaxial and Uniaxial Creep	Number of cycles to plastic flow	Permanent deformation
	Slope and intercept of accumulated permanent and total shear strains	Permanent deformation
	Plastic to resilient strain ratio	Permanent deformation
	Resilient shear modulus, total and instantaneous	Permanent deformation
Triaxial and Uniaxial Creep	Plastic and resilient shear strains	Permanent deformation
	Number of cycles to plastic flow	Permanent deformation
	Slope and intercept of total strain versus time	Permanent deformation
	Creep-compliance/creep modulus	Permanent deformation
Triaxial Compressive Strength	Time at plastic flow	Permanent deformation
	Percent strain recovery	Permanent deformation
	Angle of internal friction	Permanent deformation
	Cohesion	Permanent deformation
Wheel-Tracking, Hamburg	Compressive strength	Permanent deformation
	Fracture energy	Permanent deformation
	Rut depth at specified load cycles or load cycles at specified rut depth	X ^(a)
Asphalt Pavement Analyzer	Slope or rate of rutting	X ^(a)
	Rut depth at specified load cycles or load cycles at specified rut depth	X ^(a)
Gyratory Shear Stress	Slope or rate of rutting	X ^(a)
	Shear stress	X ^(a)
Indirect Tensile Creep Test	Rate of change of shear stress with number of gyrations	X ^(a)
	Creep-compliance/ modulus	Fracture
Indirect Tensile Fatigue/Repeated Load Test	Slope and intercept of creep-compliance versus load time	Fracture
	Number of cycles to failure	Fracture
	Resilient modulus, total and instantaneous	Fracture
	Plastic strain	Fracture
Indirect Tensile Strength Test	Slope and intercept of accumulated permanent and total strains	Fracture
	Tensile strength	Fracture
	Tensile strain at failure	Fracture
Direct Tensile Creep Test	Fracture energy	Fracture
	Creep-compliance/modulus	X ^(a)
Direct Tensile Fatigue, Repeated Load Test	Slope and intercept of the creep-compliance with load time	X ^(a)
	Number of cycles to failure	X ^(a)
Direct Tensile Strength Test	Slope and intercept of permanent and total strains versus loading cycles	X ^(a)
	Tensile strength	X ^(a)
	Tensile strain at failure	X ^(a)
	Fracture energy	X ^(a)

X^(a) designates those test methods and mixture responses that were not included in the test program of NCHRP Project 9-19, but are being evaluated under other studies.

Chapter 2 provides a discussion of the candidate test methods and mixture responses included in the test program. Chapter 3 presents the experimental factorial and details of the testing procedure for each test method. Chapters 4 and 5 compare the mixture responses with permanent deformation and fracture (both fatigue and thermal cracking), respectively.

Chapter 6 summarizes the results and test methods recommended for the SPT and presents a framework for future development of the specification criteria for the SPT and a recommended field validation experiment. The test protocols recommended for further field validation as SPTs are provided in appendixes to the report.

CHAPTER 2

CANDIDATE TESTS AND RESPONSE PARAMETERS

Table 4 listed the test methods and mixture response parameters that were ranked as the “best” candidates for the SPT for permanent deformation and fracture distresses. This chapter describes the test methods and mixture response parameters evaluated in NCHRP Project 9-19. Details of the laboratory test program are given in Chapter 3.

2.1 PERMANENT DEFORMATION TESTS

2.1.1 Triaxial Dynamic Modulus Tests

The dynamic modulus test is the oldest and best documented of the triaxial compression tests. It was standardized in 1979 as ASTM D3497, “Standard Test Method for Dynamic Modulus of Asphalt Concrete Mixtures.” The test consists of applying a uniaxial sinusoidal (i.e., haversine) compressive stress to an unconfined or confined HMA cylindrical test specimen, as shown in Figure 1.

The stress-to-strain relationship under a continuous sinusoidal loading for linear viscoelastic materials is defined by a complex number called the “complex modulus” (E^*). The absolute value of the complex modulus, $|E^*|$, is defined as the dynamic modulus. The dynamic modulus is mathematically defined as the maximum (i.e., peak) dynamic stress (σ_o) divided by the peak recoverable axial strain (ϵ_o):

$$|E^*| = \frac{\sigma_o}{\epsilon_o} \quad (1)$$

The real and imaginary portions of the complex modulus (E^*) can be written as

$$E^* = E' + iE'' \quad (2)$$

E' is generally referred to as the storage or elastic modulus component of the complex modulus; E'' is referred to as the loss or viscous modulus. The phase angle, ϕ , is the angle by which ϵ_o lags behind σ_o . It is an indicator of the viscous properties of the material being evaluated. Mathematically, this is expressed as

$$E^* = |E^*| \cos \phi + i |E^*| \sin \phi \quad (3)$$

$$\phi = \frac{t_i}{t_p} \times (360) \quad (4)$$

where

- t_i = time lag between a cycle of stress and strain (s);
- t_p = time for a stress cycle (s); and
- i = imaginary number.

For a pure elastic material, $\phi = 0$, and the complex modulus (E^*) is equal to the absolute value, or dynamic modulus. For pure viscous materials, $\phi = 90^\circ$.

2.1.2 Shear Dynamic Modulus—Superpave Shear Tester

The shear frequency sweep or shear dynamic modulus test (i.e., AASHTO TP7, “Standard Test Method for Determining the Permanent Deformation and Fatigue Cracking Characteristics of Hot Mix Asphalt [HMA] Using the Simple Shear Test [SST] Device”) conducted with the Superpave shear tester (SST) was developed under SHRP to measure mixture properties that can be used to predict mixture performance. The shear dynamic modulus is defined analogously to the triaxial dynamic modulus as the absolute value of the complex modulus in shear:

$$|G^*| = \frac{\tau_o}{\gamma_o} \quad (5)$$

where

- $|G^*|$ = shear dynamic modulus,
- τ_o = peak shear stress amplitude, and
- γ_o = peak shear strain amplitude.

With these results, both the elastic and viscous behavior can be determined through calculation of the shear storage modulus (G') and loss modulus (G''), analogous to the discussion for the dynamic modulus test.

The frequency sweep at constant height (FSCH) test is a strain-controlled test with the maximum shear strain limited to 0.0001 mm/mm. The shear strain is applied by a hor-

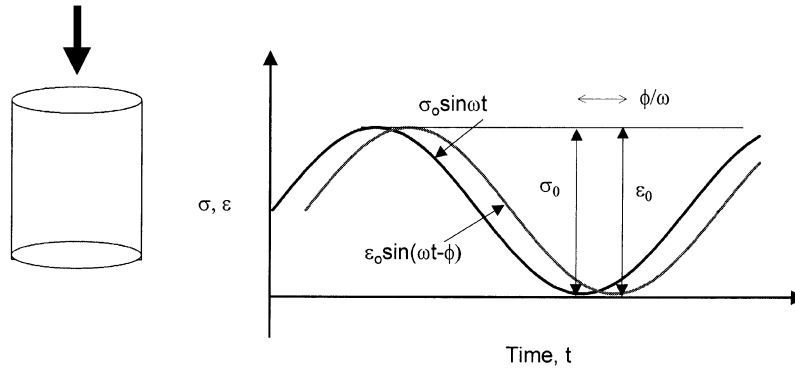


Figure 1. Haversine loading pattern or stress pulse for the dynamic modulus test.

horizontal actuator at a frequency of 10 to 0.01 Hz using a sinusoidal loading pattern, as shown in Figure 2a. The cylindrical test specimen with a diameter of 150 mm and height of 50 mm is glued between two aluminum platens. The specimen is loaded in shear from the bottom as shown in Figure 2b.

The horizontal actuator is controlled by closed loop feedback from measurements of a linear variable differential transducer (LVDT) mounted horizontally on the specimen. The specimen height is kept constant during the test by compressing or pulling the test specimen with a vertical actuator. The direction and magnitude of the axial load is controlled by closed loop feedback from measurements by a vertical LVDT attached to the top of the specimen.

2.1.3 Quasi-Direct Shear Dynamic Modulus—Field Shear Tester

The field shear tester (FST) was developed through NCHRP Project 9-7 to control Superpave-designed HMA mixtures (3). The device was designed to perform tests comparable with two of the Superpave load-related mixture tests: the FSCH (i.e., dynamic modulus in shear) test and the simple shear at constant height (SSCH) test (i.e., AASHTO TP7).

The FST control software can be used to measure the dynamic modulus in shear. The FST uses a 10-kip servo-pneumatic loading frame and is capable of applying repetitive loads of various waveforms. The FST environmental chamber used during testing is separate from the loading frame.

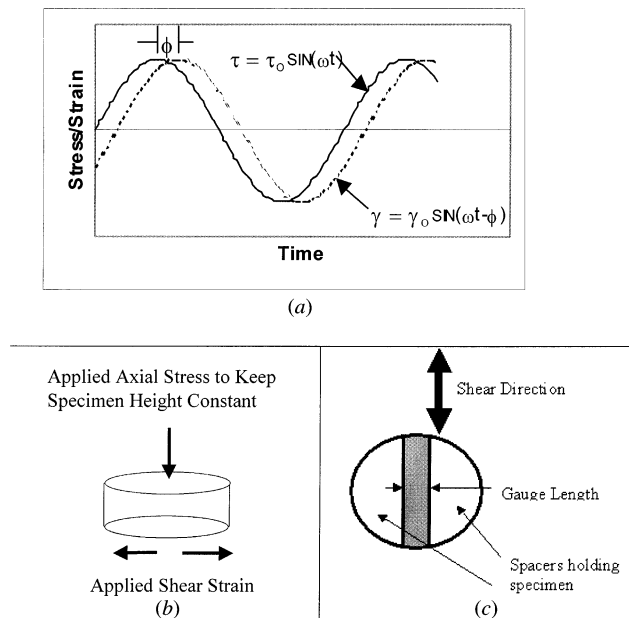


Figure 2. Dynamic modulus tests in shear. (a) Schematic of the loading pattern applied by the shear testers. (b) Superpave shear tester. (c) Field shear tester.

The key differences between the FST and SST devices are the positioning of the sample and the test control mode:

1. In the SST device, the test specimen is sheared in the upright position by moving the shear table attached to the bottom of the specimen (Figure 2b). The resulting shear strains are measured parallel to the ends of the test specimen. In the FST device, the specimen is positioned in a similar manner to the indirect tensile test using loading platens similar to the Marshall test. The test specimen is sheared along its diametral axis by moving a shaft that is attached to the loading frame holding the specimen in place, as shown in Figure 2c. The gauge length of the measured shear strain is the opening between the loading platens that are holding the specimen. Thus, the SST and FST measure the dynamic modulus along different planes and directions relative to the aggregate orientation.
2. In the SST device, the height of the specimen is kept constant by loading the specimen through a vertical actuator attached to the top of the specimen. In the FST device, the specimen height is kept constant by using rigid spacers attached to the specimen ends.
3. In the SST device, the shear frequency sweep test is conducted in a strain-control method of loading (i.e., by applying a constant sinusoidal shear strain of approximately 100 microstrains) and measuring the shear stress as a function of the applied test frequency. In the FST device, the shear frequency sweep test is conducted in a load-control method of loading (i.e. by applying a constant sinusoidal shear stress and measuring the shear strain as a function of the applied test frequency).

In this study, both the FSCH and SSCH tests were used for measuring the dynamic modulus in shear because the measured values are believed to represent different stiffness properties of the HMA mixture.

2.1.4 Elastic Modulus—Ultrasonic Wave Propagation Tests

The nondestructive pulse velocity technique is based on the measurement of wave velocities through a material. Ultrasonic wave propagation tests use a piezoelectric crystal transducer that converts a pulse of electrical energy into an ultrasonic shock wave. The crystal typically has a resonant frequency of 20 to 100 kHz.

The shock wave is normally coupled from the transducer into the material with the aid of a liquid-coupling material such as glycerin. The sound travels through the test specimen until it encounters a density change where it is reflected back towards the transducer. The density change is often the opposite end or surface of the test specimen. However, a flaw or lamination in the test specimen can cause the reflection of sound as well. The ultrasound travels back to the probe

through the coupling medium and is converted back to an electrical impulse. Figure 3 illustrates the test setup.

The velocity of an ultrasonic pulse traveling in a solid material depends on the density and the elastic properties of the material, that is, the velocity is proportional to the density and elastic properties of the material. For longitudinal waves, the pulse velocity v_{cl} is related to the density and elastic properties of a solid by Equation 6:

$$v_{cl} = \sqrt{\frac{E}{\rho} \frac{(1 - \mu)}{(1 + \mu)(1 - 2\mu)}} \quad (6)$$

where

v_{cl} = velocity of sound, m/s;
 ρ = density, kg/m³;
 E = modulus of elasticity, Pa = N/m²; and
 μ = Poisson's ratio.

If the thickness (i.e., length) of the test specimen is known, the longitudinal wave velocity can be calculated by measuring the wave pulse time. The modulus of elasticity is then calculated using Equation 6, given the longitudinal wave velocity calculated from the test (Figure 3), the known or measured density of the material, and Poisson's ratio.

2.1.5 Dynamic Modulus Calculated from Regression Equations

Regression equations are available to calculate the dynamic modulus from conventional volumetric mixture properties. These regression models were considered as SPT candidate models because of their simplicity. The two regression models that have been well documented and are in common use by the industry are the Witczak et al. (5) and Shell Oil pre-

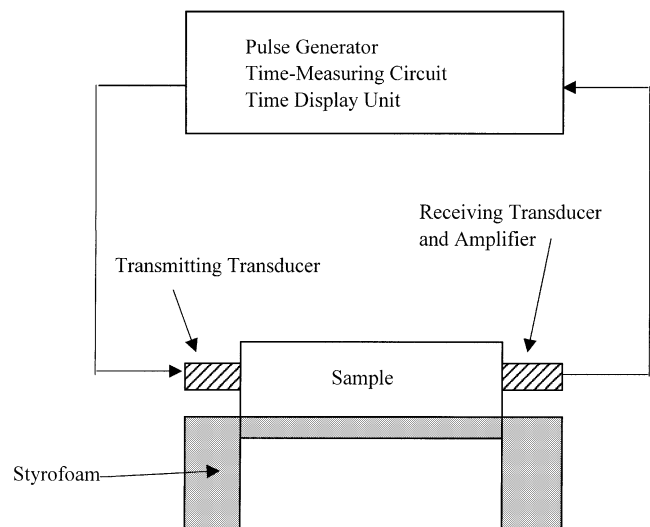


Figure 3. Schematic illustration of the ultrasonic test setup.

dictive equations (6). Both of these regression equations are listed and defined in the following paragraphs.

2.1.5.1 Witczak et al. Predictive Equation

The dynamic modulus predictive equation developed by Witczak et al. at the University of Maryland and Arizona State University over the last 30 years is one of the most comprehensive mixture dynamic modulus models available today. This regression model (Equation 7) has the capability to predict the dynamic modulus of dense-graded HMA mixtures over a range of temperatures, rates of loading, and aging conditions from information that is readily available from conventional binder tests and the volumetric properties of the HMA mixture (5).

$$\log|E^*| = -1.249937 + 0.029232(p_{200}) - 0.001767(p_{200})^2 - 0.002841(p_4) - 0.058097(V_a) - \frac{0.802208(V_{\text{eff}})}{V_{\text{eff}} + V_a} + \frac{3.871977 - 0.0021(p_4) + 0.003958(p_{38}) - 0.000017(p_{38})^2 + 0.005470(p_{34})}{1 + e^{(-0.600313 - 0.313351 \times \log(f) - 0.393532 \times \log(\eta))}}$$

where

- $|E^*|$ = dynamic modulus, 10^5 psi;
- η = bitumen viscosity, 10^6 Poise;
- f = loading frequency, Hz;
- V_a = air void content, percent;
- V_{beff} = effective bitumen content, percent by volume;
- ρ_{34} = cumulative percent retained on 19-mm sieve;
- ρ_{38} = cumulative percent retained on 9.5-mm sieve;
- ρ_4 = cumulative percent retained on 4.76-mm sieve; and
- ρ_{200} = percent passing 0.075-mm sieve.

Equation 7 is based on more than 2,800 dynamic modulus measurements from about 200 different HMA mixtures tested in the laboratories of the Asphalt Institute, the University of Maryland, and FHWA.

2.1.5.2 Shell Oil Predictive Equation

A basic assumption of the Shell Oil predictive equation is that the modulus of the dense-graded HMA mixture is related to the modulus of the binder. The binder modulus (Sb) is determined from laboratory measurements or by the use of a nomograph. Using the equations developed by Bonnaure et al., the modulus of the mixture (Sm) can be computed using equations 8 or 9 (6).

For binder moduli in the range of $5 \times 10^6 < Sb(\text{N/m}^2) < 10^9$,

$$\log Sm = \frac{\beta_4 + \beta_3}{2} \cdot (\log Sb - 8) + \frac{\beta_4 + \beta_3}{2} |\log Sb - 8| + \beta_2; \quad (8)$$

For binder moduli in the range of $10^9 < Sb(\text{N/m}^2) < 3 \times 10^9$,

$$\log Sm = \beta_2 + \beta_4 + 2.0959 \cdot (\beta_1 - \beta_2 - \beta_4) \cdot (\log Sb - 9) \quad (9)$$

where

$$\beta_1 = 10.82 - \frac{1.342 \cdot (100 - V_g)}{V_g + V_b}, \quad (10a)$$

$$\beta_2 = 8.0 + 0.00568 \cdot V_g + 0.0002135 \cdot V_g^2, \quad (10b)$$

$$\beta_3 = 0.6 \cdot \log\left(\frac{1.37 \cdot V_b^2 - 1}{1.33 \cdot V_b - 1}\right), \quad (10c)$$

$$\beta_4 = 0.7582 \cdot (\beta_1 - \beta_2), \quad (10d)$$

- Sm = modulus of the mix,
- Sb = modulus of the binder,
- V_b = percent volume of bitumen, and
- V_g = percent volume of aggregate.

2.1.6 Triaxial Shear Strength Tests

The triaxial compressive strength test has been used to a much lesser extent in evaluating an HMA mixture's susceptibility to permanent deformation compared with the dynamic modulus and repeated load tests. AASHTO T167, "Standard Test Method for Compressive Strength of Bituminous Mixtures," is the standard test typically used to measure a mixture's unconfined compressive strength. Confining pressures have also been used with the test to develop a failure envelope.

The shear strength of an HMA mixture is developed principally from two sources: (1) the cohesion, c , which reflects the adhesion or bonding mechanism of the binder and is derived from Mohr–Coulomb plots; and (2) the interlocking capability of the aggregate matrix from the applied loads, which is referred to as the angle of internal friction, ϕ . The major role and interaction of both of these terms vary substantially with the rate of loading, temperature, and volumetric properties of the HMA mixture. Triaxial tests are run at different confining pressures to obtain the Mohr–Coulomb failure envelope. The Mohr–Coulomb failure envelope is defined as follows:

$$\tau = c + \sigma \tan \phi \quad (11)$$

where

- τ = shear stress;
- σ = normal stress;

c = intercept parameter, cohesion; and
 ϕ = slope of the failure envelope or the angle of internal friction.

Typical c -values for dense-graded HMA mixtures are in the range of 5 to 35 psi; typical ϕ -values range between 35° and 48°. Triaxial tests usually require three or more levels of confinement to accurately determine the failure envelope.

An alternative to the Mohr–Coulomb failure envelope is the Drucker–Prager failure envelope, which is defined by an intercept parameter, k , and slope $\gamma^{1/2}$ (7). The Drucker–Prager failure envelope represents the combination of failure stresses expressed in terms of the first invariant stress tensor, I_1 , and the second invariant deviatoric stress tensor, $J_2^{1/2}$, by the following equation:

$$J_2^{1/2} = \gamma^{1/2} I_1 + k \quad (12)$$

where

$$J_2^{1/2} = (1/\sqrt{3}) (\sigma_1 - \sigma_3), \text{ and}$$

$$I_1 = \sigma_1 + 2\sigma_3.$$

2.1.7 Static Triaxial Creep Tests

As noted in Chapter 1, the modulus of a material is an important property that relates stress to strain and is used to predict pavement distress. For viscoelastic materials, however, it is more advantageous to use the term compliance or $D(t)$. Compliance is the reciprocal of the modulus. The main advantage of its use in viscoelasticity–viscoplasticity theory is that compliance allows for the separation of the time-independent and time-dependent components of the strain response.

In a static compressive creep test, a total strain-time relationship for a mixture is measured in the laboratory under unconfined or confined conditions. The static creep test, using either one load-unload cycle or incremental load-unload cycles, provides sufficient information to determine the instantaneous elastic (i.e., recoverable) and plastic (i.e., irrecoverable) components (which are time independent), as well as the viscoelastic and viscoplastic components (which are time dependent) of the material's response. Figure 4 shows a typical relationship between the calculated total compliance and loading time. As shown, the total compliance can be divided into three major zones:

1. The primary zone—the portion in which the strain rate decreases with loading time;
2. The secondary zone—the portion in which the strain rate is constant with loading time; and
3. The tertiary flow zone—the portion in which the strain rate increases with loading time.

Ideally, the large increase in compliance occurs at a constant volume within the tertiary zone. The starting point of

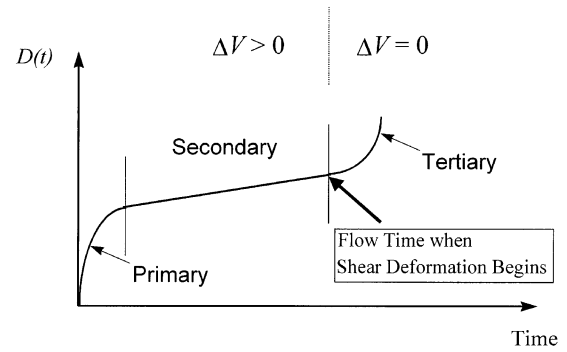


Figure 4. Typical test results between compliance and loading time.

tertiary deformation is defined as the flow time, which has been found to be a significant parameter in evaluating an HMA mixture's rutting resistance (8). The flow time also is viewed as the minimum point in the relationship of the rate of change of compliance to loading time. The flow time, F_T , is therefore defined as the time at which the shear deformation under constant volume begins.

Details on compliance models and regression parameters are available in the literature (9). In general, power models are used to model the secondary (i.e., linear) phase of the creep compliance curve, as illustrated in Figure 5.

$$D' = D(t) - D_o = a t^m \quad (13)$$

where

- D' = viscoelastic compliance component at any time,
- $D(t)$ = total compliance at any time,
- D_o = instantaneous compliance,
- t = loading time, and
- a, m = materials regression coefficients.

The regression coefficients a and m are generally referred to as the compliance parameters. These parameters are general indicators of the permanent deformation behavior of the material. In general, the larger the value of a , the larger the compliance value, $D(t)$, the lower the modulus, and the larger

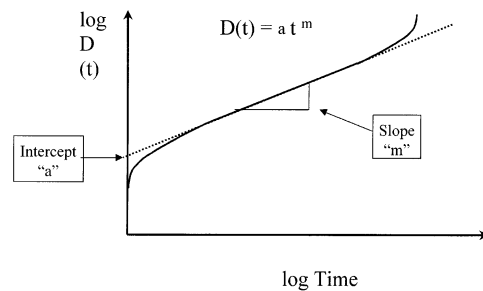


Figure 5. Regression constants a and m obtained from the secondary zone of the log compliance–log time plot.

the permanent deformation. For a constant a -value, an increase in the slope parameter m means higher permanent deformation.

Figures 6 and 7 show the actual test results and plots from a static creep test. Figure 6 shows the total compliance versus loading time on a log-log scale. The compliance parameters a and m are estimated from a regression analysis of the linear portion of the curve. Figure 7 shows a plot of the rate of change in compliance versus loading time on

a log-log scale. The calculated value of the flow time is shown on Figure 7.

2.1.8 Triaxial Repeated Load Permanent Deformation Tests

Another approach to measuring the permanent deformation characteristics of an HMA mixture is to conduct several

[F052] V1.09 Static Creep/Flow Time Strength Test

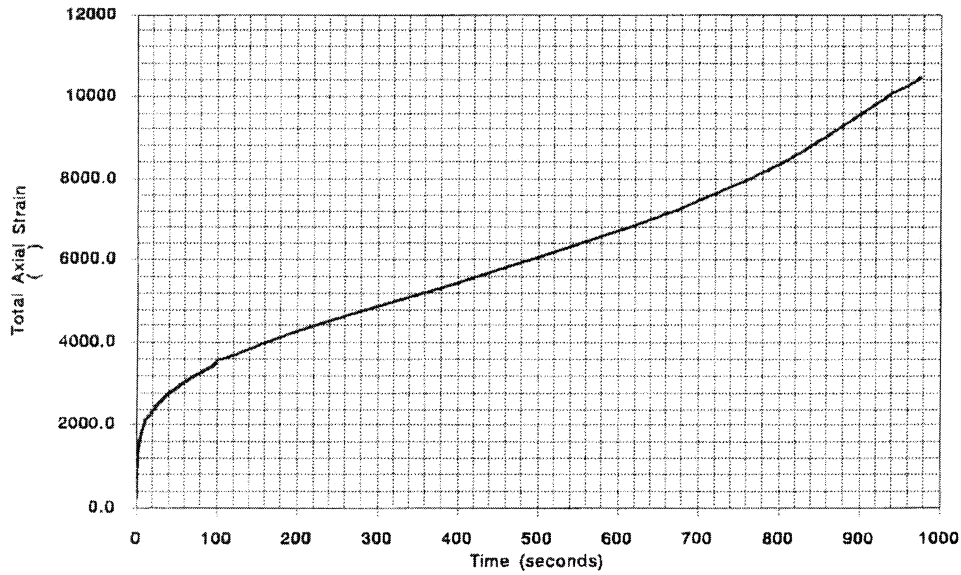


Figure 6. Total axial strain versus time from an actual static creep test.

[F052] V1.09 Static Creep/Flow Time Strength Test

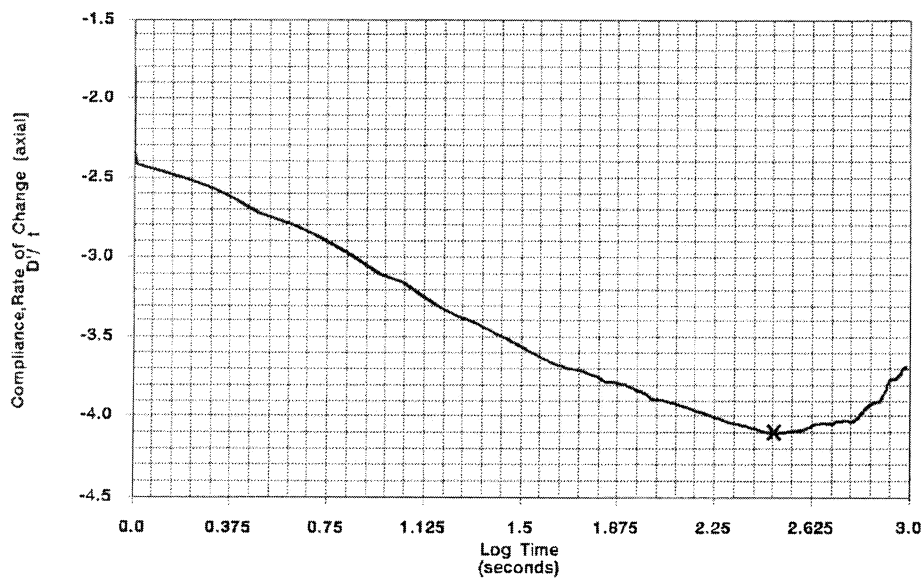


Figure 7. Plot of the rate of change in compliance versus loading time on a log-log scale for a static creep test.

thousand repetitions of a repeated load test and to record the cumulative permanent deformation as a function of the number of load cycles (i.e., repetitions). A load cycle consisting of a 0.1-s haversine pulse load and a 0.9-s dwell (i.e., rest) time is applied for the test duration—typically about 3 h or 10,000 loading cycles.

Results from repeated load tests are typically presented in terms of the cumulative permanent strain versus the number of loading cycles. Figure 8 illustrates such a relationship. Similar to the creep test, the cumulative permanent strain (ϵ_p) curve can be divided into three zones: primary, secondary, and tertiary. The cycle number at which tertiary flow starts is referred to as the “flow number.”

Figure 9 illustrates the same relationship plotted on a log–log scale. The intercept a represents the permanent strain at $N = 1$ whereas the slope b represents the rate of change of the permanent strain as a function of the change in loading cycles ($\log [N]$). These two permanent deformation parameters are derived from the linear (i.e., secondary) portion of the cumulative plastic strain–repetitions relationship. The classic power-law model, mathematically expressed by Equation 14, is typically used to analyze the test results:

$$\epsilon_p = aN^b \tag{14}$$

The regression constants a and b ignore the tertiary zone of material deformability (Figure 9) and are dependent on the material–test combination conditions. Figures 10 through 12 show plots from an actual repeated load test. Figure 11 is a plot of the total permanent strain versus loading cycles on a log–log scale. The estimation of parameters a and b are obtained from a regression analysis of the linear portion of the permanent strain versus number of cycles. Figure 12 shows a plot of the rate of change in permanent strain versus loading cycle on a log–log scale. The flow number is recorded where the minimum slope occurs.

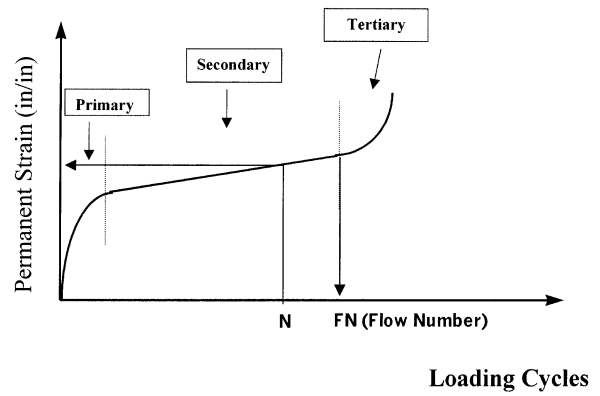


Figure 8. Typical relationship between total cumulative plastic strain and loading cycles.

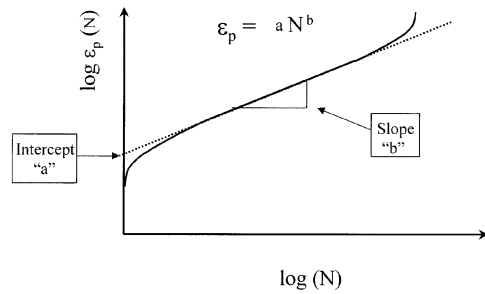


Figure 9. Regression constants a and b when plotted on a log–log scale.

Three other mixture response parameters from the triaxial repeated load test have been correlated to permanent deformation or rutting: resilient modulus (E_R), plastic strain (ϵ_p) per load cycle, and strain ratio (ϵ_p/ϵ_r). The resilient strain (ϵ_r) is the recoverable axial strain during the rest period of the load cycle. The resilient shear modulus is defined as the ratio

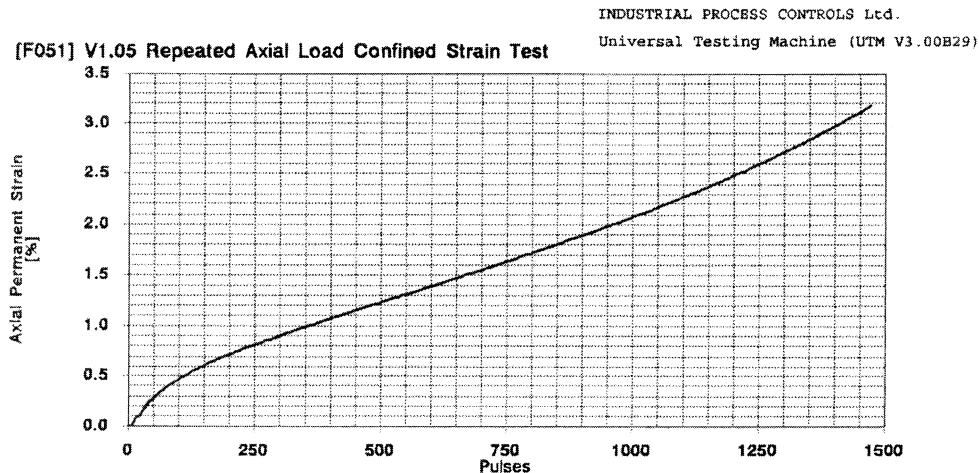


Figure 10. Cumulative permanent strain versus loading cycles from a repeated load test.

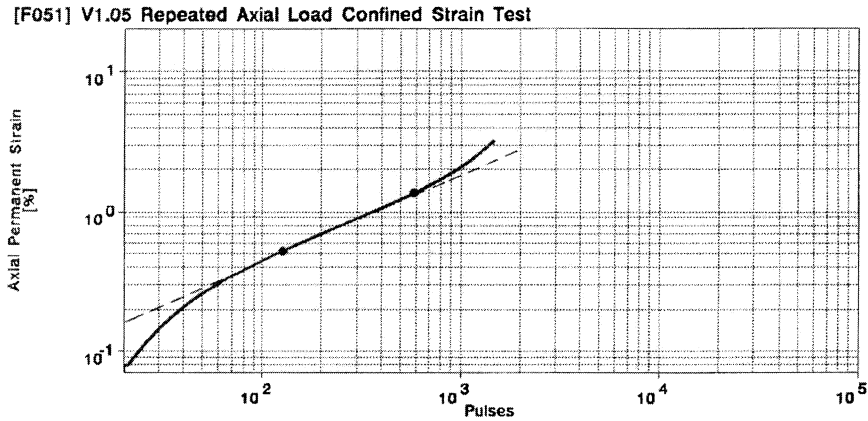


Figure 11. Regression constants *a* and *b* from log permanent strain versus log number of loading cycles plot for a repeated load test.

of the applied compressive stress to the resilient axial strain. The strain ratio is defined as the ratio of the permanent or plastic strain to the resilient strain.

2.1.9 SST Repeated Shear Permanent Deformation Tests

In development of the repeated load SSCH test using the SST, two mechanisms were hypothesized. The first is related to the asphalt binder modulus: stiffer binders help in resisting permanent deformation because the magnitude of the shear strains is reduced under each load application. The rate of accumulation of permanent deformation is strongly related to the magnitude of the shear strains. A stiffer asphalt binder, therefore, will have increased rutting resistance because it minimizes shear strains in the aggregate skeleton.

The second mechanism is the aggregate structure stability: the axial stresses act as a confining pressure and tend to stabilize the mixture. A well-compacted mixture with a strong aggregate structure will develop high axial forces at very

small shear strain levels. Poorly compacted mixtures can also generate similar levels of axial stresses, but they will require much higher shear strain. In the SSCH test, these two mechanisms are free to fully develop their relative contribution to the resistance of permanent deformation, because they are not constrained by imposed axial or confining stresses.

Figure 13 shows how the accumulated permanent deformation increases with increasing load applications. The specimen deforms quite rapidly at the beginning of the test. The amount of unrecoverable deformation per cycle decreases and remains steady for many cycles in the secondary region. At some point or number of loading cycles, the deformation begins to accelerate, leading towards failure in the tertiary portion of the curve.

Similar to the triaxial repeated load permanent deformation test, the permanent shear strain versus the number of load repetitions plotted on a log-log scale is linear. The slope and intercept are used to characterize the permanent deformation of the HMA mixture. The flow number defines the number of loading cycles at the beginning of the tertiary

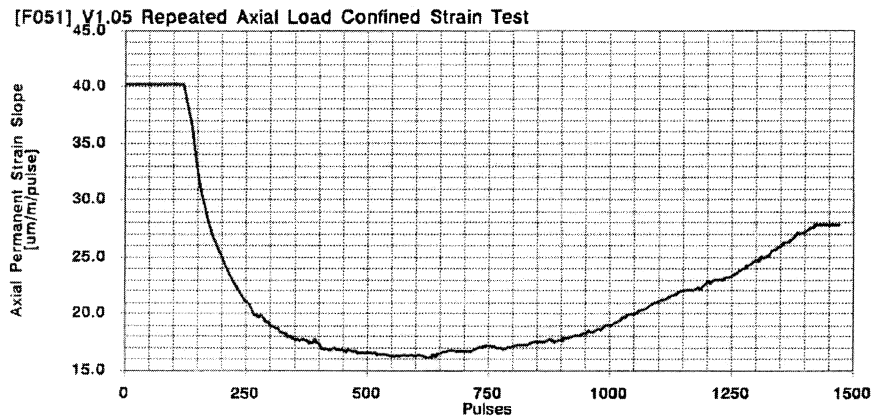


Figure 12. Typical plot of the rate of change in permanent strain versus loading cycles for a repeated load test.

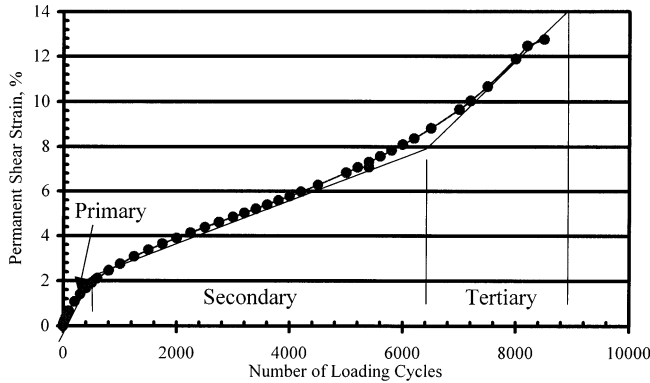


Figure 13. Permanent shear strain versus number of loading cycles using the SST.

zone. The resilient shear strain is the recoverable shear strain. The resilient shear modulus is defined as the ratio of the shear stress to the recoverable shear strain, and the strain ratio is defined as the ratio of the permanent shear strain to the resilient shear strain.

2.2 FRACTURE TESTS

2.2.1 Triaxial Dynamic Modulus Tests

The dynamic modulus test previously described in this chapter was also used in the correlation study for fatigue cracking. However, the dynamic modulus for the fatigue cracking test plan was measured at lower test temperatures than those temperatures used in the permanent deformation test plan. Details on the test temperatures and stress levels used for both correlation studies are provided in Chapter 3.

2.2.2 Indirect Tensile Tests

The indirect tensile test has been extensively used in structural design research for flexible pavements since the 1960s and, to a lesser extent, in HMA mixture design research. It is the test recommended for mixture characterization in the Long-Term Pavement Performance (LTPP) Program (10) and to support structural designs in the 1986 and 1993 AASHTO Guide for Design of Pavement Structures (10 and 11). The indirect tensile test is one of the most popular tests used for HMA mixture characterization in evaluating pavement structures. The primary reason for the test's popularity is that cores from thin lifts can be tested directly in the laboratory.

The indirect tensile test is the test specified in AASHTO T283, "Resistance of Compacted Bituminous Mixture to Moisture-Induced Damage," for evaluating an HMA mixture's susceptibility to moisture damage. Properties that have been used for evaluating moisture damage and fracture-related distresses are the resilient modulus (under repeated loadings) and the indirect tensile strength and failure strain (at

a constant rate of loading) (12). Although the reliability of the indirect tensile test to detect and predict moisture damage is questionable, no other test has been found to provide consistent results at a higher reliability. In addition, SHRP recommended use of the indirect tensile creep test method to characterize HMA mixtures for thermal-cracking predictions.

The indirect tensile method is used to develop tensile stresses along the diametral axis of the test specimen. The test is conducted by applying a compressive load to a cylindrical specimen through two diametrically opposed, arch-shaped rigid platens, as shown in Figure 14.

Based upon the theory of elasticity, the strain can be expressed in three dimensions. Ideally, the 3-D analysis can be reduced to a 2-D analysis for special element-size and loading conditions. For the case of a circular disk, the 2-D analysis can be categorized as plane stress.

2.2.3 Indirect Tensile Strength Tests

The indirect tensile strength is measured by loading the specimen at a constant strain rate until it fails by splitting along the diametral axis. The horizontal tensile stress at the center of the test specimen is calculated using Equation 15; the tensile strain is calculated using Equation 16:

$$\text{Horizontal Tensile Stress} = \sigma_{xy} = \frac{2P}{\pi td} \quad (15)$$

where

- d = the diameter of the specimen,
- P = the applied load, and
- t = the thickness of the test specimen or core; and

$$\text{Horizontal Tensile Strain} = \epsilon_{xx} = \delta_{xx} \left(\frac{2(1+3\mu)}{d(a+b\mu)\pi} \right) \quad (16)$$

where

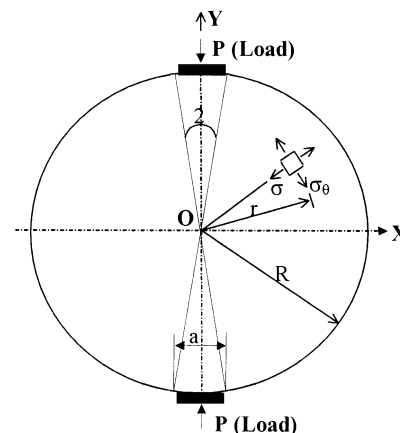


Figure 14. Schematic of the indirect tensile test.

δ_{xx} = horizontal deformation across the test specimen,
 μ = Poisson's ratio, and
 a, b, d = integration constants that are specimen geometry dependent.

The only unknowns in the equation are Poisson's ratio and the integration constants. The integration constants are dependent on the geometry of the test specimen. The determination of Poisson's ratio requires both horizontal and vertical deformation measurements made on the specimen, or it can be calculated from the regression equation developed by Witczak and Mirza, as shown below (13):

$$\mu = 0.15 + \frac{0.35}{1 + \exp(3.1849 - 0.04233 \times Temp)} \quad (17)$$

Temperature in the above equation is expressed in degrees Fahrenheit.

Parameters from the indirect tensile strength test that have been correlated to actual cracking values include indirect tensile strength (S_t), horizontal strain at failure (ϵ_{ff}), total fracture energy (Γ_{ff}), and fracture energy to failure (Γ_{fa}). These indirect tensile strength parameters are defined below.

1. The maximum horizontal tensile stress at the center of the specimen and the horizontal tensile strain are calculated from the plot shown in Figure 15. The indirect tensile strength is the maximum stress developed at the center of the specimen in the radial direction during the loading operation for a fixed geometry.
2. The fracture energy is calculated as the area under the load-vertical deformation curve as shown in Figure 16.
3. The energy until failure is calculated from the results of this test as shown in Figure 17.

2.2.4 Indirect Tensile Resilient Modulus Tests

The resilient modulus can be obtained for a known corresponding deflection value, which can be obtained from the

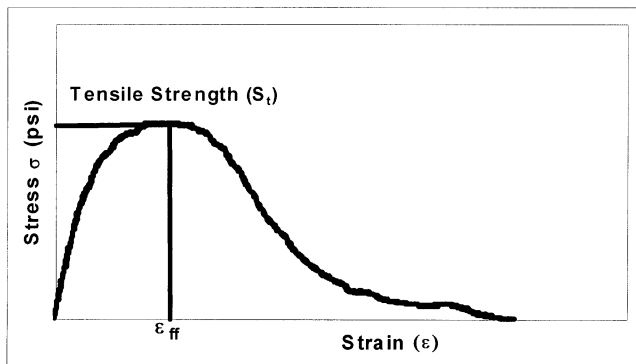


Figure 15. Illustration showing the determination of the indirect tensile strength.

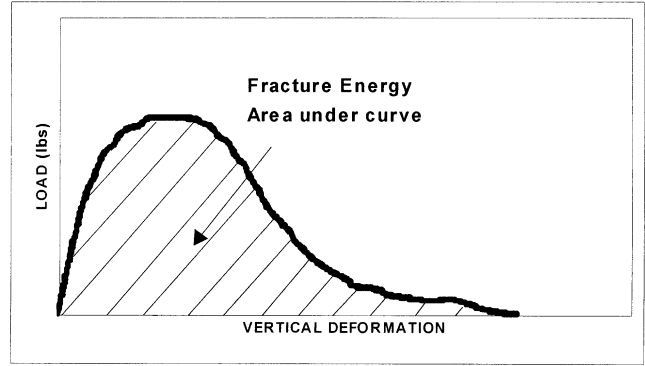


Figure 16. Determination of total fracture energy.

laboratory indirect tensile test. The resilient modulus is calculated with Equation 18:

$$Resilient\ Modulus = E_R = M_R = \frac{P}{t\delta_{xx}}(a + b\mu) \quad (18)$$

where

- E_R, M_R = resilient modulus,
- P = applied load,
- t = thickness of the test specimens,
- δ_{xx} = horizontal deformation across the test specimen,
- a, b = integration constants that are dependent on the gauge length or the length over which the deformation measurements were made, and
- μ = Poisson's ratio.

The values of the integration constants a and b depend upon the gage length or the length over which the deformation measurements were made.

2.2.5 Indirect Tensile Fatigue Tests

The fatigue life of a material is defined as the number of load cycles to specimen fracture. The horizontal deformation

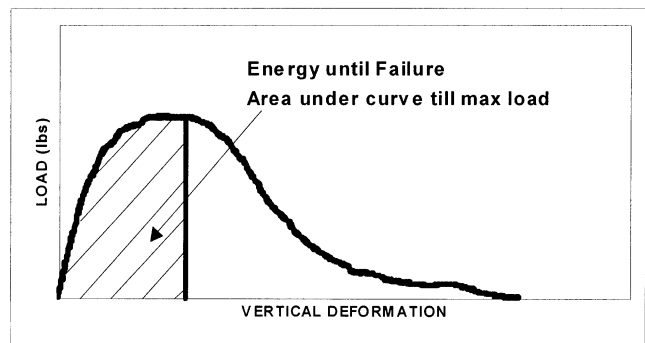


Figure 17. Determination of energy to peak load.

during the indirect tensile fatigue test is recorded as a function of load cycle, and the horizontal strains are calculated using Equation 16. Two criteria were used to define failure. The first is the number of cycles to complete failure (N_f); the second is the number of cycles at which the resilient modulus is reduced to 50 percent of its original value (N_{50}).

The loading pattern used in the indirect tensile fatigue test is a haversine load. The loading time was 0.1 s, and the rest period was 0.4 s. The amplitude of the load for a specific tensile stress was kept constant during the test, and deformations were recorded at various loading cycles.

Each specimen is subjected to a different level of stress (or strain) so that a range of values is obtained for both N_f and N_{50} repetitions. This range allows the development of the classical fatigue relationship between N_f and σ (stress) or ϵ (strain) on a log-log model form, as shown in Figure 18 and mathematically represented by Equations 19 or 20:

$$N_f = K_1 * \sigma^{k_2}, \quad (19)$$

or

$$N_f = K_1 * \epsilon^{k_2}. \quad (20)$$

2.2.6 Indirect Tensile Creep Tests

The static creep test used in the study is a single load-unload cycle. A constant static load is applied to the specimen for 1,000 s, and the horizontal deformation is recorded. The applied load is a percentage of the horizontal tensile strength of the material (Equation 15). The horizontal deformations are recorded for another 1,000 s after the load is removed to measure the recovery of the specimen. The stresses and strains are calculated using Equations 15 and 16.

Both horizontal and vertical LVDTs are used in the test to measure the deformations under the static load for calcula-

tion of Poisson's ratio. Poisson's ratio can also be calculated using Equation 18, when only horizontal deformations are measured.

2.2.6.1 Strain-Time Response Curve

The phenomenon of the static creep test is shown in Figure 19, which illustrates the typical strain-time response of an HMA mixture and shows the salient components of the load-unload cycle. The total strain (ϵ_T) can be divided into recoverable and irrecoverable components or time-dependent and time-independent components, just as it is for the triaxial compressive creep test. Equation 21 describes the four components composing the total strain:

$$\epsilon_T = \epsilon_e + \epsilon_p + \epsilon_{ve} + \epsilon_{vp} \quad (21)$$

where

ϵ_T = the total strain;

ϵ_e = the elastic strain, recoverable and time-independent;

ϵ_p = the plastic strain, irrecoverable and time-independent;

ϵ_{ve} = the viscoelastic strain, recoverable and time-dependent; and

ϵ_{vp} = the viscoplastic strain, irrecoverable and time-dependent.

The elastic and viscoelastic strain components exist during both loading and unloading conditions; the plastic and viscoplastic components exist during the loading portion.

2.2.6.2 Modulus-Compliance Components

The modulus from the creep test is calculated using Equation 15, so the compliance is defined as follows:

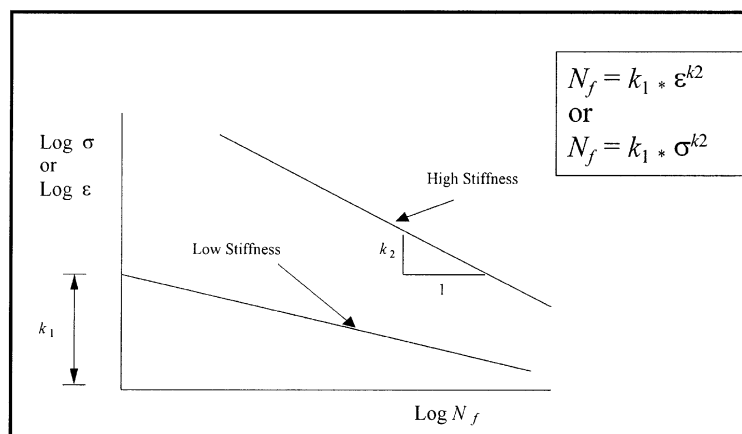


Figure 18. Stress-strain versus number of load repetitions.

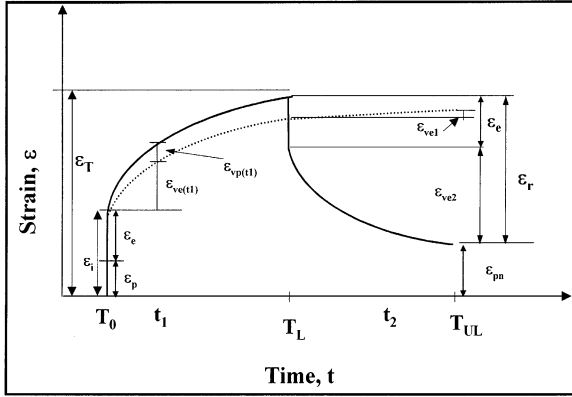


Figure 19. Typical strain-time response for HMA mixtures for a static creep test.

$$D(t)_h = E(t)^{-1} = \frac{\delta_{xx} * t}{p(a + b\mu)} \tag{22}$$

where h is the horizontal height.

The mathematical form to represent the compliance from the indirect tensile test is similar to the compliance determined from the triaxial compressive creep test and is given by Equation 23:

$$D(t) = D_1 T^{m_1} \tag{23}$$

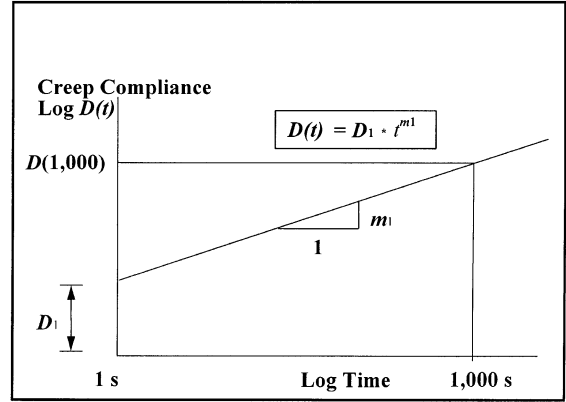


Figure 20. Illustration of creep-compliance versus time from a static creep test.

where

$D(t)$ = total compliance at any time,

t = loading time, and

D_1, m_1 = material regression coefficients.

The regression coefficients D_1 and m_1 are generally referred to as the compliance parameters and are shown in Figure 20. These parameters are general indicators of the creep behavior of the materials, similar to those parameters determined from the triaxial compressive creep test. The Paris law's fracture parameters were also calculated in accordance with the procedure recommended by Roque et al. (14).

CHAPTER 3

EXPERIMENTAL FACTORIAL AND TESTING PLAN

3.1 EXPERIMENTAL PLAN

The experimental plan was designed to investigate separately both major distresses—deformability and fracture. A practical, reliable HMA mix design method must be based on a set of compromising principles that balance the volumetric components to optimize the mix’s flexibility to prevent fracture while maintaining adequate stiffness to resist deformation. This balance was clearly recognized by the individuals responding to the utility analysis questionnaire discussed in Chapter 1.

Although both major distress manifestations were pursued in this work, it is important to recognize that rutting was rated as the most significant HMA mixture problem in current practice. Thus, the experimental plan for selecting the SPT employs the higher level of effort to quantify the deformability of HMA mixtures. Table 5 shows the three test sites and mixture distresses included in the experimental factorial. Each test site is discussed in this chapter.

3.1.1 Experimental Goal

The goal of the experimental plan was to use field projects with a diverse range of distress magnitudes to select the test methods and mixture response parameters that are most highly correlated to rutting and cracking. Table 6 shows the experimental factorial for the test methods and responses for each distress.

The HMA materials and mixtures were sampled from these projects to recompact test specimens with the SGC to the volumetric properties reported during mixture placement. The measured responses from those test methods (Table 6) were compared with the observed distress at each project. The projects identified for use in this study were those having multiple test sections that are identical with the exception of the composition of the HMA mixture. Thus, the individual goal of each field project was to allow for the relative comparison of the measured response parameters to distress within that project.

3.1.2 Tiered Factorial Approach

The testing plan was to concentrate on those “mechanistic and fundamental” response parameters that could be linked

to the advanced material characterization tests, which also are being developed as a part of NCHRP Project 9-19. This linkage is one of the major requirements of the SPT.

The initial work completed under Phase II of the FHWA contract resulted in a significant number of candidates for the SPT (Table 4). Rather than subjectively eliminating some of the candidate test methods, it was decided to actually evaluate as many of the candidate test protocols as possible in a phased laboratory study. As a consequence, the laboratory experimental factorial was divided into different projects.

A wide variety of test methods and responses were used in the laboratory effort in the first part of the experimental plan. The HMA mixture responses were compared with each distress on a project-by-project basis. Those test methods that were found to have inconsistent relationships or that resulted in poor correlations with the distress magnitude were removed from further consideration in the other projects. The test methods and response parameters found to be highly correlated with the distress observations at a project then were evaluated in the other projects.

3.1.3 Experimental Analysis Plan

For the experiment design, it was hypothesized that the test methods and responses ranked as the “best” candidates for the SPT could be used to identify HMA mixtures that are susceptible to permanent deformation and fracture over a diverse range of materials, climates, pavement structures, and support conditions. The experimental analysis plan was devised to quantify the correlation between mixture response and distress on a project-by-project basis.

Statistical analyses were conducted to evaluate all measured laboratory responses on how they compared with observed distress measurements. The analysis was completed for each distress by developing plots of the distress for each test section against the laboratory-measured test parameter. Trends and regression models were statistically evaluated based on the goodness-of-fit parameters: coefficient of determination, R^2 , standard error of estimate, Se , relative accuracy, Se/Sy , and assessment of the model rationality. Two types of regression models were used in the comparisons, a linear and nonlinear model. The nonlinear model was based on the power law.

TABLE 5 Experimental site factorial for selection of the SPT

Field Project and Individual Test Sections	Distress		
	Permanent Deformation	Fracture	
		Fatigue Cracking	Thermal Cracking
MnRoads: Cells 16, 17, 18, 20, & 22	√ (Cells 16–18, 20, & 22)		√ (Cells 16–18, 20, & 22)
ALF: Lanes 1, 2, 3, 4, 5, 7, 8, 9, 10, 11, & 12	√ (Lanes 5 & 7–12)	√ (Lanes 1–4)	
WesTrack: Sections 2, 4, 5, 6, 7, 15, 23, & 24	√ (Sections 2, 4, 7, 15, 23, & 24)	√ (Sections 2, 5, 6, & 24)	

For linear models, the coefficient of determination, R^2 , is a measure of model accuracy. The standard error of estimate, Se , reflects the likely error in our prediction. This value is good when it is small compared with the average value of the criterion variable. The model coefficients can sometimes be a limiting value, as they measure the model rationality. The coefficients should accurately indicate the effect of the test parameters on the rut depth.

It is important to recognize that in evaluating nonlinear models, the R^2 is not always a good measure of model accuracy because it depends on a linear separation of variation and is only applicable to linear models. Model accuracy can be assessed by the standard error ratio, Se/S_y , in which S_y is the standard deviation of the criterion variable. When R^2 was computed for comparison purposes, that computation was based on the Se/S_y ratio as follows:

$$R^2 = 1 - [(n - v)/(n - 1)](S_e/S_y)^2 \quad (24)$$

where

n = the sample size, and
 v = the number of regression coefficients.

3.1.4 Evaluation Criteria

In an effort to standardize the statistical results in a “subjective goodness” classification, a criterion was used to rate the statistical analysis results. The subjective classification criteria is shown in Table 7. Generally, linear trends were observed for most parameters; however, for nonlinear trends, a nonlinear power model was evaluated based on the goodness-of-fit statistics and rationality of the regression coefficients.

TABLE 6 Experimental test method factorial for selecting the SPT

Test Method		Distress	
Type of Test / Load	Equipment / Test Geometry*	Permanent Deformation	Fracture
Dynamic Modulus Tests	Uniaxial, Unconfined	√	√
	Triaxial, Confined	√	√
	SST, Constant Height	√	
	FST	√	
	Ultrasonic Wave Propagation	√	√
	Predictive Equations	√	√
Strength Tests	Triaxial Shear Strength	√	
	Unconfined Compressive Strength	√	
	Indirect Tensile Strength		√
Creep Tests	Uniaxial, Unconfined	√	
	Triaxial, Confined	√	
	Indirect Tensile		√
Repeated Load Tests	Uniaxial, Unconfined	√	
	Triaxial, Confined	√	
	SST, Constant Height	√	
	FST	√	
	Indirect Tensile		√

*Refer to Table 4 for the response parameters considered for each test method.

TABLE 7 Subjective classification of the goodness-of-fit statistical parameters

CRITERIA	R^2	Se/Sy
Excellent	> 0.90	< 0.350
Good	0.70–0.89	0.36–0.55
Fair	0.40–0.69	0.56–0.75
Poor	0.20–0.39	0.76–0.90
Very Poor	< 0.19	> 0.90

Finally, when a weighted average correlation of all test sites was obtained, the number of test sections for each project was the weight factor used in the analysis. For MnRoad, the permanent deformation weight factor was 5; for the Accelerated Loading Facility (ALF) at Turner–Fairbanks it was 7; and for WesTrack it was 4 (Sections 2 and 15 were excluded).

3.2 TEST SITES AND MIXTURES

Three projects were selected for use in the experimental plan, as shown in Table 5. These projects were selected because each one has multiple test sections that are identical with the exception of the HMA mixtures, and there is a range in distress magnitudes between the individual test sections along a project. Each project is discussed in the following sections.

3.2.1 MnRoad

Five MnRoad test sites were selected for the test factorial (Table 5): Cells 16, 17, 18, 20, and 22. Table 8 shows the target binder and air void contents, rut depth measured in inches, and cracking measured in feet for each cell. Two different binders were used: an AC-20 was used for Cells 16, 17, and 18, and a 120/150Pen asphalt was used for Cells 20 and 22.

The original mixture design for Cells 17, 18, 20, and 22 was completed in accordance with the Marshall method; Cell

16 was designed with the Superpave volumetric mix design method. Table 9 shows the target gradations for the each cell.

In-place mixture composition was measured from bulk samples taken behind the paver. The in-place air void contents were obtained from cores recovered from each cell. Complete documentation of the MnRoad test section properties are found in the references (15–25).

3.2.2 Accelerated Loading Facility—Turner Fairbanks

Seven of the test lanes constructed at the ALF at Turner–Fairbanks were used in the experimental plan. These test sections included Lanes 5, 7, 8, 9, 10, 11, and 12. The fatigue cracking sections included Lanes 1, 2, 3, and 4. Table 10 lists the target binder content, air void content, and rut depths measured in millimeters after 10,000 passes for each lane used in the permanent deformation experimental plan. Table 11 lists the target binder content, air void content, and number of passes at 100 m of cracking for each lane.

Three conventional binders and two modified binders were used, as identified in Tables 10 and 11. All mixtures were designed with the Superpave volumetric mix design method. Table 12 shows the average in-place gradations for each lane. Complete documentation of the ALF test lane properties are provided in the references (26–35).

3.2.3 WesTrack

Eight of the WesTrack test sections were included in the experimental plan. Six of the test sections (Sections 2, 4, 15, 7, 23, and 24) were included in the permanent deformation experiment, and four sections were included in the fatigue cracking experiment (Sections 2, 5, 6, and 24). Table 13 lists the target binder content, air void content and rut depths measured in millimeters after 1.5 million equivalent single axle load (MESAL) applications for each section. Table 14 lists the same information for the cracking sections and the percent fatigue cracking reported at 2.8 MESALs.

Upon completion of the lab evaluation study, it was found that Sections 2 and 15 plotted as significant outliers for

TABLE 8 Target test specimen volumetric properties, in-place mixture composition at MnRoad

Cell	Binder Type	Asphalt Content, %	Air Void Content, %	Mix Design	1998 Rut Depth (in.)	1998 Cracking (ft)
16	AC-20	5.08	8.2	Gyratory	0.175	595
17	AC-20	5.45	7.7	75 Marshall	0.205	275
18	AC-20	5.83	5.6	50 Marshall	0.195	355
20	120/150Pen	6.06	6.3	35 Marshall	0.670	215
22	120/150Pen	5.35	6.5	75 Marshall	0.280	205

TABLE 9 Target test specimen gradation, in-place gradation at MnRoad

Sieve Size, mm	Cell 16	Cell 17	Cell 18	Cell 20	Cell 22
19	100	100	100	100	100
16	98.8	99.3	98.5	99.3	98.5
12.5	93.3	93.3	92.8	93.8	94.0
9.5	84.5	85	84.5	85.0	85.0
4.75	68.3	68.8	68.8	69.3	69.5
2.36	58.8	59.3	59.0	60.1	60.4
1.18	47.6	48	47.9	48.7	48.4
0.6	32.5	33.0	33.0	33.2	32.9
0.3	19.5	19.6	19.6	19.6	19.8
0.15	6.5	6.8	6.4	7.0	7.0
0.075	4.6	4.2	4.4	4.8	4.3

TABLE 12 Average in-place gradation for the ALF test lanes, percent passing

Sieves, mm	Lanes 1, 2, 3, 4, 5, 7, 8, 9, 10	Lanes 11, 12
	19-mm mix	37.5-mm mix
	% passing	% passing
37.5	100	100
25	100	85.6
19	98.7	73.9
12.5	76.0	65.1
9.5	62.0	59.0
4.75	44.0	47.6
2.36	32.5	32.5
1.18	23.5	24.0
0.6	17.5	17.4
0.3	11.5	12.3
0.15	8.0	8.0
0.075	5.1	5.7

TABLE 10 Target test specimen volumetric properties for the ALF lanes based on the in-place mixture composition—rutting lanes

ALF Lane	Binder Type	Nominal Size, mm	Asphalt Content, %	Air Void Content, %	Rut Depth, (10,000 Passes) mm
5	AC-10	19.0	4.80	8.6	39.3
7	Styrelf	19.0	4.90	11.9	12.0
8	Novophalt	19.0	4.70	11.9	4.4
9	AC-5	19.0	4.90	7.7	48.1
10	AC-20	19.0	4.90	9.3	36.3
11	AC-5	37.5	4.05	6.0	22.3
12	AC-20	37.5	4.05	7.4	15.2

TABLE 11 Target test specimen volumetric properties for the ALF lanes based on in-place mixture composition—cracking lanes

ALF Lane	Binder Type	AC Layer Thickness mm	Nominal Size, mm	Asphalt Content, %	Air Void Content, %	ALF Passes @ 100 m of Line Cracking	
						66 °F (19 °C)	82 °F (28 °C)
1	AC-5	100	19.0	4.80	6.1	7,500	221,000
2	AC-20	100	19.0	4.90	6.5	75,000	177,000
3	AC-5	200	19.0	4.70	7.7	164,000	354,000
4	AC-20	200	19.0	4.90	9.7	544,000	528,000

TABLE 13 Target test specimen volumetric properties for WesTrack test sections based on in-place mixture composition—rutting sections

WesTrack Section	Binder Type	Nominal Size, mm	Asphalt Content, %	Air Void Content, %	Rut Depth, (1.5 MESAL*) mm
2**	PG 64-22	12.5 Fine	5.02	10.4	6
4	PG 64-22	12.5 Fine	5.24	6.6	7
15**	PG 64-22	12.5 Fine	6.28	6.9	8
7	PG 64-22	12.5 Coarse	6.28	6.9	36
23	PG 64-22	12.5 Coarse	5.78	4.9	13
24	PG 64-22	12.5 Coarse	5.91	7.2	22

*MESALS = million equivalent single axle loads.

**After lab test evaluation, it was concluded that the target volumetrics shown for Sections 2 and 15 were not the same as those found in the field test sections.

TABLE 14 Target test specimen volumetric properties for WesTrack test sections based on in-place mixture composition—cracking sections

WesTrack Section	Binder Type	Nominal Size, mm	Asphalt Content, %	Air Void Content, %	% Cracking, (2.8 MESAL)
2	PG 64-22	12.5 Fine	4.76	9.3	7
5	PG 64-22	12.5 Coarse	5.61	7.0	51
6	PG 64-22	12.5 Coarse	5.89	11.3	100
24	PG 64-22	12.5 Coarse	5.78	7.5	0

almost every SPT test parameter examined. In addition, it was also discovered that differences in the reported in situ mix volumetrics were found in other WesTrack reports compared with the final values noted in Table 13. As a consequence, the research team decided to discard these test results for these two sections and not to incorporate them in the final statistical analysis. For all practical purposes, it was concluded that all specimens compacted for these sections had mix volumetrics that differed from the in situ properties.

One conventional binder (i.e., PG 64-22) and two aggregate blends (i.e., gradations) were used. All mixtures were designed with the Superpave volumetric mix design method. Table 15 lists the average in-place gradations for each test section. Complete documentation of the WesTrack test section properties are provided in the references (36–45).

3.3 TEST SPECIMEN PREPARATION AND CONDITIONING

All test specimens were prepared according to the Test Protocol UMD 9808, “Method for Preparation of Triaxial Specimens” (46). The air voids and other volumetric properties (i.e., asphalt content and gradation) of the test specimens were matched with the in-place properties measured after

TABLE 15 Average in-place gradation for the WesTrack test sections

Sieves, mm	Sections: 2, 4, 15	Sections: 5, 6, 7, 23, 24
	<i>12.5-mm fine mix</i>	<i>12.5-mm coarse mix</i>
	<i>% passing</i>	<i>% passing</i>
25	100	100
19	100	100
12.5	87.8	80.8
9.5	75.9	65.8
4.75	49.4	42.0
2.36	38.0	28.2
1.18	33.6	20.6
0.6	27.4	15.6
0.3	15.6	11.6
0.15	7.8	8.5
0.075	4.7	6.1

placement and compaction of the HMA mixtures for each individual test section.

The mixing and compaction temperatures were determined using binder consistency test results and viscosity-temperature relationships for both binders. The mixing and compaction temperatures used to prepare the specimens are shown in Table 16. All mixtures were short-term oven-aged for 4 h at 135°C, according to the AASHTO Test Method AASHTO PP2, “Standard Practice for Short and Long Term Aging of Hot Mix Asphalt,” before compaction.

The specimens were compacted with a Servopac gyratory compactor into a 150-mm diameter gyratory mold to approximately 160 mm in height. The test specimen’s “ideal” geometry was based on the specimen size and the aggregate effects study that was completed by the Superpave models team (47). Test specimens, 100 mm in diameter, were cored from the center of the gyratory compacted specimen, and approximately 5 mm were sawed from each end of the test specimen.

The bulk specific gravities, as well air void contents, for each test specimen were measured before the specimens were tested. The air void tolerance used to accept or reject the test specimens for testing was ± 0.5 percent from the mean air void content after placement.

3.3.1 Triaxial Dynamic Modulus Specimens

The dynamic (i.e., complex) modulus-testing program included the measurement of the dynamic modulus of each mixture at four to five temperatures and six frequencies. Testing was conducted at levels of confinement ranging from 0 to 275 kPa (40 psi).

A servohydraulic test system was used to load the specimens. The dynamic modulus and phase angle were measured by applying a compressive sinusoidal (i.e., haversine) loading. The diameter of the test specimens was 100 mm (4 in.), and the height was 150 mm (6 in.). Testing was conducted in an environmental chamber capable of holding temperatures from -16 to 60°C (3.2 to 140°F).

Each specimen was tested in an order of increasing test temperature and for each temperature; specimens were tested in an order of decreasing test frequency. This temperature-frequency sequence was carried out to cause minimum damage to the specimen before the next sequential test. Two replicates were used for all mixtures.

TABLE 16 Mixing and compaction temperatures for all mixtures used in the experimental plan

Experimental Site	Binder	Mixing Temperature, °C (°F)	Compaction Temperature, °C (°F)
MnRoad	120-150 Pen	143 (290)	132 (270)
MnRoad	AC-20	152 (305)	141 (285)
ALF	AC-5	152 (305)	141 (286)
ALF	AC-10	146 (295)	136 (277)
ALF	AC-20	154 (309)	143 (289)
ALF	Novophalt	168 (334)	154 (309)
ALF	Styrelf	173 (343)	158 (316)
WesTrack	PG 64-22	152 (305)	141 (285)

The deformations were measured through two spring-loaded LVDTs. The LVDTs were placed vertically on diametrically opposite sides of the specimen. Parallel brass studs, glued 100-mm (4-in.) apart and located approximately 25 mm (1 in.) from the top and bottom of the specimen, were used to secure the LVDTs in place.

3.3.1.1 Unconfined Testing

Two different stress levels were used for unconfined testing. The stress levels for a given test temperature were selected to produce resilient strains of less than 100 microstrains. This limit on the resilient strain ensured that the response of the material would be linear. The same specimens were retested at 37.8, and 54.4°C (100 and 130°F) using stress levels that result in high dynamic strains (500 to 1000 microstrains) and nonlinear material response.

The unconfined dynamic (i.e., complex) modulus tests were conducted at five temperatures: 9, 4.4, 21.2, 37.8, and 54.4°C (15.8, 40, 70, 100, and 130°F) using frequencies of 25, 10, 5, 1, 0.5, and 0.1 Hz. Each specimen was tested in an order of increasing temperatures using dynamic stress levels of 138 to 965 kPa (20 to 140 psi) for colder temperatures (i.e., 9, 4.4, and 21.1°C). For the warmer temperatures, 37.8 and 54.4°C, stress levels of 46 to 48 kPa (7 to 10 psi) and about 21 kPa (3 psi) were used, respectively. Upon completion of this test sequence, each specimen was retested at 37.8 and 54.4°C using a stress level of 138 kPa (20 psi). This high stress level caused some damage to the specimens. The extent of the damage depended on the mixture's unconfined compressive strength.

3.3.1.2 Confined Testing

The confined testing was conducted using the same temperatures and frequencies as were used for the unconfined tests. The stress levels were determined based upon the stress-

to-strength ratio determined using the cohesion and friction parameters (c , ϕ) from the triaxial strength test for the warmer test temperatures of 70, 100, and 130°F (21.1, 37.8, and 54.4°C). For the colder test temperatures, the deviatoric stress was changed to produce at least a 20-microstrain response. Table 17 summarizes the stress levels used for the testing at all temperatures.

3.3.2 SST Specimens

Values of the complex shear modulus and phase angle were collected for various combinations of strain level, temperature, and frequency of loading. More temperature and frequency combinations than are required by AASHTO TP7 were added to facilitate construction of master curves. The tests were performed at additional strain levels to evaluate the nonlinear response.

The initial experimental plan for the dynamic shear modulus test included testing at five temperatures (0, 40, 70, 100, and 130°F) and five frequencies (0.01, 0.1, 1, 10, and 25 Hz). This combination was selected to provide sufficient data for construction of sigmoid-shaped master curves by shifting the data from different temperatures to 70°F using numerical optimization techniques. However, the 0°F-testing temperature was dropped because temperatures significantly below 40°F could not be maintained on a consistent basis based on the initial testing with the Interlaken SST.

During the MnRoad testing, the 25-Hz data were found to be unreliable; therefore, these data were eliminated from the ALF section testing. The other frequencies included in AASHTO TP7 were included. Finally, the tests were conducted at the normal AASHTO TP7 strain level of 100 microstrains, about 1.5 and 2.0 times the normal strain level.

Table 18 summarizes the final data collection plan. Tests at each strain level were conducted on replicate 50-mm-thick specimens sawed from the top and bottom of a single gyratory specimen. Air void contents were measured after sawing the final test specimens. For each of the ALF test sections, the overall testing program required testing six test specimens

TABLE 17 Stress levels, temperatures and frequencies used in dynamic modulus testing

Stress State	Temperature		MnRoad Dynamic Stress Level	ALF and WesTrack Dynamic Stress Level
	$^{\circ}F$	$^{\circ}C$	<i>Psi (kPa)</i>	<i>psi (kPa)</i>
Unconfined low stress	15.8	-9	18 (124)	80-140 (552-965)
Unconfined low stress	40	4.4	18 (124)	60-80 (414-552)
Unconfined low stress	70	21.1	18 (124)	20-40 (138-275)
Unconfined low stress	100	37.8	7 (48)	7-10 (46-68)
Unconfined low stress	130	54.4	3 (21)	3 (21)
Unconfined high stress	100, 130	37.8, 54.4	18 (124)	20 (138)
Confined—20 psi	15.8	-9	20 (138)	80-140 (552-965)
Confined—20 psi	40	4.4	20 (138)	60-140 (414-965)
Confined—20 psi	70	21.1	20 (138)	60-40 (138-275)
Confined—20 psi	100, 130	37.8, 54.4	20 (138)	20 (138)
Confined—20 psi	15.8	-9	30 (206)	80-140 (552-965)
Confined—20 psi	40	4.4	30 (206)	60-140 (414-965)
Confined—20 psi	70	21.1	30 (206)	80-100 (552-689)
Confined—20 psi	100, 130	37.8, 54.4	30 (206)	80-100 (552-689)

obtained from three gyratory specimens. For each strain level, 40 combinations of G^* and δ were collected for analysis and for the construction of the master curves. A thermocouple mounted at the middle of a dummy specimen that was the same size as the test specimen was used to monitor the test temperature. The test temperature tolerance was $\pm 1.0^{\circ}F$.

3.3.3 FST Specimens

The FST shear frequency sweep tests were conducted using 150-mm diameter gyratory compacted specimens. The specimens were sawed to a height of 2.76 ± 0.1 in. (70.0 ± 2.5 mm). The specimens were tested at $100^{\circ}F$ ($37.87^{\circ}C$) and $130^{\circ}F$ ($54.4^{\circ}C$), and each specimen was tested three times.

The first test was conducted using test frequencies of 10, 5, 2, and 1 Hz (i.e., the first decade); the second test at test frequencies of 1, 0.5, 0.2, and 0.1 Hz (i.e., the second decade); and the third test was at test frequencies of 0.1, 0.05, 0.02, and 0.01 Hz (i.e., the third decade). For the test temperature of $100^{\circ}F$ ($37.7^{\circ}C$), three magnitudes of shear stresses

were used: 2.90, 5.80, and 8.70 psi (20, 40, and 60 kPa). The stress levels resulted in shear strains of approximately 50 to 150 microstrains, 150 to 300 microstrains, and 300 to 500 microstrains at a frequency of 10 Hz. For tests conducted at $130^{\circ}F$ ($54.4^{\circ}C$), the shear stress levels used were 1.45, 2.90, and 4.35 psi (10, 20, and 30 kPa).

3.3.4 Ultrasonic Wave Propagation Specimens

The basic procedure used in the experimental plan follows ASTM C597, "Standard of Test Method for Pulse Velocity Through Concrete." A cylindrical 6×6 -in. (150×150 -mm) specimen was used for the ultrasonic testing. Both ends of each specimen were sawn to obtain a smooth surface for the transducers. A block of Styrofoam $4.7 \times 7.9 \times 4$ -in. ($130 \times 200 \times 100$ -mm) was used as a base medium for all testing. The samples were placed in a temperature chamber 3 to 4 h before testing and then individually transferred to room temperature for testing. Testing time was kept under 1 min to minimize the temperature loss during testing.

TABLE 18 Summary of the final testing program for each mixture

Strain Levels, (microstrain)	Temperature, ($^{\circ}F$)	Frequency, (Hz)	Replicates
100, 150, 200	40, 70, 100, 130	10, 5, 2, 1, 0.5, 0.2, 0.1, 0.05, 0.02, 0.01	2

The sample dimensions were measured to obtain the needed path length for the ultrasonic measurements. High vacuum grease was applied to the transducer faces and to the test surface of specimens to avoid entrapped air between the contact surfaces. Three separate pulse time measurements were taken from one location and then averaged. The transit time displayed on the display unit in microseconds was recorded. The density (D) of specimens was determined using the surface saturated (SSD) test method (AASHTO-T166, "Standard Test Method for Bulk Specific Gravity of Compacted Asphalt Mixtures Using Saturated Surface-Dry Specimens").

The pulse velocity (V) was calculated dividing the measured path length by the measured pulse time:

$$V = \frac{L}{T} \quad (25)$$

where

V = pulse velocity, ft/s (m/s);

L = distance between transducers, ft (m); and

T = effective transit time, s (measured time minus zero correction, and corrected for calibration errors).

The elastic modulus (E) was calculated using Equation 26:

$$E = (K) DV^2 \quad (26)$$

where

K = a constant, $K = 1$, used for all initial calculations and data analysis;

E = the modulus of elasticity, psi (kPa);

D = density, γ/g , where g -force = 32.19 ft/s^2 ($\rho = \text{kg/m}^3$);

V = pulse velocity, ft/s (m/s).

Because the value of Poisson's ratio was not known for the tested material, a constant, $K = 1$, was used for all elastic modulus calculations. In the analysis of the test results, an attempt was made to estimate the value of Poisson's ratio to correct the measured elastic modulus values.

3.3.5 Triaxial Shear Strength Specimens

Four triaxial strength tests, one unconfined and three confined, were conducted for each mixture in the three experimental sites to evaluate the cohesion (c) and the angle of internal friction (ϕ). The test was carried out on cylindrical samples 100 mm (4 in.) in diameter and 150 mm (6 in.) in height. Test temperatures were similar to the other tests described. MnRoad mixtures were tested at 37.8 and 54.4°C (100 and 130°F); ALF and WesTrack mixtures were only tested at 54.4°C (130°F). In addition to the unconfined test, three additional confining pressures were used: 138, 276, and 414 kPa (20, 40, and 60 psi). The samples were loaded axi-

ally to failure, at the selected constant confining pressure at a strain rate of 0.05 in./in./min (1.27 mm/mm/min).

An IPC universal testing machine (UTM 100) electro-hydraulic system was used to load the specimens. The machine is equipped to apply up to 100 psi (690 kPa) confining pressure and 22,000 lbs (100 KN) maximum vertical load. The load was measured through the load cell; the deformations were measured through the actuator LVDT. Thin and fully lubricated membranes at the sample ends were used to reduce end friction. All tests were conducted within an environmentally controlled chamber throughout the testing sequence, controlled within $\pm 1^\circ\text{F}$ throughout the entire test.

3.3.6 Static Creep and Repeated Load Specimens

Static creep and repeated load tests, confined and unconfined, were conducted using at least two replicate test specimens for each of the mixtures to evaluate the compliance properties and the flow time and flow number. Three replicates were used for the coarser mixtures. The test was carried out on cylindrical specimens, 100 mm (4 in.) in diameter and 150 mm (6 in.) in height.

An IPC universal testing machine (UTM 25-14P) electro-pneumatic system was used to load the specimens. The machine is equipped to apply up to 90 psi (620 kPa) confining pressure and 5,500 lb (24.9 KN) maximum vertical load. The load was measured through the load cell; the deformations were measured through six spring-loaded LVDTs. Two axial LVDTs were mounted vertically on diametrically opposite specimen sides. Parallel studs—mounted on the test specimen, placed 100-mm (4-in.) apart, and located at the center of the specimen—were used to secure the LVDTs in place. The studs were glued using a commercial 5-min epoxy.

An alignment rod with a frictionless bushing was used to keep the studs aligned at extreme failure conditions. For radial deformations, four externally mounted LVDTs aligned on diametrical and perpendicular lines were located at the center of the specimen and along opposite specimen sides. Thin and fully lubricated membranes at the test specimen ends were used to warrant frictionless surface conditions. All tests were conducted within an environmentally controlled chamber throughout the testing sequence (i.e., the temperature was held constant within the chamber to $\pm 1^\circ\text{F}$ throughout the entire test). Figure 21 shows typical unconfined test setup for either a static creep or the repeated load unconfined test. Figures 22 and 23 show the same for a confined test setup.

3.3.6.1 MnRoad Tests

MnRoad tests were performed at two temperatures, 37.8°C (100°F) and 54.4°C (130°F). Unconfined tests were conducted at one deviatoric stress level of 207 kPa (30 psi)



Figure 21. Vertical and radial LVDTs setup for an unconfined test.

for the 37.8°C (100°F) and two deviatoric stress levels of 69 and 207 kPa (10 and 30 psi) for the 54.4°C (130°F). For the static creep tests, a static constant load was applied with a variable time of load until tertiary flow occurred. For the repeated load tests, a haversine pulse load of 0.1 s and a 0.9-s dwell (i.e., rest time) was applied for a total of 10,000 cycles. This number was less if the test specimen failed under tertiary flow before reaching this target level.

3.3.6.2 ALF Tests

ALF tests were performed at a temperature of 54.4°C (130°F), which was similar to the field test temperature of 58°C (136°F). Unconfined tests were conducted at two deviatoric stress levels of 69 and 138 kPa (10 and 20 psi), and confined tests were conducted at 138 kPa (20 psi) confining pressure and 828 kPa (120 psi) deviatoric stress level. WesTrack tests were performed at a temperature of 54.4°C (130°F). Unconfined tests were conducted at a stress level of 69 kPa (10 psi), and confined tests were conducted at 138 kPa (20 psi) confining pressure and 828 kPa (120 psi) deviatoric stress level.

3.3.7 Repeated Shear Permanent Deformation Specimens

The repeated shear test at constant height is a stress-controlled test. A repetitive shear haversine load is applied to the specimen, and the shear deformation is measured. Testing is done according to AASHTO TP7. However, some modifications were necessary for this study to harmonize the test method with the triaxial repeated load permanent deformation test.

AASHTO TP7 requires the shear load be applied with a maximum shear stress of 69 kPa (10 psi) for a loading time of 0.1 s and a rest period of 0.6 s. The number of repetitions applied is a total of 5,000 or until 5-percent shear strain is reached. An axial stress is applied to maintain constant



Figure 22. Confined test setup.

height. The test is conducted at the maximum 7-day pavement temperature.

In this test program, test temperatures of 37.8 and 54.4°C (100 and 130°F) were used, and three shear stresses were used for each of the test temperatures. At 100°F, the shear stresses were 69, 138, and 207 kPa (10, 20, and 30 psi). At 130°F, the shear stresses were 35, 69, and 104 kPa (5, 10, and 15 psi). The dwell period between load pulses was 0.9 s and the number of load pulses was 10,000 or until the test specimen failed.

Two test specimens—150 mm (6 in.) in diameter and approximately 130 to 140 mm (5.1 to 5.5 inches) in height—were cut from each gyratory specimen, as illustrated in Figure 24. The test specimens met the AASHTO TP7 height requirements of 50 ± 2.5 mm. The test specimens were glued to the aluminum platens for mounting in the SST (Figure 25). The specimens were instrumented in the SST to measure both shear and vertical deformations. Figure 26 shows a test specimen with LVDT instrumentation mounted on the side. Two L-shaped brackets are attached to the side of the specimen.

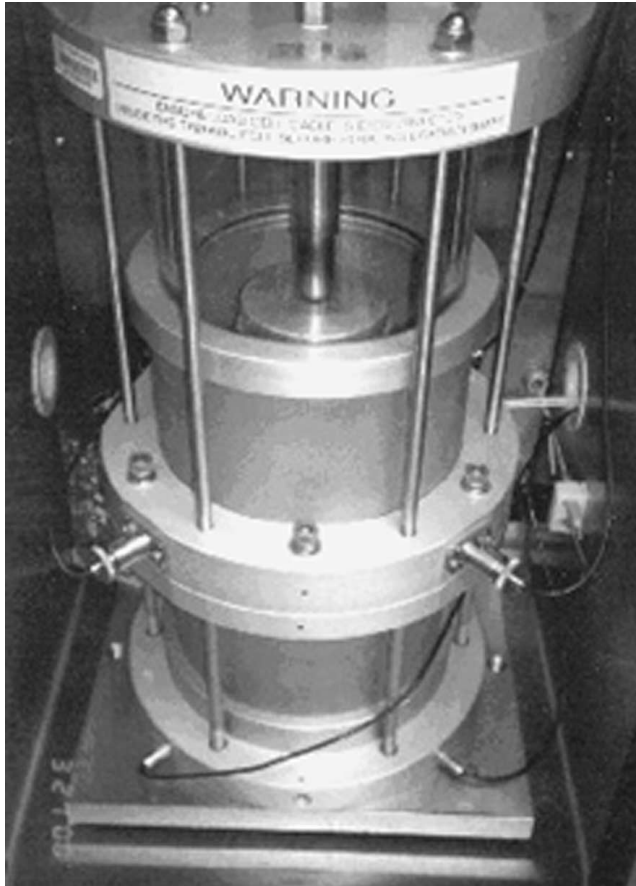


Figure 23. Test setup within triaxial cell with mounted radial LVDTs.

3.3.8 Indirect Tensile Specimens

All three indirect tensile cracking tests were carried out according to the procedure described in the “Superpave Models Team Inter-Laboratory Testing Manual” (46). All test specimens were sawed from gyratory fabricated specimens. The test specimen had a dimension of 38 mm (1.5-in.) in thickness by 150 mm (6 in.) in diameter. Two replicates were tested for each test. Vertical or horizontal LVDTs were used on the specimen for measuring the horizontal and vertical deformation using a gage length of 76.2 mm (3 in.) for both. The tests were carried out at one temperature—12.8°C (55°F) for MnRoad and Wes Track and 21.1°C (70°F) for ALF.

3.3.8.1 Indirect Tensile Strength Test

The load was applied using a constant rate of deformation of 50.8 mm/min (2 in./min). The strength test was stopped when the applied load went to zero (i.e., total failure of the specimen occurred).

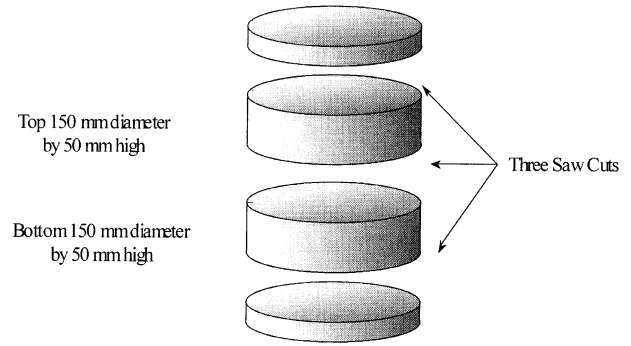


Figure 24. Manufacture of shear test specimens from gyratory specimen.



Figure 25. Test specimen prepared for testing with aluminum platens glued to top and bottom.

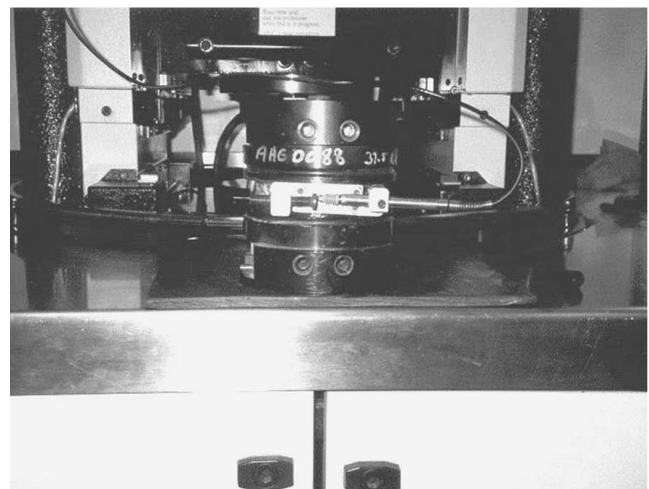


Figure 26. Specimen ready for testing showing horizontal LVDT setup.

3.3.8.2 Indirect Tensile Creep Test

The static creep test used in the study was one cycle load-unload. Two stress levels were used: a high stress level that equaled 10 percent of the indirect tensile strength of the material and a low stress level that corresponded to 2 percent of the indirect tensile strength of the material. A 1,000-s static loading time was used for the test followed by another 1,000 s for unloading. The indirect tensile creep test was used to provide the vertical and horizontal deformations as a function of time. These deformations were then used to estimate the creep compliance parameters, as presented in Chapter 2.

3.3.8.3 Indirect Tensile Fatigue Test

Eight to twelve replicates were tested for each of the experimental sites sections considered in the study. The loading pattern followed in the fatigue test was a haversine load

with a rest period. The loading period selected was 0.1 s. The rest duration selected was 0.4 s. The stress amplitude was kept constant and corresponding deformations were recorded at different times. The load was applied until the sample fractured along the vertical diameter.

In the indirect fatigue test, horizontal deformations (i.e., strains) are recorded as a function of load repetitions. This method of recording allows the resilient modulus to be estimated as a function of a specific load cycle. Each specimen is subjected to a different level of stress (or strain) so that the N_f or N_{50} will result in a range of values for fracture life. This will allow for the development of the classic fatigue relationship between N_f and σ (stress) or ϵ (strain) on a log-log model form. Different stress levels were used for each sample in order to obtain fatigue life between 100 to 100,000 load cycles. These fracture relations then can be evaluated to see whether a relationship exists between these parameters and the fatigue cracking measured from the road tests.

CHAPTER 4

ANALYSES AND COMPARISONS OF MIXTURE RESPONSE TO PERMANENT DEFORMATION

The analysis of the permanent deformation experiment followed the general methodology discussed in Chapter 3. Statistical analysis using regression techniques was used to determine the level of correlation between the measured laboratory mixture response and rut depth. Graphical comparisons were also prepared to judge the reasonableness of the trends in the data. This chapter summarizes the test results, graphical comparisons, and statistical analyses of the measured response parameters and rut depths measured in each project.

4.1 MODULUS PARAMETERS VERSUS RUTTING

4.1.1 Triaxial Dynamic Modulus

All dynamic modulus test data are presented in the individual test–experimental site reports developed by the project team (25, 26, 35, 36, 45, and 46). Dynamic moduli measured at 100 and 130°F at 5 Hz were selected for the correlation analysis. The mixture response parameters included in the statistical analysis and graphical comparisons to rutting were $|E^*|$ and a calculated parameter $|E^*|/\sin\phi$.

Linear and nonlinear regression were used to fit a linear and power model form through the data. The analysis was performed for all test data measured at different stress levels, which included (1) unconfined low stress levels in the linear region; (2) unconfined high stress levels in the nonlinear region; and (3) two levels of confinement (138 and 206 kPa [20 and 30 psi]) with a high deviatoric stress level in the nonlinear region.

Table 19 presents the correlation between $|E^*|$ and $|E^*|/\sin\phi$ and the rut depths measured at all three experimental sites. Typical plots and analyses of the test results using the power model for the unconfined test are shown in Figures 27 through 32. Plots of the confined tests and all analyses using the linear regression model are provided in the individual test–experimental site project reports.

Table 20 presents a summary of the weighted average correlation between dynamic modulus and rutting for all experimental projects. The statistical results show that the unconfined tests in the linear range had the best correlation to rutting. This was the case for both $|E^*|$ and $|E^*|/\sin\phi$. The correlation between rutting and dynamic modulus for the

unconfined tests in the nonlinear range was slightly less. The statistical measures for confined testing were very poor to fair. Overall, the stiffness parameter $|E^*|/\sin\phi$ had the best statistical correlation with rutting.

4.1.2 Ultrasonic Wave Propagation Elastic Modulus

All ultrasonic wave propagation test data are presented in the individual test–experimental site reports (24, 34, and 44). The parameter obtained from the ultrasonic testing is the elastic modulus, E_d . The measured modulus was corrected using Poisson’s ratio because of the lateral confinement effects. Without the correction, the elastic modulus was much larger than the dynamic modulus, $|E^*|$. Table 21 shows two other moduli, E_{CORA} and E_{CORB} . These moduli were corrected using Methods A and B as is described in the individual site reports.

Table 21 presents the correlation between rut depths and the three wave-propagation parameters for all three experimental projects. Table 22 presents the weighted average of the correlation between elastic modulus and rutting for all experimental sites. As shown, the correlation between the ultrasonic test parameters and rutting was only poor to fair.

4.1.3 SST and FST Dynamic Shear Modulus

All dynamic shear modulus test data are presented in the individual test–experimental site reports developed by the team (19, 20, 30, and 40). Similar to the dynamic modulus testing, two stiffness parameters were compared with rutting: $|G^*|$ and $|G^*|/\sin\phi$. Both the SST and FST were used to measure the dynamic shear modulus of the HMA mixtures for the MnRoad test sections. As is summarized in Table 23, the correlation between the rut depths measured on the MnRoad sections and the stiffness parameters measured with the FST were very poor. As a result, the FST was dropped from further evaluation and from use on the other experimental sites.

The SST was used to measure the two stiffness parameters at three strain amplitudes: 100, 150, and 200 microstrains. Table 24 shows the correlation of $|G^*|$ and $|G^*|/\sin\phi$ measured at all strain amplitudes to rutting for all three experi-

TABLE 19 Summary of the goodness-of-fit statistics, rationality and ratings of the models investigated for the dynamic modulus testing

TEST PARAMETER	STRESS LEVEL	SITES	STATISTICAL MEASURE									
			TEST TEMP 100°F					TEST TEMP 130°F				
			Se	R2	Se/Sy	Rational	Rating	Se	R2	Se/Sy	Rational	Rating
E*	UnC-Lin	WST	0.302	0.753	0.609	Yes	Fair	0.357	0.656	0.719	Yes	Fair
		ALF	0.404	0.660	0.637	Yes	Fair	0.292	0.820	0.460	Yes	Good
		MnR	0.063	0.930	0.305	Yes	Excellent	0.092	0.853	0.443	Yes	Good
E*	UnC-NonL	WST	0.368	0.633	0.742	Yes	Fair	0.470	0.402	0.947	Yes	Very Poor
		ALF	0.331	0.770	0.521	Yes	Good	0.341	0.760	0.537	Yes	Good
		MnR	0.086	0.876	0.407	Yes	Good	0.090	0.861	0.431	Yes	Good
	Con-20-NonL	WST	0.510	0.296	1.028	Yes	Very Poor	0.595	0.041	1.199	Yes	Very Poor
		ALF	0.407	0.660	0.641	Yes	Fair	0.408	0.660	0.643	Yes	Fair
	Con-30-NonL	WST	0.224	0.865	0.450	Yes	Good	0.290	0.772	0.585	Yes	Fair
ALF		0.633	0.170	0.996	Yes	Very Poor	0.528	0.430	0.831	Yes	Poor	
E*/sinφ	UnC-Lin	WST	0.196	0.896	0.394	Yes	Good	0.041	0.996	0.082	Yes	Excellent
		ALF	0.311	0.800	0.489	Yes	Good	0.222	0.900	0.350	Yes	Good
		MnR	0.066	0.925	0.316	Yes	Excellent	0.087	0.868	0.420	Yes	Good
E*/sinφ	UnC-NonL	WST	0.307	0.896	0.353	Yes	Good	0.212	0.879	0.426	Yes	Good
		ALF	0.224	0.900	0.353	Yes	Good	0.250	0.870	0.394	Yes	Good
		MnR	0.086	0.872	0.413	Yes	Good	0.047	0.962	0.225	Yes	Excellent
	Con-20-NonL	WST	0.541	0.209	1.089	Yes	Very Poor	0.607	0.348	0.885	Yes	Poor
		ALF	0.334	0.770	0.526	Yes	Good	0.562	0.350	0.890	Yes	Poor
	Con-30-NonL	WST	0.608	0.000	1.225	Yes	Very Poor	0.539	0.215	1.085	Yes	Very Poor
ALF		0.581	0.300	0.914	Yes	Very Poor	0.681	0.040	1.071	Yes	Very Poor	

mental sites. Table 25 shows the summary of the weighted averages for these data. Figures 33 through 35 show the plots of shear modulus versus rutting for the stiffness parameter $|G^*|$. The $|G^*|$ measured at 100 microstrains had the best correlation to rutting for the SST. Plots for the other response parameters are included in the individual test–experimental site reports.

4.1.4 Predictive Equations for Dynamic Modulus

The two predictive models (Witczak et al. and Bonnaure et al. [5 and 6]) were used to calculate the dynamic modulus from volumetric properties of the HMA mixture and material properties of its components. All test section data and

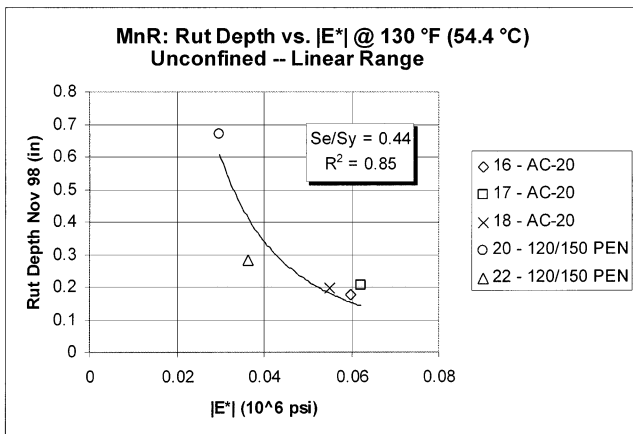


Figure 27. Linear $|E^*|$ versus rutting for the MnRoad test sections.

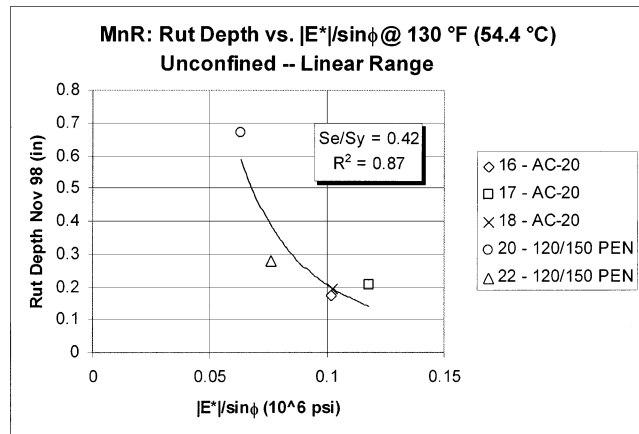


Figure 28. Linear $|E^*|/\sin\phi$ versus rutting for the MnRoad test sections.

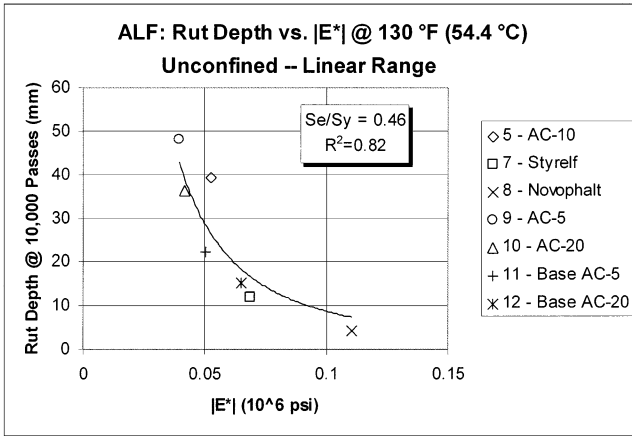
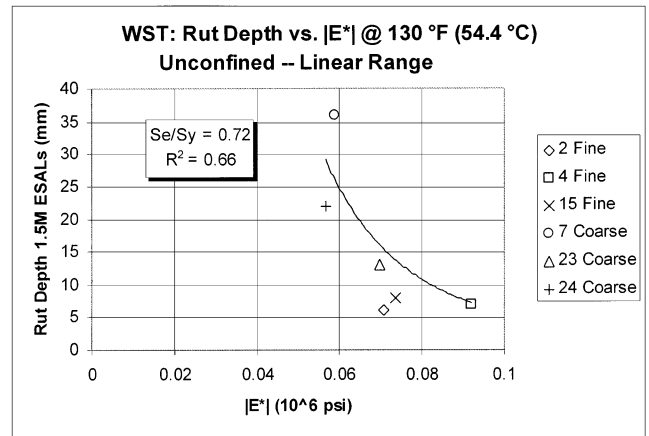


Figure 29. Linear $|E^*|$ versus rutting for the ALF test sections.



NOTE: Sections 2 and 15 were treated as outliers and were not included in statistical analysis.

Figure 31. Linear $|E^*|$ versus rutting for the WesTrack test sections.

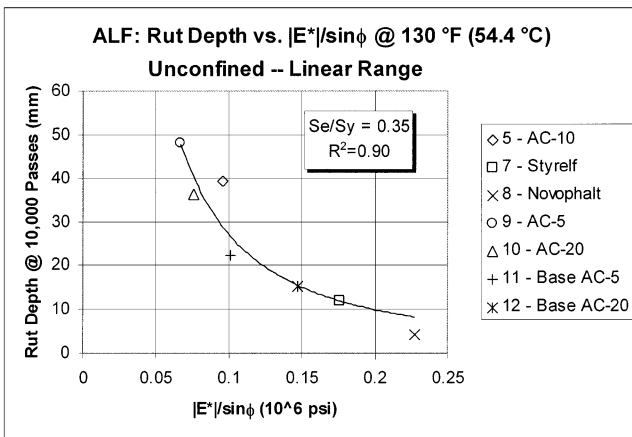
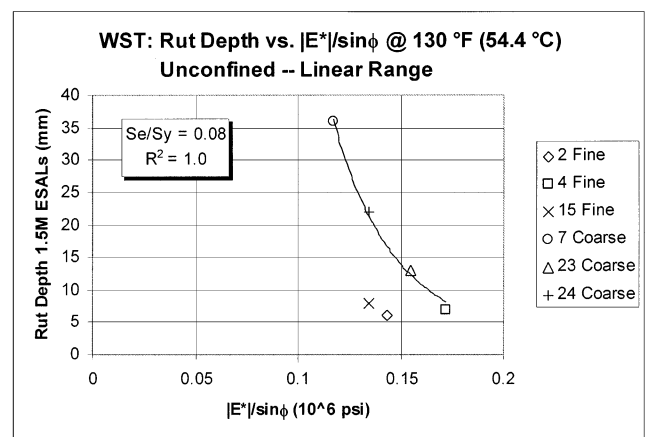


Figure 30. Linear $|E^*|/\sin\phi$ versus rutting for the ALF test sections.



NOTE: Sections 2 and 15 were treated as outliers and were not included in statistical analysis.

Figure 32. Linear $|E^*|/\sin\phi$ versus rutting for the WesTrack test sections.

TABLE 20 Summary of the goodness-of-fit statistics, rationality and ratings for the dynamic modulus tests, weighted by all experimental sites

Dynamic Modulus SPT 2J-K (5 Hz)	STRESS/ STRAIN LEVEL	100 °F				130 °F			
		R ²	Se/Sy	Rational	Rating	R ²	Se/Sy	Rational	Rating
E*	UnC-Linear	0.768	0.526	Yes	Good	0.789	0.519	Yes	Good
E*	UnC-NonL	0.769	0.541	Yes	Good	0.702	0.606	Yes	Fair
E*	C-20psi-NonL	0.528	0.782	Yes	Poor	0.435	0.845	Yes	Poor
E*	C-30psi-NonL	0.423	0.797	Yes	Poor	0.554	0.742	Yes	Fair
E*/sinφ	UnC-Linear	0.863	0.411	Yes	Good	0.914	0.305	Yes	Excellent
E*/sinφ	UnC-NonL	0.890	0.372	Yes	Good	0.901	0.349	Yes	Excellent
E*/sinφ	C-20psi-NonL	0.566	0.731	Yes	Fair	0.349	0.888	Yes	Poor
E*/sinφ	C-30psi-NonL	0.191	1.027	Yes	Very Poor	0.104	1.076	Yes	Very Poor

TABLE 21 Summary of the goodness-of-fit statistics, rationality and ratings of the models investigated for the ultrasonic wave propagation test parameters

TEST PARAMETER	STRESS LEVEL	SITES	STATISTICAL MEASURE									
			TEST TEMP 100°F					TEST TEMP 130°F				
			Se	R2	Se/Sy	Rational	Rating	Se	R2	Se/Sy	Rational	Rating
E_{CORA}	Linear	WST	0.3215	0.72	0.648	Yes	Fair	0.32	0.709	0.66	Yes	Fair
		ALF	0.4291	0.62	0.676	Yes	Fair	0.4504	0.581	0.709	Yes	Fair
		MnR	0.074	0.905	0.357	Yes	Good	0.222	0.144	1.068	Yes	Very Poor
E_{CORB}		WST	0.3286	0.708	0.662	Yes	Fair	0.3525	0.664	0.71	Yes	Fair
		ALF	0.4284	0.621	0.675	Yes	Fair	0.4511	0.58	0.71	Yes	Fair
		MnR	0.1	0.826	0.482	Yes	Good	0.171	0.491	0.823	Yes	Poor
E_d		WST	0.4859	0.361	0.979	Yes	Very Poor	0.4491	0.454	0.905	Yes	Very Poor
		ALF	0.3126	0.798	0.492	Yes	Good	0.2076	0.911	0.327	Yes	Excellent
		MnR	0.159	0.56	0.76	Yes	Poor	0.162	0.54	0.78	Yes	Poor

TABLE 22 Summary of the goodness-of-fit statistics, rationality and ratings for the ultrasonic wave propagation test, weighted for all experimental sites

E_d Wave Propag. SPT 2J-K	STRESS/ STRAIN LEVEL	100 °F				130 °F			
		R ²	Se/Sy	Rational	Rating	R ²	Se/Sy	Rational	Rating
E_{CORA}	Linear	0.750	0.554	Yes	Good	0.462	0.823	Yes	Poor
E_{CORB}	Linear	0.719	0.602	Yes	Fair	0.572	0.750	Yes	Fair
E_d (54 kHz)	Linear	0.588	0.727	Yes	Fair	0.648	0.654	Yes	Fair

mixture properties required by these two predictive equations are provided for each experimental project in the individual test–experimental site reports developed by the project team (25, 35, and 45). A total of 9 test sections were used for the comparison studies from the MnRoad project, 7 sections from the ALF project, and 26 sections from the Wes-Track project.

The stiffness parameter predicted was $|E^*|$ from the Witczak et al. predictive equation (5) and Sm from the Bonnaure et al. equation (6). In addition, the phase-angle models proposed for use by Azari et al. (48) and Bonnaure et al. were used to predict the phase angle of each mixture. Using the computed phase angle, the stiffness parameters of $|E^*|/\sin\phi$ and $Sm/\sin\phi$ were also predicted by both equations. The stiffness parameters were computed at 37.8 and 54.4°C (100 and 130°F).

Table 26 summarizes the correlation between the measured rut depths and the predicted mixture stiffness parameters for

all test sections at the three experimental sites. Table 27 summarizes the same information, but only for the test sections used in the experimental laboratory test plan. As shown, the correlation between rut depth and calculated dynamic modulus increased when only those test sections included in the experimental laboratory test plan were used in the analysis. However, the correlation between the predicted $|E^*|$ and rutting was less than that for the measured $|E^*|$ in either case. One possible reason for this observation is that the Witczak et al. equation (5) was not developed from a data set containing numerous mixtures with very high air voids.

Overall, the Bonnaure et al. equation (6) had slightly better correlation to the measured rut depths than did the Witczak et al. equation (5). However, the magnitude of the predicted modulus values in the Bonnaure et al. model are substantially lower than those obtained from the Witczak et al. model. An excellent correlation exists, however, between the Witczak et al. model and the measured E^* lab values. In con-

TABLE 23 Summary of the goodness-of-fit statistics, rationality and ratings of the models investigated for the FST shear modulus tests

TEST PARAMETER FST	SITE	STATISTICAL MEASURE									
		TEST TEMP 100°F					TEST TEMP 130°F				
		Se	R2	Se/Sy	Rational	Rating	Se	R2	Se/Sy	Rational	Rating
G^*	MnRoad	0.123	0.07	1.115	Yes	Very Poor	0.119	0.13	1.074	Yes	Very Poor
$G^*/\sin\phi$	MnRoad	0.123	0.07	1.112	Yes	Very Poor	0.129	-0.03	1.170	No	Very Poor
G^*	MnRoad	0.238	0.02	1.144	Yes	Very Poor	0.221	0.15	1.060	Yes	Very Poor
$G^*/\sin\phi$	MnRoad	0.236	0.03	1.135	Yes	Very Poor	0.246	-0.05	1.180	No	Very Poor

TABLE 24 Summary of the goodness-of-fit statistics, rationality and ratings of the models investigated for the SST shear modulus tests

TEST PARAMETER SST	STRESS LEVEL	SITE	STATISTICAL MEASURE									
			TEST TEMP 100 °F					TEST TEMP 130 °F				
			Se	R ²	Se/Sy	Rational	Rating	Se	R ²	Se/Sy	Rational	Rating
G*	1.0	MnRoad	0.097	0.838	0.465	Yes	Good	0.105	0.809	0.505	Yes	Good
		ALF	0.010	0.625	0.670	Yes	Fair	0.006	0.858	0.413	Yes	Good
		WesTrack	0.174	0.680	0.570	Yes	Fair	0.220	0.660	0.720	Yes	Fair
	1.5	MnRoad	0.229	0.093	1.099	Yes	Very poor	0.194	0.347	0.933	Yes	Very poor
		ALF	0.009	0.708	0.593	Yes	Fair	0.005	0.886	0.370	Yes	Good
		WesTrack	0.106	0.880	0.350	Yes	Good	0.261	0.510	0.860	Yes	Poor
	2.0	MnRoad	0.204	0.276	0.983	Yes	Very Poor	0.098	0.832	0.473	Yes	Good
		ALF	0.008	0.722	0.577	Yes	Fair	0.007	0.804	0.485	Yes	Good
		WesTrack	0.282	0.420	0.920	Yes	Very Poor	0.225	0.640	0.740	Yes	Fair
G*/sinφ	1.0	MnRoad	0.099	0.828	0.478	Yes	Good	0.130	0.707	0.625	Yes	Fair
		ALF	0.009	0.653	0.646	Yes	Fair	0.006	0.856	0.414	Yes	Good
		WesTrack	0.193	0.730	0.630	Yes	Fair	0.242	0.580	0.790	Yes	Poor
	1.5	MnRoad	0.214	0.207	1.028	Yes	Very Poor	0.186	0.402	0.893	Yes	Poor
		ALF	0.008	0.722	0.577	Yes	Fair	0.005	0.885	0.370	Yes	Good
		WesTrack	0.113	0.910	0.430	Yes	Good	0.304	0.340	1.000	Yes	Very Poor
	2.0	MnRoad	0.197	0.330	0.945	Yes	Very Poor	0.098	0.832	0.473	Yes	Good
		ALF	0.008	0.742	0.558	Yes	Fair	0.007	0.779	0.516	Yes	Fair
		WesTrack	0.292	0.390	0.960	Yes	Very Poor	0.211	0.680	0.690	Yes	Fair

TABLE 25 Summary of the goodness-of-fit statistics, rationality and ratings of the models investigated for the SST shear modulus, weighted by all experimental sites

Shear Modulus SPT 2F (5Hz)	STRAIN LEVEL (μSTRAIN)	100 °F				130 °F			
		R ²	Se/Sy	Rational	Rating	R ²	Se/Sy	Rational	Rating
G*	100	0.705	0.580	Yes	Good	0.790	0.520	Yes	Good
G*/sinδ	100	0.740	0.570	Yes	Good	0.780	0.574	Yes	Good
G*	150	0.559	0.690	Yes	Fair	0.624	0.668	Yes	Fair
G*/sinδ	150	0.608	0.681	Yes	Fair	0.597	0.691	Yes	Fair
G*	200	0.507	0.789	Yes	Fair	0.772	0.545	Yes	Good
G*/sinδ	200	0.525	0.779	Yes	Fair	0.771	0.546	Yes	Good

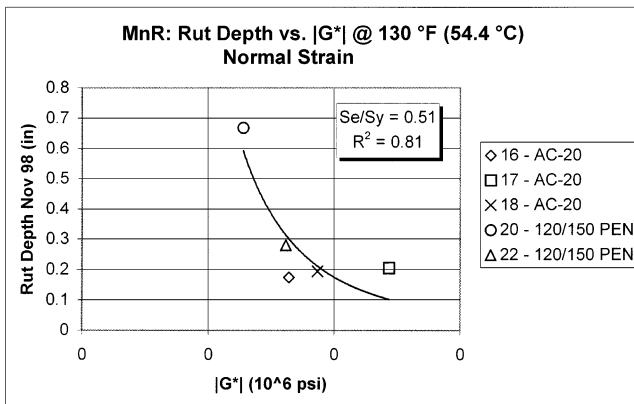


Figure 33. Linear |G*| versus rutting for the MnRoad test sections.

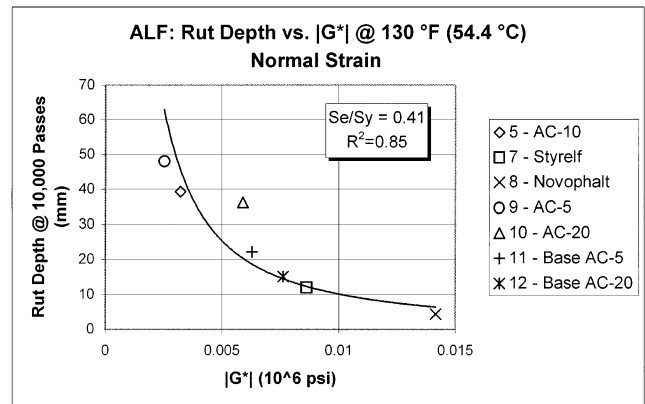


Figure 34. Linear |G*| versus rutting for the ALF test sections.

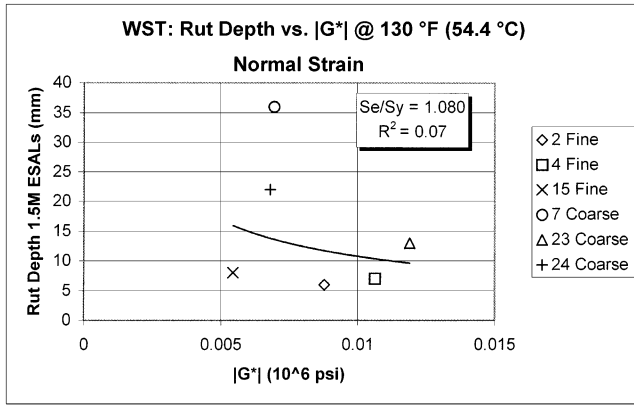


Figure 35. Linear $|G^*|$ versus rutting for the WesTrack test sections.

trast, the lab measured E^* values are significantly different than the Bonnaure et al. predictive model. Table 28 summarizes the summary of the weighted average analysis for both predictive equations.

4.2 STATIC CREEP PARAMETERS VERSUS RUTTING

The results from the static confined and unconfined creep tests for all three projects are included in the individual test-experimental site reports (23, 33, and 43). Conventional compliance and tertiary flow parameters were calculated and reported for each test replicate. These response parameters included the intercept (a), slope (m), total compliance at a loading time of 1 s ($D1$), and the flow time (F_T). The averages,

TABLE 26 Summary of the goodness-of-fit statistics, rationality and ratings of the models investigated for the prediction stiffness versus rutting using all test sections

TEST PARAMETER	SITE	STATISTICAL MEASURE									
		TEST TEMP 100°F					TEST TEMP 130°F				
		Se	R ²	Se/Sy	Rational	Rating	Se	R ²	Se/Sy	Rational	Rating
E^*	WST	8.133	0.116	0.959	No	Very Poor	8.146	0.113	0.961	No	Very Poor
	MnR	0.128	0.559	0.728	Yes	Fair	0.128	0.554	0.731	Yes	Fair
	ALF	5.547	0.506	0.770	Yes	Poor	3.089	0.768	0.528	Yes	Good
S_m	WST	8.345	0.070	0.984	Yes	Very Poor	7.963	0.153	0.939	Yes	Very Poor
	MnR	0.058	0.910	0.328	Yes	Excellent	0.053	0.923	0.303	Yes	Excellent
	ALF	4.414	0.855	0.417	Yes	Good	4.912	0.834	0.446	Yes	Good
$E^*/\sin\phi$	WST	8.133	0.116	0.959	No	Very Poor	8.146	0.113	0.961	No	Very Poor
	MnR	0.128	0.559	0.728	Yes	Fair	0.134	0.513	0.764	Yes	Fair
	ALF	4.940	0.500	0.774	Yes	Poor	2.811	0.770	0.525	Yes	Good
$S_m/\sin\phi$	WST	8.210	0.099	0.969	Yes	Very Poor	7.825	0.182	0.923	Yes	Very Poor
	MnR	0.056	0.914	0.322	Yes	Excellent	0.050	0.931	0.287	Yes	Excellent
	ALF	4.163	0.859	0.412	Yes	Good	4.910	0.835	0.444	Yes	Good

TABLE 27 Summary of the goodness-of-fit statistics, rationality and ratings of the models investigated for the predictive stiffness versus rutting using all laboratory test sections

TEST PARAMETER	SITE	STATISTICAL MEASURE									
		TEST TEMP 100°F					TEST TEMP 130°F				
		Se	R ²	Se/Sy	Rational	Rating	Se	R ²	Se/Sy	Rational	Rating
E^*	WST	6.417	0.827	0.509	Yes	Good	6.295	0.834	0.499	Yes	Good
	ALF	3.386	0.929	0.309	Yes	Excellent	2.881	0.948	0.263	Yes	Excellent
	MnR	0.139	0.665	0.669	Yes	Fair	0.137	0.675	0.658	Yes	Fair
S_m	WST	1.383	0.992	0.110	Yes	Excellent	0.434	0.999	0.034	Yes	Excellent
	ALF	5.713	0.796	0.521	Yes	Good	6.304	0.752	0.575	Yes	Fair
	MnR	0.074	0.905	0.356	Yes	Good	0.063	0.932	0.302	Yes	Excellent
$E^*/\sin\phi$	WST	6.460	0.825	0.512	Yes	Good	6.347	0.831	0.503	Yes	Good
	ALF	3.180	0.937	0.290	Yes	Excellent	2.551	0.959	0.233	Yes	Excellent
	MnR	0.140	0.661	0.673	Yes	Fair	0.140	0.661	0.673	Yes	Fair
$S_m/\sin\phi$	WST	0.967	0.996	0.077	Yes	Excellent	0.240	1.000	0.019	Yes	Excellent
	ALF	5.773	0.792	0.526	Yes	Good	6.305	0.752	0.575	Yes	Fair
	MnR	0.073	0.908	0.350	Yes	Good	0.073	0.908	0.350	Yes	Good

TABLE 28 Weighted summary of the goodness-of-fit statistics, rationality and ratings for the predictive stiffness versus rutting using laboratory test sections

Predicted Modulus SPT 2L (5Hz)	100 °F				130 °F			
	R ²	Se/Sy	Rational	Rating	R ²	Se/Sy	Rational	Rating
E^*_{max}	0.806	0.495	Yes	Good	0.818	0.472	Yes	Good
$E^*_{max}/\sin\phi$	0.806	0.490	Yes	Good	0.816	0.467	Yes	Good
Sm	0.891	0.345	Yes	Excellent	0.887	0.323	Yes	Excellent
$Sm/\sin\phi$	0.892	0.335	Yes	Excellent	0.879	0.336	Yes	Excellent

standard deviations, and coefficient of variation from the two replicates are included in the individual test–experimental site reports.

Statistical analyses were completed on all response parameters to determine how well these parameters correlated to the measured rut depths. Tables 29 and 30 summarize the goodness-of-fit statistics, the rationality of the trends for the uncon-

finied and confined test results, and the subjective ratings of the correlations for each response parameter and regression model. Table 31 presents the final rating weighted by all experimental projects.

The flow time was the highest ranked test parameter for the static creep test. Figures 36 through 41 are plots of the measured rut depths for each test section versus the flow time

TABLE 29 Summary of the goodness-of-fit statistics, rationality and ratings of the models investigated for the unconfined static creep–flow time test

TEST PARAMETER	STRESS (psi)	PROJECT	MODEL TYPE	STATISTICAL MEASURE									
				TEST TEMP 100 °F					TEST TEMP 130 °F				
				Se	R ²	Se/Sy	Rational	Rating	Se	R ²	Se/Sy	Rational	Rating
Flow Time (FT)	30@100 F 10@130 F	MnRoad	Power	0.032	0.99	0.137	Yes	Excellent	0.036	0.98	0.155	Yes	Excellent
	10	ALF	Power						0.181	0.92	0.310	Yes	Excellent
	20		Power						0.296	0.82	0.466	Yes	Good
	10	WesTrack	Power						0.152	0.94	0.306	Yes	Excellent
Slope (m)	30@100 F 10@130 F	MnRoad	Linear	0.175	0.62	0.758	Yes	Fair	0.045	0.98	0.193	Yes	Excellent
	10	ALF	Linear						0.292	0.82	0.459	Yes	Good
	20		Linear						0.495	0.49	0.779	Yes	Fair
	10	WesTrack	Linear						0.407	0.48	0.882	Yes	Fair
Compliance D(t) at Low Time	30@100 F 10@130 F	MnRoad	Linear	0.038	0.98	0.163	Yes	Excellent	0.061	0.95	0.265	Yes	Excellent
	10	ALF	Linear						0.635	0.17	0.999	Yes	Very Poor
	20		Linear						0.347	0.75	0.546	Yes	Good
	10	WesTrack	Linear						0.248	0.81	0.537	Yes	Good
Compliance D(t) at High Time	30@100 F 10@130 F	MnRoad	Linear	0.061	0.95	0.262	Yes	Excellent	0.026	0.99	0.112	Yes	Excellent
	10	ALF	Linear						0.491	0.50	0.774	Yes	Fair
	20		Linear						0.264	0.86	0.416	Yes	Good
	10	WesTrack	Linear						0.206	0.87	0.447	Yes	Good
Intercept (a)	30@100 F 10@130 F	MnRoad	Linear	0.136	0.77	0.588	Yes	Good	0.170	0.64	0.735	Yes	Fair
	10	ALF	Linear						0.692	0.01	1.089	-	Very Poor
	20		Linear						0.483	0.52	0.760	Yes	Fair
	10	WesTrack	Linear						0.305	0.71	0.661	Yes	Good

TABLE 30 Summary of the goodness-of-fit statistics, rationality and ratings of the models investigated for the confined static creep–flow time test

TEST PARAMETER	STRESS $\sigma_3 - \sigma_1$ psi	PROJECT	MODEL TYPE	STATISTICAL MEASURE									
				TEST TEMP 100 °F					TEST TEMP 130 °F				
				Se	R ²	Se/Sy	Rational	Rating	Se	R ²	Se/Sy	Rational	Rating
Flow Time (<i>FT</i>)	20-120	MnRoad	Power	0.167	0.61	0.719	Yes	Fair	0.107	0.84	0.462	Yes	Good
	20-140	ALF	Power						0.133	0.97	0.206	Yes	Excellent
	20-140	WesTrack	Power						0.304	0.75	0.613	Yes	Fair
Slope (<i>m</i>)	20-120	MnRoad	Linear	0.253	0.20	1.095	Yes	Poor	0.184	0.58	0.794	Yes	Fair
	20-140	ALF	Linear						0.373	0.71	0.588	Yes	Good
	20-140	WesTrack	Linear						0.209	0.86	0.453	Yes	Good
Compliance <i>D(t)</i> at Low Time	20-120	MnRoad	Linear	0.256	0.18	1.109	No	Very Poor	0.038	0.98	0.166	Yes	Excellent
	20-140	ALF	Linear						0.691	0.01	1.088	-	Very Poor
	20-140	WesTrack	Linear						0.416	0.46	0.901	Yes	Fair
Compliance <i>D(t)</i> at High Time	20-120	MnRoad	Linear	0.274	0.06	1.186	-	Very Poor	0.083	0.91	0.360	Yes	Excellent
	20-140	ALF	Linear						0.675	0.06	1.062	-	Very Poor
	20-140	WesTrack	Linear						0.391	0.52	0.848	Yes	Fair
Intercept (<i>a</i>)	20-120	MnRoad	Linear	0.236	0.19	1.020	No	Poor	0.259	0.16	1.122	-	Very Poor
	20-140	ALF	Linear						0.664	0.09	1.046	No	Very Poor
	20-140	WesTrack	Linear						0.480	0.28	1.039	Yes	Poor

for the unconfined and confined static creep test, respectively. As shown, the flow time was found to have an excellent comparison with the measured rut depths for all projects and test sections with the exception of Test Sections 2 and 15 of the WesTrack project (Figures 40 and 41).

This poor correlation between measured rutting and mixture response for these two WesTrack sections was also evident for all other tests evaluated within this project; thus, it appears that the reported volumetric properties of these two sections may be inaccurate. As a result, these two sections were treated as outliers in all further comparison studies because the results were consistent for all test methods and response parameters for these two sections. The comparisons between the rutting and mixture responses for these two sections, however, are shown on the plots for completeness.

The following provides a summary of the findings for each of the response parameters from the static creep test. Plots for

all other static creep parameters were included in the individual test–experimental site reports.

4.2.1 Unconfined Static Creep Test Parameters

In summary, all of the graphical comparisons at both temperatures for the unconfined static creep test demonstrated good-to-excellent relationships between the test parameters and the measured rutting. The flow time showed the best rational correlation. The following are specific findings from the analyses of the unconfined static creep test.

- **Intercept Parameter (*a*)**—The intercept showed rational relationships with the rut depth. The graphical analysis for this parameter showed reasonable distinction between the mixtures. The statistics obtained for the lin-

TABLE 31 Summary of the goodness-of-fit statistics, rationality and ratings for the static creep-flow time tests, weighted by all experimental sites

Unconfined Static Creep	Model	100°F				130°F			
		R ²	Se/Sy	Rational	Rating	R ²	Se/Sy	Rational	Rating
Flow Time (<i>F_T</i>)	Power	0.99	0.137	Yes	Excellent	0.91	0.323	Yes	Excellent
Slope (<i>m</i>)	Linear	0.62	0.758	Yes	Fair	0.70	0.572	Yes	Good
Compliance <i>D(t)</i> at Low Time	Linear	0.98	0.163	Yes	Excellent	0.63	0.621	Yes	Fair
Compliance <i>D(t)</i> at High Time	Linear	0.95	0.262	Yes	Excellent	0.78	0.464	Yes	Good
Intercept (<i>a</i>)	Linear	0.77	0.588	Yes	Good	0.42	0.837	Yes	Fair

Confined Static Creep	Model	100°F				130°F			
		R ²	Se/Sy	Rational	Rating	R ²	Se/Sy	Rational	Rating
Flow Time (<i>F_T</i>)	Power	0.61	0.719	Yes	Fair	0.87	0.388	Yes	Good
Slope (<i>m</i>)	Linear	0.20	1.095	Yes	Poor	0.71	0.619	Yes	Fair
Compliance <i>D(t)</i> at Low Time	Linear	0.18	1.109	No	Very Poor	0.43	0.753	Yes	Fair
Compliance <i>D(t)</i> at High Time	Linear	0.06	1.186	-	Very Poor	0.44	0.789	Yes	Fair
Intercept (<i>a</i>)	Linear	0.19	1.020	No	Poor	0.16	1.068	Yes	Very Poor

ear models showed fair-to-good measures of model accuracy.

- **Slope Parameter (*m*)**—The slope parameter showed a positive and rational relationship with the rut depth. The linear models had fair-to-good measures of accuracy. The graphical analysis showed a reasonable distinction among the mixtures.
- **Compliance *D(t)* at Short Time**—The compliance at short-time (i.e., low) values showed a positive and rational relationship with the rut depth. The graphical analysis also showed a very good distinction among the mixtures. The statistics had fair measures of model accuracy.

- **Compliance *D(t)* at Long Time**—The compliance at longer time values showed rational relationships with the rut depth. The linear model statistics were good, and the distinction among mixtures was also very good.
- **Flow Time (*F_T*)**—The statistics indicate excellent model accuracy. The relationships obtained in the correlation models were rational and provided good distinction among the different mixtures.

Overall, the flow-time and the compliance parameters showed stronger correlations with rut depth than did the

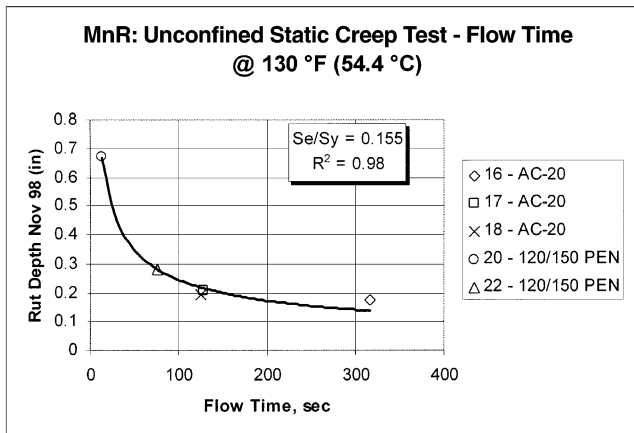


Figure 36. Rut depth versus unconfined flow time for the MnRoad test sections.

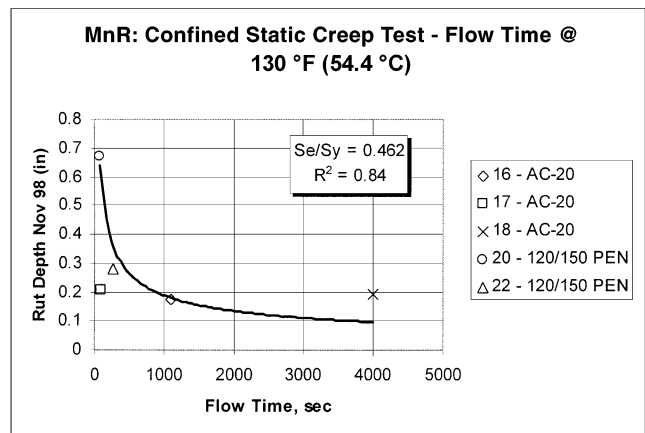


Figure 37. Rut depth versus confined flow time for the MnRoad test sections.

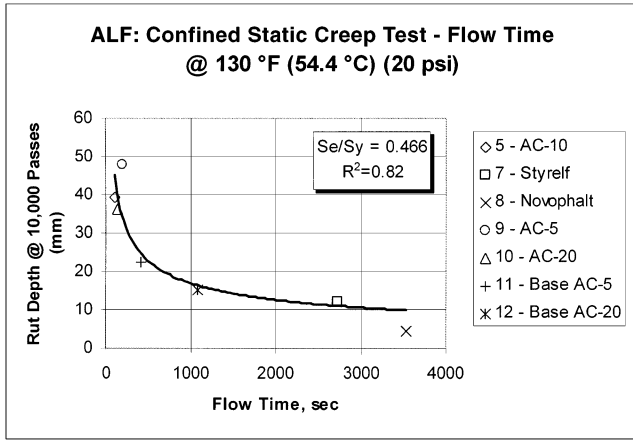


Figure 38. Rut depth versus unconfined flow time for the ALF test sections.

intercept and slope parameters when analyzed separately. All of the models were rational in that the flow time decreased as the rut depth increased. The flow-time models showed a very good distinction among the different mixtures. Poor-performing mixtures had the lowest flow time (i.e., the shortest time to failure); the good-performing mixtures had the largest flow time (i.e., the longest time to failure).

The ALF experiment provided a particularly good assessment of the flow-time parameter. The high-and-wide range of air void levels present among the different ALF mixtures might be expected to interfere with the relationship to the performance because densification has a strong influence on parameters such as the intercept and compliance. The densification range, however, did not affect the onset of tertiary flow as can be observed by the excellent relationship that was found between the flow parameters and the observed section rutting.

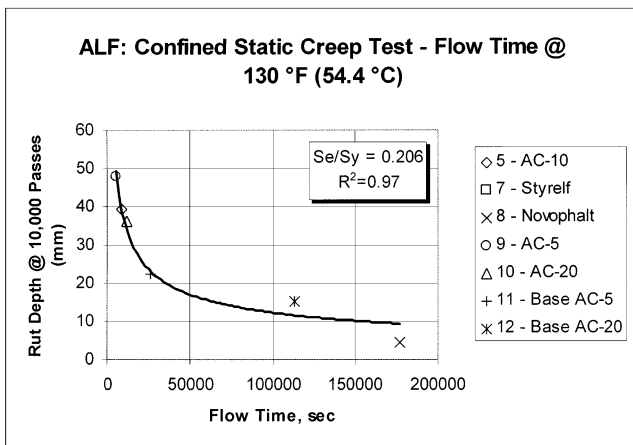
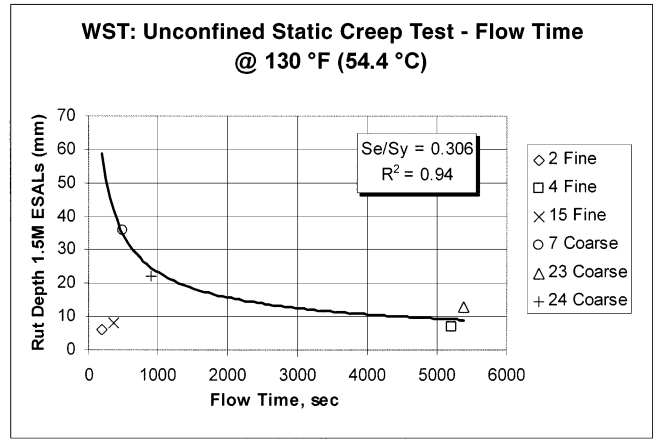


Figure 39. Rut depth versus confined flow time for the ALF test sections.



NOTE: Sections 2 and 15 treated as outliers and are not included in statistical analysis.

Figure 40. Rut depth versus unconfined flow time for the WesTrack test sections.

4.2.2 Confined Static Creep Test Parameters

All of the plots for the confined testing at 130°F (except for the intercept) demonstrated fair-to-good relationships between the test parameters and the permanent deformation (i.e., rutting) behavior in the field. The following are specific findings from the analyses of the confined static creep test.

- **Intercept Parameter (*a*)**—The intercept did not show a rational relationship with the rut depth and had very poor measures of model accuracy. No clear trend was observed with the rut-depth measurements.
- **Slope Parameter (*m*)**—The slope parameter showed positive and rational relationships with the rut depth. The linear-model statistics were indicative of good measures of model accuracy.

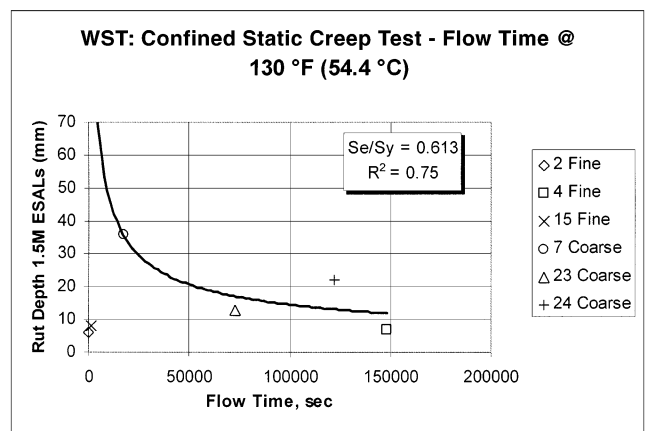


Figure 41. Rut depth versus confined flow time for the WesTrack test sections.

- **Compliance $D(t)$ at Short and Long Times**—The compliance at both short- and long-time values showed a rational correlation with the rut depth. The linear-model statistics indicated fair measures of model accuracy.
- **Flow Time (F_T)**—The flow time for the confined tests also showed good correlation with field rut depth measurements. The statistics obtained for the power models were good. All of the models were rational in that the flow time decreased as the rut depth increased. The tests conducted at 130°F showed better goodness-of-fit statistics than did the tests conducted at 100°F.

The correlation results obtained at 130°F were generally better than those obtained at 100°F. The slope and the flow-time parameters can discriminate among the different mixtures even when a wide range of volumetric properties are present among the different mixtures. Overall, the flow time showed the best rational correlation and statistical measures.

4.3 TRIAXIAL REPEATED LOAD PERMANENT DEFORMATION PARAMETERS VERSUS RUTTING

All of the repeated load permanent deformation data are presented in the individual test–experimental site reports (22, 32, and 42). The permanent deformation parameters included the conventional intercept (a) and slope (b), resilient strain (ϵ_r), the permanent deformation characteristics of alpha (α) and mu (μ), the flow number (F_N), the permanent strain at selected number of cycles, the resilient modulus at flow, and the strain ratio (ϵ_p/ϵ_r) at a selected number of cycles. The averages, standard deviations, and coefficient of variations for the replicate test specimens were determined and are included in the individual site reports produced by the project team.

Statistical analyses were completed on all response parameters to determine how well those parameters correlated to the measured rut depths. Tables 32 and 33 summarize the goodness-of-fit statistics, the rationality of the trends for the unconfined and confined test results, and the subjective ratings on the correlation for each response parameter and regression model. Table 34 presents the final rating weighted by all experimental projects.

The flow number was the highest ranked test parameter for the triaxial repeated load permanent deformation test. Figures 42 through 46 are plots of the measured rut depths for each test section versus the flow number for the unconfined and confined tests. As shown, the flow number compares well with the measured rut depths for all projects and test sections with the exception of Test Sections 2 and 15 of the WesTrack

project. The reason and possible explanation for this divergence was discussed earlier in this chapter.

The following are specific findings for each of the response parameters from both the confined and unconfined triaxial repeated load permanent deformation test. All graphical comparisons of the repeated load permanent deformation parameters and measured rut depths are included in the individual test–experimental site reports.

- **Confined Versus Unconfined Tests**—The statistical measures for the correlation between the unconfined test parameters and rutting were slightly higher than the measures for the confined test parameters, especially for the slope, permanent strain, and flow number. However, the weighted average statistical results and final ratings were similar for both the unconfined and confined tests.
- **Intercept Parameter**—The intercept did not show any clear trends with rut depth. The linear-model statistics were indicative of poor measures of model accuracy.
- **Slope Parameter**—The slope parameter showed a positive and rational relationship with the rut depth. The linear models had good measures of accuracy and good distinction among the mixtures.
- **Resilient Strain (ϵ_r)**—The resilient strain showed a positive and rational relationship with the rut depth. The linear models had fair statistical measures of accuracy.
- **Mu Parameter (μ)**—The linear model statistics were poor, and the distinction among the mixtures was not clear.
- **Flow Number (F_N)**—All of the tertiary-flow models were rational in that the flow number decreased as the rut depth increased. The power model provided good (nearly excellent) statistical measures of accuracy.
- **Permanent Strain**—The permanent strain showed a positive and rational relationship with the rut depth. The graphical analysis also showed a very good distinction among the mixtures. The models had good measures of model accuracy.
- **Resilient Modulus**—The data showed a good and rational relationship with the rut depth. The graphical analysis also showed a good distinction among the mixtures.
- **Ratio of Permanent to Elastic Strain (ϵ_p/ϵ_r)**—The ratio at 2,000 cycles showed a positive and rational relationship with the rut depth. The results also showed a reasonable distinction among the mixtures. The model statistics were indicative of fair measures of model accuracy.

In summary, many mixture-response parameters for both the unconfined and confined repeated load test correlated well with the measured rut depths. These parameters cover a

TABLE 32 Summary of the goodness-of-fit statistics, rationality and ratings of the models investigated for the unconfined repeated load tests

TEST PARAMETER	STRESS	PROJECT	MODEL TYPE	STATISTICAL MEASURE									
				TEST TEMP 100°F					TEST TEMP 130°F				
				Se	R ²	Se/Sy	Rational	Rating	Se	R ²	Se/Sy	Rational	Rating
Flow Number (F_N)	30@100 F 10@130 F	MnRoad	Power	0.07	0.86	0.313	Yes	Excellent	0.09	0.85	0.453	Yes	Good
	10	ALF	Power						0.17	0.94	0.295	Yes	Excellent
	20		Power						0.28	0.84	0.435	Yes	Good
	10	WesTrack	Power						0.21	0.88	0.424	Yes	Good
Slope (b)	30@100 F 10@130 F	MnRoad	Linear	0.154	0.59	0.743	Yes	Fair	0.055	0.95	0.264	Yes	Excellent
	10	ALF	Linear						0.20	0.92	0.310	Yes	Excellent
	20		Linear						0.26	0.86	0.410	Yes	Good
	10	WesTrack	Linear						0.31	0.70	0.672	Yes	Good
Permanent Strain at $N=1000$	30@100 F 10@130 F	MnRoad	Linear	0.053	0.95	0.256	Yes	Excellent	0.052	0.95	0.249	Yes	Excellent
	10	ALF	Linear						0.26	0.86	0.416	Yes	Good
	20		Linear						0.33	0.78	0.520	Yes	Good
	10	WesTrack	Linear						0.19	0.89	0.408	Yes	Good
Resilient Strain ϵ_{200}	30@100 F 10@130 F	MnRoad	Linear	0.075	0.90	0.362	Yes	Excellent	0.141	0.65	0.680	Yes	Fair
	10	ALF	Linear						0.34	0.76	0.533	Yes	Good
	20		Linear						0.40	0.67	0.629	Yes	Fair
	10	WesTrack	Linear						0.41	0.47	0.881	Yes	Fair
Resilient Modulus at Flow		MnRoad											
	10	ALF	Linear						0.14	0.96	0.225	Yes	Excellent
	20		Linear						0.48	0.52	0.761	Yes	Fair
	10	WesTrack	Linear						0.34	0.64	0.739	Yes	Fair
ϵ_p/ϵ_r Ratio	30@100 F 10@130 F	MnRoad	Linear	0.098	0.83	0.472	Yes	Good	0.240	0.00	1.153	-	Very Poor
	10	ALF	Linear						0.41	0.66	0.638	Yes	Fair
	20		Linear						0.24	0.88	0.379	Yes	Good
	10	WesTrack	Linear						0.31	0.70	0.667	Yes	Good
μ (μ)	30@100 F 10@130 F	MnRoad	Linear	0.110	0.79	0.530	-	Good	0.225	0.12	1.081	-	Very Poor
	10	ALF	Linear						0.65	0.13	1.021	-	Very Poor
	20		Linear						0.68	0.05	1.068	-	Very Poor
	10	WesTrack	Linear						0.03	0.99	0.060	-	Excellent

wide range of material behavior from elastic properties, such as the resilient modulus, to plastic properties, such as tertiary flow. Overall, the slope, permanent strain, and the flow number showed good correspondence with rut depth. Among these parameters, the flow number had the best statistical measures.

4.4 SST REPEATED LOAD PERMANENT DEFORMATION PARAMETERS VERSUS RUTTING

All of the shear repeated load permanent deformation data are presented in the individual test-experimental site reports (21, 31, and 41). The response parameters for the repeated

TABLE 33 Summary of the goodness-of-fit statistics, rationality and ratings of the models investigated for the confined repeated load test

TEST PARAMETER	STRESS $\sigma_3 - \sigma_1$ psi	PROJECT	MODEL TYPE	STATISTICAL MEASURE									
				TEST TEMP 100°F					TEST TEMP 130°F				
				Se	R ²	Se/Sy	Rational	Rating	Se	R ²	Se/Sy	Rational	Rating
Flow Number (FN)	20 - 120	MnRoad	-	-	-	-	Yes	-	0.08	0.93	0.32	Yes	Excellent
	20 - 140	ALF	Power						0.35	0.75	0.520	Yes	Good
	20 - 130	WesTrack	Power									Yes	
Slope (b)	20 - 120	MnRoad	Linear	0.080	0.89	0.386	Yes	Good	0.149	0.62	0.715	Yes	Fair
	20 - 140	ALF	Linear						0.43	0.62	0.672	Yes	Fair
	20 - 130	WesTrack	Linear						0.28	0.75	0.609	Yes	Good
Permanent Strain at N=1000	20 - 120	MnRoad	Linear	0.128	0.71	0.617	Yes	Good	0.171	0.49	0.821	Yes	Fair
	20 - 140	ALF	Linear						0.41	0.66	0.638	Yes	Fair
	20 - 130	WesTrack	Linear						0.24	0.82	0.517	Yes	Good
Permanent Strain at N>5000	20 - 120	MnRoad	Linear	0.091	0.86	0.438	Yes	Good	0.129	0.71	0.621	Yes	Good
	20 - 140	ALF	Linear						0.37	0.71	0.589	Yes	Good
	20 - 130	WesTrack	Linear						0.160	0.89	0.399	Yes	Good
Resilient Strain ϵ_r	20 - 120	MnRoad	Linear	0.157	0.58	0.753	Yes	Fair	0.197	0.33	0.949	Yes	Poor
	20-140	ALF	Linear						0.46	0.61	0.721	Yes	Fair
	20-130	WesTrack	Linear						0.32	0.68	0.697	Yes	Fair
Resilient Modulus at Flow	20 - 120	MnRoad	Linear										
	20 - 140	ALF	Linear						0.42	0.63	0.663	Yes	Fair
	20 - 130	WesTrack	Linear						0.28	0.75	0.611	Yes	Good
ϵ_p/ϵ_r Ratio	20 - 120	MnRoad	Linear	0.099	0.82	0.478	Yes	Good	0.196	0.33	0.944	Yes	Poor
	20 - 140	ALF	Linear						0.37	0.73	0.569	Yes	Good
	20 - 130	WesTrack	Linear						0.32	0.68	0.690	Yes	Fair
Mu (μ)	20 - 120	MnRoad	Linear	0.237	0.02	1.142	-	Very Poor	0.228	0.09	1.101	-	Very Poor
	20 - 140	ALF	Linear						0.65	0.13	1.024	-	Very Poor
	20 - 130	WesTrack	Linear						0.32	0.68	0.68	-	Fair
Intercept (a)	20 - 120	MnRoad	Linear	0.231	0.07	1.113	No	Very Poor	0.224	0.13	1.078	No	Very Poor
	20 - 140	ALF	Linear						0.69	0.02	1.087	-	Very Poor
	20 - 130	WesTrack	Linear						0.55	0.04	1.199	Yes	Very Poor

load permanent deformation test included the permanent shear strain at a selected number of load repetitions, the conventional slope and intercept parameters, the flow number, the resilient shear strain (i.e., recoverable shear strain), the resilient shear modulus, and the ratio of the permanent shear strain to total shear strain. The averages, standard deviations, and coefficient of variations for the replicate test specimens were determined and are included in the site project reports.

Statistical analyses were completed on all response parameters to determine how well those parameters correlated with the measured rut depths. Table 35 summarizes the goodness-of-fit statistics, the rationality of the trends for the test results, and the subjective ratings on the correlation for each response

parameter and regression model. Table 36 presents the final rating weighted by all experimental projects.

The permanent shear strain at 3,000 load repetitions was the highest ranked test parameter for the SST repeated shear constant height (RSCH) test. Figures 47 through 52 are plots of the measured rut depths for each test section versus the permanent shear strain at 1,000 and 3,000 load repetitions. All other repeated load-parameter plots are included in the individual test-experimental site reports along with all combinations of statistical models, temperatures, and stress levels used in the study.

The SST repeated shear data showed rational trends and fair-to-good relationships with the measured rut depths. The permanent deformation increased with the number of load

TABLE 34 Summary of the goodness-of-fit statistics, rationality and ratings for the repeated load tests, weighted by all experimental sites

Unconfined Repeated Load	Model	100°F				130°F			
		R ²	Se/Sy	Rational	Rating	R ²	Se/Sy	Rational	Rating
Flow Number (F _N)	Power	0.96	0.229	Yes	Excellent	0.90	0.359	Yes	Good
Slope (b)	Linear	0.59	0.743	Yes	Fair	0.87	0.393	Yes	Good
Permanent Strain	Linear	0.95	0.256	Yes	Excellent	0.86	0.410	Yes	Good
Resilient Strain	Linear	0.90	0.362	Yes	Excellent	0.66	0.652	Yes	Fair
Resilient Modulus at Flow	Linear					0.72	0.548	Yes	Good
ε _p /ε _r Ratio	Linear	0.83	0.472	Yes	Good	0.59	0.676	Yes	Fair
Mu (μ)	Linear	0.79	0.530	-	Good	0.25	0.881	-	Poor
Intercept (a)	Linear	0.30	0.964	Yes	Poor	0.13	1.055	Yes	Very Poor

Confined Repeated Load	Model	100°F				130°F			
		R ²	Se/Sy	Rational	Rating	R ²	Se/Sy	Rational	Rating
Flow Number (F _N)	Power			Yes		0.75	0.520	Yes	Good
Slope (b)	Linear	0.89	0.386	Yes	Good	0.65	0.670	Yes	Fair
Permanent Strain	Linear	0.86	0.438	Yes	Good	0.76	0.552	Yes	Good
Resilient Strain	Linear	0.58	0.753	Yes	Fair	0.54	0.786	Yes	Fair
Resilient Modulus at Flow	Linear					0.46	0.443	Yes	Fair
ε _p /ε _r Ratio	Linear	0.82	0.478	Yes	Good	0.59	0.716	Yes	Fair
Mu (μ)	Linear	0.02	1.142	-	Very Poor	0.26	0.962		Poor
Intercept (a)	Linear	0.07	1.113	No	Very Poor	0.02	1.088		Very Poor

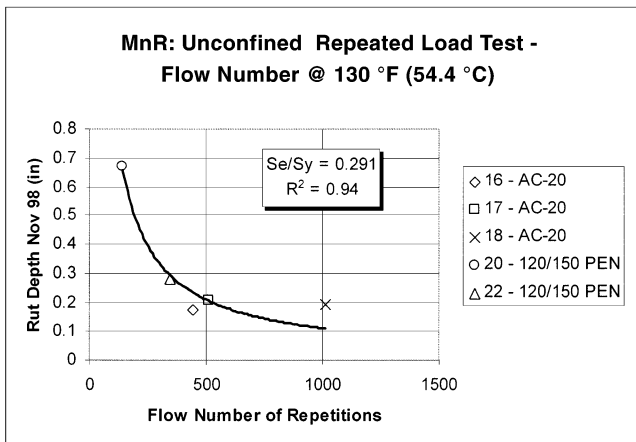


Figure 42. Rut depth versus unconfined flow number for the MnRoad test sections.

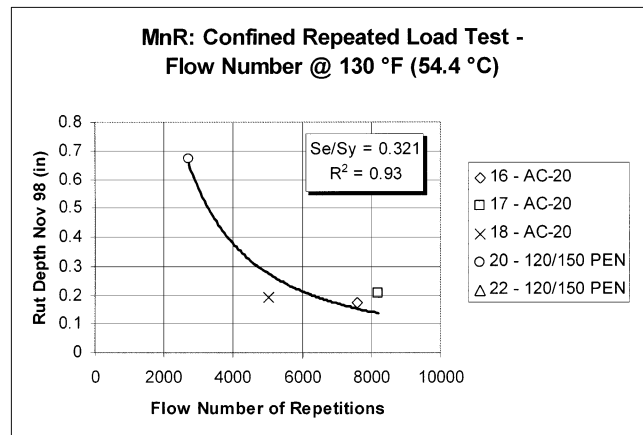


Figure 43. Rut depth versus confined flow number for the MnRoad test sections.

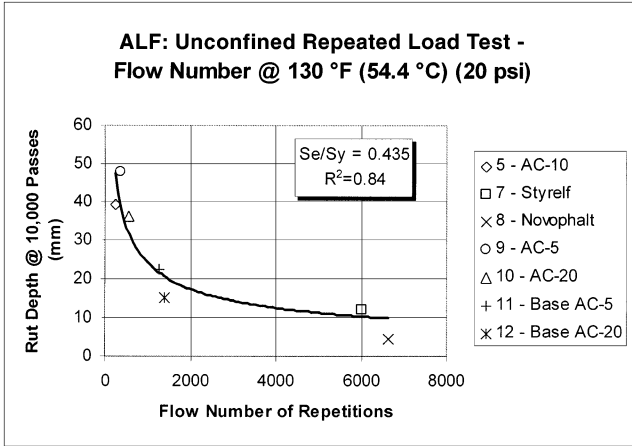
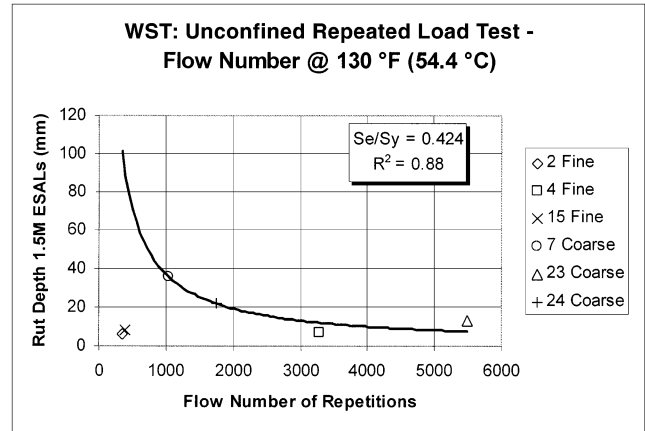


Figure 44. Rut depth versus unconfined flow number for the ALF test sections.



NOTE: Sections 2 and 15 were excluded from the analysis.

Figure 46. Rut depth versus unconfined flow number for the WesTrack test sections.

repetitions, shear stress, and temperature. The following are specific findings for each of the response parameters from the SST repeated shear load permanent deformation test. All graphical comparisons of the repeated load permanent deformation parameters and measured rut depths are included in the individual site reports.

- **Intercept Parameter**—The intercept linear-model statistics were indicative of poor measures of model accuracy.
- **Slope Parameter**—The slope parameter showed a positive and rational relationship with the rut depth. The linear models had fair measures of accuracy and good distinction among the mixtures.

- **Resilient Strain**—The resilient strain also showed a positive and rational relationship with the rut depth. The linear models had fair statistical measures of accuracy.
- **Flow Point**—In most cases, no tertiary flow was induced. The models evaluated for the cases obtained provided fair statistical measures of accuracy.
- **Resilient Modulus**—The data showed a fair and rational relationship with rutting. The graphical analysis also showed a reasonable distinction among the mixtures.
- **Shear Strain**—The shear strain showed a positive and rational relationship with the rut depth. The results at 3,000 cycles were better than those at 1,000 cycles. The graphical analysis also showed a very good distinction among the mixtures. The models had good measures of model accuracy.

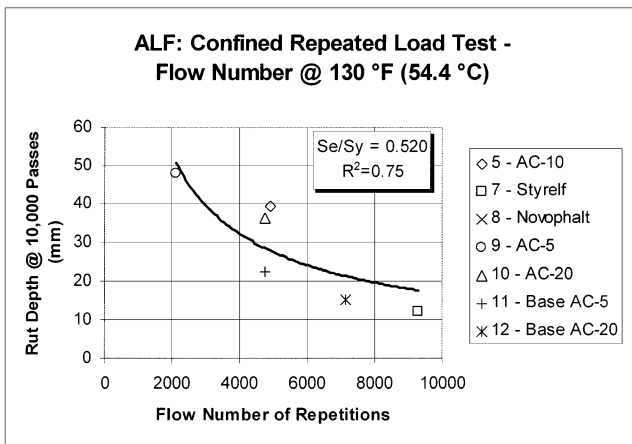


Figure 45. Rut depth versus confined flow number for the ALF test sections.

In summary, the accumulated shear strain is the response parameter from the SST RSCH test that had the best correlation to the measured rut depth. The best correlation was obtained at the higher test temperature and higher number of load cycles.

4.5 TRIAXIAL SHEAR STRENGTH PARAMETERS VERSUS RUTTING

All of the triaxial shear strength data are presented in the individual test-experimental site reports (18, 29, and 40). These reports summarize the maximum deviatoric stress, normal stress, and percent strain at failure for each test condition and project. The triaxial shear strength parameters from the Mohr-Coulomb failure envelope included the cohesion (c) and friction angle (ϕ); the shear strength, the intercept parameter (k), and the slope ($\gamma^{1/2}$) were from the Drucker-Prager failure

TABLE 35 Summary of the goodness-of-fit statistics, rationality and ratings of the models investigated for the repeated shear tests

TEST PARAMETER	STRESS (psi)	PROJECT	MODEL TYPE	STATISTICAL MEASURE										
				TEST TEMP 100°F					TEST TEMP 130°F					
				Se	R ²	Se/Sy	Rational	Rating	Se	R ²	Se/Sy	Rational	Rating	
γ _p 100 Cycles	10	MnRoad												
		ALF	Log-Log					8.389	0.77	0.520	Yes	Good		
		WesTrack												
γ _p 1000 Cycles	10	MnRoad												
		ALF	Log-Log					5.324	0.91	0.330	Yes	Excellent		
		WesTrack												
γ _p 3000 Cycles	10	MnRoad												
		ALF	Linear					4.517	0.93	0.280	Yes	Excellent		
		WesTrack												
γ _p 100 Cycles	15	MnRoad	Linear					0.108	0.80	0.519	Yes	Good		
		ALF	Semi-Log					5.001	0.92	0.310	Yes	Excellent		
		WesTrack	Linear					7.302	0.67	0.640	Yes	Fair		
γ _p 1000 Cycles	15	MnRoad	Linear					0.105	0.81	0.503	Yes	Good		
		ALF	Semi-Log					5.646	0.91	0.35	Yes	Excellent		
		WesTrack	Linear					8.443	0.56	0.740	Yes	Fair		
γ _p 3000 Cycles	15	MnRoad	Linear					0.015	1.00	0.072	Yes	Excellent		
		ALF	Semi-Log					3.549	0.96	0.220	Yes	Excellent		
		WesTrack	Linear					9.927	0.40	0.870	-	Poor		
Slope	15	MnRoad	Linear	0.240	0.00	1.154	-	Very Poor	0.240	0.00	1.154	-	Very Poor	
		ALF	Semi-Log					7.098	0.84	0.440	Yes	Good		
		WesTrack	Linear					5.591	0.80	0.490	Yes	Good		
Total Strain per Cycle	15	MnRoad												
		ALF	Log-Log					6.614	0.86	0.410	Yes	Good		
		WesTrack	Linear					6.047	0.77	0.530	Yes	Good		
Resilient Strain per Cycle	15	MnRoad	Linear	0.227	0.11	1.089	-	Very Poor	0.216	0.19	1.039	-	Very Poor	
		ALF	Log-Log					6.614	0.86	0.410	Yes	Good		
		WesTrack	Linear					6.161	0.77	0.540	Yes	Good		
Resilient Shear Modulus	15	MnRoad	Linear	0.208	0.25	1.000	-	Very Poor	0.202	0.29	0.973	-	Very Poor	
		ALF	Log-Log					5.969	0.88	0.370	Yes	Good		
		WesTrack	Power					6.960	0.70	0.610	Yes	Fair		
Strain Ratio per Cycle	15	MnRoad	Linear	0.208	0.01	1.149	-	Very Poor	0.215	0.20	1.033	-	Very Poor	
		ALF	Linear					14.841	0.30	0.920	-	Very Poor		
		WesTrack	Linear					7.645	0.64	0.670	Yes	Fair		
Plastic Strain per Cycle	15	MnRoad												
		ALF	Linear					10.486	0.65	0.650	Yes	Fair		
		WesTrack	Linear					8.215	0.59	0.720	Yes	Fair		
Intercept	15	MnRoad	Linear	0.227	0.11	1.091	-	Very Poor	0.217	0.18	1.044	-	Very Poor	
		ALF	Log-Log					6.937	0.85	0.430	Yes	Good		
		WesTrack	Log-Log					11.410	0.20	1.000	-	Very Poor		
Flow Point	15	MnRoad	Linear	0.224	0.13	1.077	-	Very Poor	0.198	0.320	0.952	-	Very Poor	
		ALF	Linear					8.873	0.75	0.550	Yes	Good		
		WesTrack												
γ _p 100 Cycles	30	MnRoad	Linear	0.221	0.15	1.062	-	Very Poor						
		ALF												
		WesTrack												
γ _p 1000 Cycles	30	MnRoad	Linear	0.221	0.15	1.065	-	Very Poor						
		ALF												
		WesTrack												
γ _p 3000 Cycles	30	MnRoad	Linear	0.199	0.31	0.956	-	Very Poor						
		ALF												
		WesTrack												

TABLE 36 Summary of the goodness-of-fit statistics, rationality and ratings for the repeated shear tests, weighted by all experimental sites

Repeated Shear SPT 2(G)	MODEL	130 °F			
		R ²	Se/Sy	Rational	Rating
γ _p @ 1000 cycles	Linear	0.75	0.577	Yes	Good
γ _p @ 3000 cycles	Linear	0.88	0.392	Yes	Good
slope	Linear	0.60	0.728	Yes	Fair
Intercept	Linear	0.28	0.982	Yes	Poor
Flow Point	Linear	0.60	0.730	Yes	Fair
Total Shear Strain / cycle	Linear	0.64	0.696	Yes	Fair
Resilient Strain / cycle	Linear	0.60	0.728	Yes	Fair
Resilient Modulus	Linear	0.42	0.878	Yes	Fair

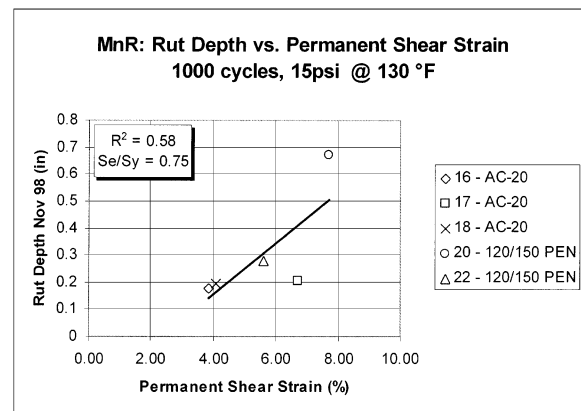


Figure 47. Rut depth versus permanent shear strain at 1,000 load cycles for the MnRoad test sections.

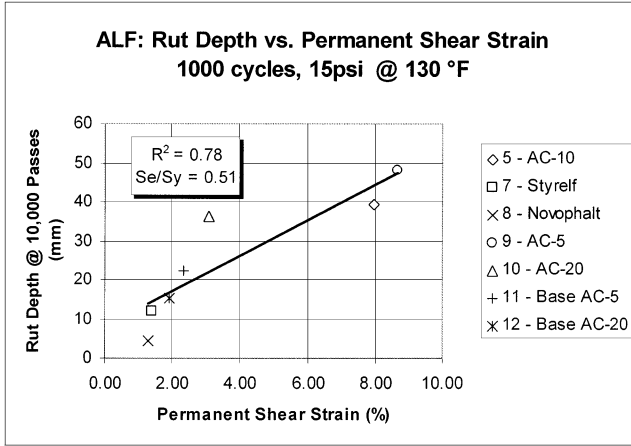


Figure 48. Rut depth versus permanent shear strain at 1,000 load cycles for the ALF test sections.

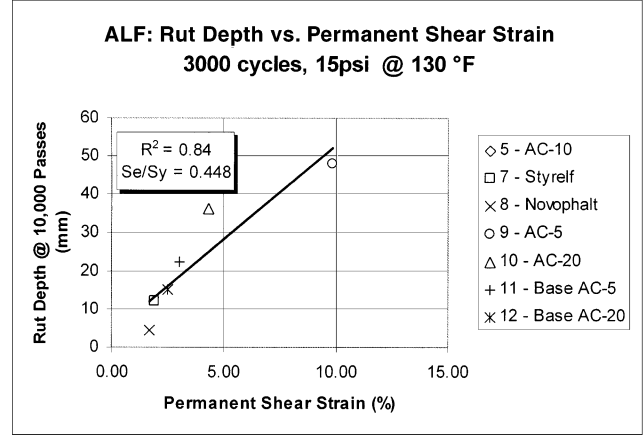
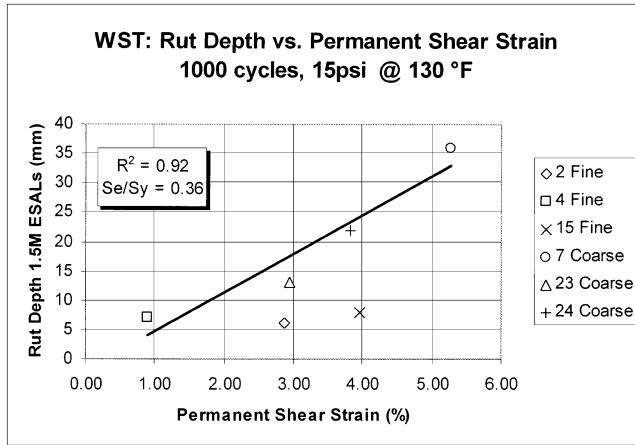
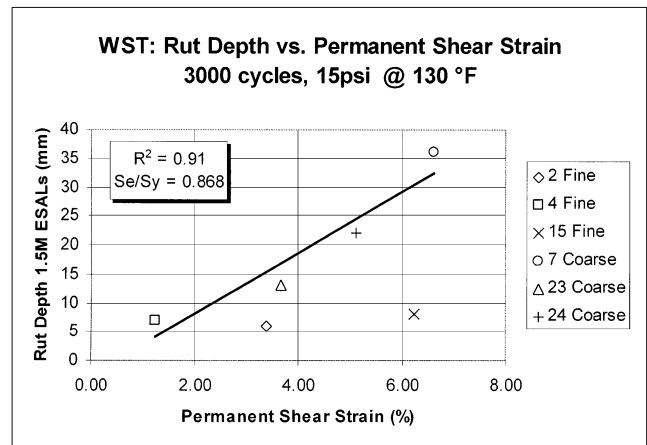


Figure 51. Rut depth versus permanent shear strain at 3,000 load cycles for the ALF Test sections.



NOTE: Sections 2 and 15 treated as outliers and are not included in statistical analysis.

Figure 49. Rut depth versus permanent shear strain at 1,000 load cycles for the WesTrack test sections.



NOTE: Sections 2 and 15 treated as outliers and are not included in statistical analysis.

Figure 52. Rut depth versus permanent shear strain at 3,000 load cycles for the WesTrack test sections.

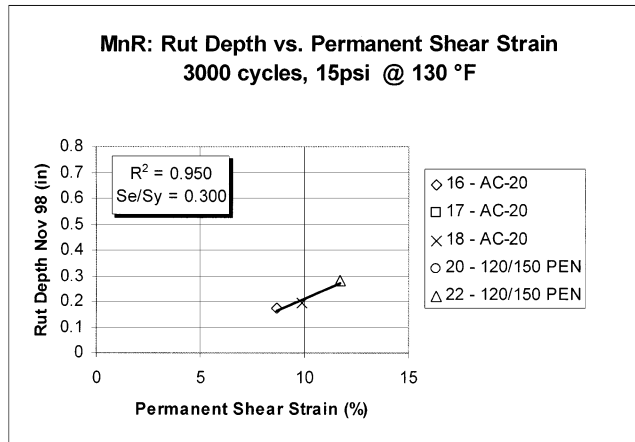


Figure 50. Rut depth versus permanent shear strain at 3,000 load cycles for the MnRoad test sections.

envelope. The averages, standard deviations, and coefficient of variations from the replicates are included in the site reports.

Statistical analyses were completed on all response parameters to determine how well these parameters correlated to the measured rut depths. Table 37 summarizes the goodness-of-fit statistics, the rationality of the trends for the triaxial shear strength test results, and the subjective ratings of the correlation for each response parameter and regression model. Table 38 presents the final rating weighted by all experimental projects.

Figures 53 through 55 are plots of the measured rut depths for each test section versus the shear strength at a selected normal stress for each project. The shear strength was the highest-ranked test parameter from the triaxial shear strength test. The following are detailed findings for each of the

TABLE 37 Summary of the goodness-of-fit statistics, rationality and ratings of the models investigated for the triaxial shear strength tests

TEST PARAMETER	PROJECT	MODEL TYPE	STATISTICAL MEASURE									
			TEST TEMP 100°F					TEST TEMP 130°F				
			Se	R ²	Se/Sy	Rational	Rating	Se	R ²	Se/Sy	Rational	Rating
Shear Strength	MnRoad	Power	0.116	0.77	0.559	Yes	Good	0.078	0.90	0.374	Yes	Good
	ALF	Power						11.970	0.54	0.742	Yes	Fair
	WesTrack	Power						10.560	0.35	0.901	No	Poor
Cohesion (c)	MnRoad	Power	0.113	0.78	0.546	Yes	Good	0.235	0.04	1.133	-	Very Poor
	ALF	Power						13.860	0.38	0.859	Yes	Poor
	WesTrack	Power						9.720	0.45	0.829	No	Poor
Intercept (k)	MnRoad	Power	0.125	0.73	0.601	Yes	Fair	0.237	0.02	1.141	-	Very Poor
	ALF	Power						14.030	0.37	0.870	Yes	Poor
	WesTrack	Power						9.450	0.48	0.806	No	Poor
Friction Angle (φ)	MnRoad	Power	0.154	0.59	0.743	Yes	Fair	0.134	0.69	0.647	Yes	Fair
	ALF	Power						17.220	0.05	1.068	Yes	Very Poor
	WesTrack	Power						11.940	0.17	1.019	No	Very Poor
Slope ($\gamma^{1/2}$)	MnRoad	Power	0.118	0.76	0.567	Yes	Fair	0.078	0.90	0.374	Yes	Good
	ALF	Power						17.210	0.05	1.067	Yes	Very Poor
	WesTrack	Power						12.220	0.13	1.043	No	Very Poor

TABLE 38 Summary of the goodness-of-fit statistics, rationality and ratings for the triaxial shear strength tests, weighted by all experimental sites

Triaxial Strength Test	Model	100°F				130°F			
		R ²	Se/Sy	Rational	Rating	R ²	Se/Sy	Rational	Rating
Shear Strength	Power	0.77	0.559	Yes	Good	0.52	0.692	Yes	Fair
Cohesion (c)	Power	0.78	0.546	Yes	Good	0.18	0.980	-	Very Poor
Intercept (k)	Power	0.73	0.601	Yes	Fair	0.17	0.987	-	Very Poor
Friction Angle (φ)	Power	0.59	0.743	Yes	Fair	0.24	0.919	-	Very Poor
Slope ($\gamma^{1/2}$)	Power	0.76	0.567	Yes	Fair	0.30	0.834	-	Poor

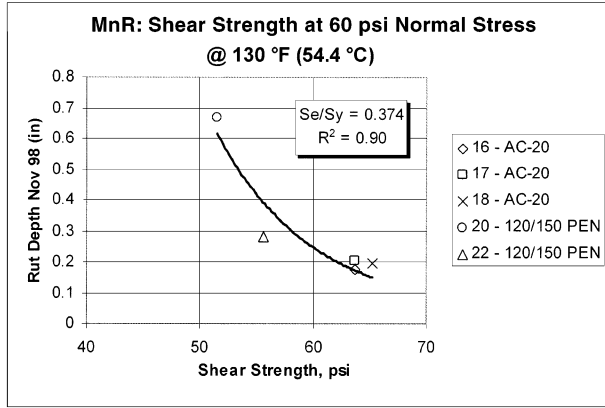


Figure 53. Rut depth versus shear strength for the MnRoad test sections.

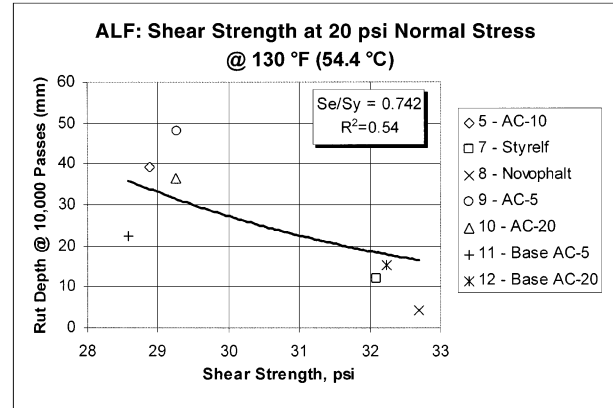
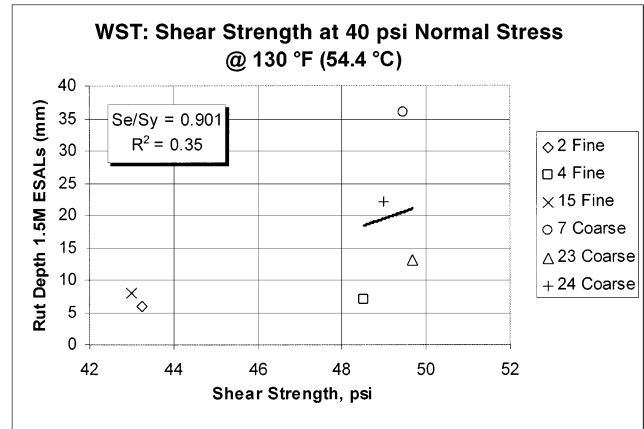


Figure 54. Rut depth versus shear strength for the ALF test sections.

response parameters from the shear strength test. Plots for all other shear strength test parameters are included in the individual test–experimental site reports.

- **Cohesion (*c*) and Intercept Parameter (*k*)**—The statistics for the cohesion parameter (*c*) indicated good relative accuracy of model prediction at 100°F, but very poor measures were observed at 130°F. Similar results were found for the intercept parameter (*k*).
- **Friction Angle (ϕ) and Slope Parameter ($\gamma^{1/2}$)**—The results showed a fair relationship between the rut depth and the friction angle at 100°F. The results at 130°F showed a very poor relationship between the rut depth and friction angle.
- **Shear Strength Values at Selected Normal Stress**—The statistics for this parameter were indicative of good-to-fair model accuracy. The trends between the measured rut depths and shear strength were rational and did distinguish between the extreme mixtures, except for the WesTrack test sections.

In summary, the shear strength exhibited a rational, fair-to-good correspondence with rutting that was measured on each of the test sections.



NOTE: Sections 2 and 15 treated as outliers and are not included in statistical analysis.

Figure 55. Rut depth versus shear strength for the WesTrack test sections.

CHAPTER 5

ANALYSES AND COMPARISONS OF MIXTURE RESPONSE TO FRACTURE

The analysis of the fatigue (i.e., load) and thermal (i.e., environmental) fracture experiment followed the general methodology discussed in Chapter 3. Statistical analysis using regression techniques was used to determine the level of correlation between the measured laboratory mixture response to both fatigue and thermal cracking. However, it must be recognized that not all of the experimental sites investigated possessed both load-associated fatigue cracking and thermal fracture. For the MnRoad test sites, the observed cracking on the selected test sections was thermal cracking. In contrast, the ALF and WesTrack sections were the only experimental sites to exhibit fatigue cracking (Table 5). Because a limited number of sections selected for the FHWA–ALF study possessed fatigue cracking (i.e., 2 thickness levels by 2 stiffness levels), a detailed statistical correlation analysis, as done for all other main experimental sites could not be done with only the two points. Wherever possible, graphical comparisons were also prepared to judge the reasonableness of the trends in the data. This chapter summarizes the test results, graphical comparisons, and statistical analyses of the measured response parameters and fracture (i.e., fatigue cracking and thermal cracking) on specific projects.

5.1 MODULUS PARAMETERS VERSUS CRACKING

The mixture modulus for the cracking study was obtained only from the triaxial dynamic modulus and ultrasonic wave propagation tests. All dynamic modulus test data are presented in the individual test–experimental site reports previously cited in Chapter 4. It is important for the reader to recall the specific types of fracture that were present for each of the three main experimental sites evaluated.

The response parameters used in the comparison studies for the dynamic modulus test were the same as the parameters used for the rutting analysis (i.e., $|E^*|$ and ϕ). However, the stiffness factor used in the statistical analysis was $|E^*| \sin\phi$ rather than $|E^*|/\sin\phi$. The response parameters from the ultrasonic wave propagation test were the same as the parameters used in the rutting analysis: E_d , E_{CORA} , and E_{CORB} .

The correlation between modulus and cracking for all test sections is provided in Table 39. Both the dynamic modulus and elastic modulus from the ultrasonic wave propagation

tests were used in the statistical comparison. The ALF project had only two data points. Only the rationality of the test results could therefore be assessed. Overall, the correlation between mixture modulus or stiffness and cracking is fair.

5.2 INDIRECT TENSILE TEST PARAMETERS VERSUS CRACKING—GENERAL

Three indirect tensile tests were performed on the mixtures recovered from the three experimental projects: the indirect tensile strength, the indirect tensile fatigue, and the indirect tensile creep. Numerous parameters were computed from these tests and then regressed against the cracking data measured on each test section.

All test data that were used in the comparisons are presented in the individual test–experimental site reports (15, 17, 26, 28, 36, and 38). Statistical analyses were completed on all response parameters to determine how well these parameters correlated to the measured cracking at each test section. The statistical goodness-of-fit values are presented in Tables 40 through 42 for each test. In general, the correlation between the response parameters from the indirect tensile test and cracking was poor and site dependent. The exception to this observation was the compliance values and the tensile strain at failure–modulus relationship. The creep compliance from the indirect tensile creep test had the best correlation to cracking for the test section included in this study.

5.3 INDIRECT TENSILE CREEP PARAMETERS VERSUS CRACKING

The indirect tensile creep test results and computations of creep compliance for all three projects are included in the individual site reports (16, 27, and 37). The creep compliance was calculated as a function of time for each test section and mixture tested. The two parameters (i.e., D_1 and m_1) of the creep compliance equation (Equation 23) were evaluated by fitting a regression model through the data. Creep compliance at a time of 1,000 s was calculated for each cell tested in the study and for two stress levels. The statistical results for this parameter are summarized in Table 43.

TABLE 39 Summary of the goodness-of-fit statistics, rationality and ratings of the models investigated for the stiffness versus cracking for dynamic modulus and ultrasonic wave propagation tests

TEST PARAMETER	STRESS LEVEL	SITE	STATISTICAL MEASURE									
			TEST TEMP 40°F					TEST TEMP 70°F				
			Se	R ²	Se/Sy	Rational	Rating	Se	R ²	Se/Sy	Rational	Rating
E*max	UnC-Lin	WST	54.03	0.09	1.17	No	Very Poor	54.87	0.06	1.19	No	Very Poor
		MnR	126.28	0.53	0.79	Yes	Poor	170.08	0.15	1.06	Yes	Very Poor
		ALF				Yes					Yes	
E*	Con-20 -	WST	56.24	0.01	1.22	No	Very Poor	55.53	0.04	1.20	No	Very Poor
		ALF				Yes					Yes	
	Con-30 -	WST	20.60	0.87	0.45	Yes	Good	25.90	0.79	0.56	Yes	Fair
		ALF				Yes					Yes	
E*maxsinφ	UnC-Lin	WST	5.89	0.99	0.13	No	Excellent	54.20	0.08	1.17	Yes	Very Poor
		MnR	136.65	0.45	0.85	Yes	Poor	176.24	0.09	1.10	Yes	Very Poor
		ALF				Yes					Yes	
E*sinφ	Con-20-	WST	56.09	0.02	1.21	No	Very Poor	53.94	0.35	0.89	No	Poor
		ALF				Yes					Yes	
	Con-30-	WST	33.64	0.65	0.73	Yes	Fair	25.87	0.79	0.56	No	Fair
		ALF				Yes					Yes	
E _{CORA}	Linear	WST	36.32	0.59	0.79	Yes	Poor	36.65	0.58	0.79	Yes	Poor
E _{CORB}		WST	26.19	0.79	0.57	No	Fair	22.37	0.84	0.48	No	Good
E _{US}		WST	35.85	0.60	0.78	Yes	Poor	35.87	0.60	0.78	Yes	Poor

TABLE 40 Summary of the goodness-of-fit statistics, rationality and ratings of the models investigated for the indirect tensile strength tests

TEST PARAMETER	PROJECT	MODEL TYPE	STATISTICAL MEASURE									
			TEST TEMP 55°F					TEST TEMP 70°F				
			S _e	R ²	Se/Sy	Rational	Rating	S _e	R ²	Se/Sy	Rational	Rating
Tensile Strength	MnRoad	Linear	181.55	0.04	1.133	No	Very Poor					
	ALF										Yes	
	WesTrack	Log.	38.16	0.55	0.826	Yes	Fair					
Horizontal Tensile Strain	MnRoad	Exp.	167.88	0.18	1.048	Yes	Very Poor					
	ALF										Yes	
	WesTrack	Linear	55.20	0.05	1.194	Yes	Very Poor					
Fracture Energy	MnRoad	Log.	156.70	0.28	0.978	Yes	Poor					
	ALF										Yes	
	WesTrack	Linear	47.80	0.29	1.034	Yes	Poor					
Energy at Failure	MnRoad	Log.	182.70	0.03	1.14	Yes	Very Poor					
	ALF										Yes	
	WesTrack	Linear	56.57	0.00	1.224	Yes	Very Poor					

TABLE 41 Summary of the goodness-of-fit statistics, rationality and ratings of the models investigated for the indirect tensile fatigue tests

TEST PARAMETER	PROJECT	MODEL TYPE	STATISTICAL MEASURE											
			TEST TEMP 55°F					TEST TEMP 70°F						
			S _e	R ²	Se/Sy	Rational	Rating	S _e	R ²	Se/Sy	Rational	Rating		
Tensile Stress versus (N _f) <i>Intercept</i>	MnRoad	Power	156.42	0.29	0.976	Yes	Poor							
	ALF											Yes		
	WesTrack	Logarithm	51.70	0.17	1.119	Yes	Very poor							
Tensile Stress versus (N _f) <i>Slope</i>	MnRoad	Power	156.22	0.29	0.975	Yes	Poor							
	ALF											Yes		
	WesTrack	Linear	54.85	0.06	1.187	Yes	Very poor							
Horizontal Tensile Strain versus (N _f) <i>Intercept</i>	MnRoad	Power	29.90	0.97	0.187	Yes	Excellent							
	ALF											Yes		
	WesTrack	Logarithm	54.71	0.07	1.184	No	Very poor							
Horizontal Tensile Strain versus (N _f) <i>Slope</i>	MnRoad	Power	31.39	0.97	0.196	Yes	Excellent							
	ALF											Yes		
	WesTrack	Linear	53.30	0.01	1.218	No	Very poor							
Tensile Stress versus (N ₅₀) <i>Intercept</i>	MnRoad	Power	142.45	0.41	0.889	Yes	Poor							
	ALF											Yes		
	WesTrack	Logarithm	53.40	0.11	1.155	Yes	Very poor							
Tensile Stress versus (N ₅₀) <i>Slope</i>	MnRoad	Power	140.66	0.42	0.878	Yes	Poor							
	ALF											Yes		
	WesTrack	Linear	55.81	0.03	1.207	Yes	Very poor							
Horizontal Tensile Strain versus (N ₅₀) <i>Intercept</i>	MnRoad	Power	27.25	0.98	0.170	Yes	Excellent							
	ALF											Yes		
	WesTrack	Logarithm	53.73	0.10	1.163	No	Very poor							
Horizontal Tensile Strain versus (N ₅₀) <i>Slope</i>	MnRoad	Power	23.94	0.98	0.149	Yes	Excellent							
	ALF											Yes		
	WesTrack	Linear	55.89	0.03	1.209	No	Very poor							
Initial Resilient Modulus (M _{ro})	MnRoad	Power	169.69	0.16	1.060	No	Very poor							
	ALF											Yes		
	WesTrack	Logarithm	33.00	0.66	0.714	Yes	Fair							
Stress-strength ratio	MnRoad	Power	35926	0.74	0.516	Yes	Good							
	ALF											Yes		
	WesTrack	Power	524614	0.67	0.597	Yes	Fair							
N _f from Equation 2.1	MnRoad	Power	179.95	0.05	1.123	No	Very Poor						No	
	ALF													
	WesTrack	Linear	54.46	0.08	1.178	Yes	Very poor							

5.3.1 MnRoad

Figure 56 shows the creep compliance values at a time of 1,000 s [$D(1,000)$] for low-stress levels plotted as a function of the MnRoad thermal cracking data. Higher correlation was observed for the low-stress level compared with the high-stress level. The average observed cracking decreased with the increase of creep compliance. The models had good measures of model accuracy.

5.3.2 ALF

Figure 57 shows the values of $D(1,000)$ for low-stress levels plotted as a function of the number of wheel repetitions at the ALF project to obtain 100-m fatigue cracking. At the low-stress level, Lane 4 (i.e., stiffer binder and thick pavement) had the highest compliance at 1,000 s. Lane 2 on the other hand had the least compliance. The trend of the pavement thickness is reversed in the low-stress level. In other words, using a stiffer binder gave higher compliance for the thick pavement but lower compliance for the thin pavement.

No correlation could be obtained from the ALF mixtures because of the difference in pavement thickness between the sections.

5.3.3 WesTrack

Figure 58 shows the values of $D(1,000)$ for low-stress levels plotted as a function of the percentage area of fatigue cracking for the WesTrack project. Fair correlation was obtained for the low-stress level compared with the high-stress level. The observed percent fatigue cracking increased with an increase in creep compliance.

5.4 INDIRECT TENSILE STRENGTH PARAMETERS VERSUS CRACKING

All indirect tensile strength test data are presented in the individual test-experimental site reports developed by the project team (15, 26, and 36). The response parameters from the indirect tensile strength test included the tensile strength,

TABLE 42 Summary of the goodness-of-fit statistics, rationality and ratings of the models investigated for the indirect tensile creep tests

TEST PARAMETER	PROJECT	MODEL TYPE	STATISTICAL MEASURE									
			HIGH STRESS LEVEL					LOW STRESS LEVEL				
			S_e	R^2	Se/Sy	Rational	Rating	S_e	R^2	Se/Sy	Rational	Rating
Compliance @ 1000 sec	MnRoad	Power	172.48	0.13	1.076	Yes	Very Poor	66.36	0.87	0.414	Yes	Good
	ALF					Yes					Yes	
	WesTrack	Linear	32.11	0.68	0.695	Yes	Fair	38.93	0.53	0.842	Yes	Fair
(D1)	MnRoad	Power	178.29	0.07	1.113	Yes	Very Poor	104.50	0.68	0.652	Yes	Fair
	ALF					Yes					Yes	
	WesTrack	Linear	36.55	0.58	0.791	Yes	Fair	52.55	0.14	1.137	Yes	Poor
(m1)	MnRoad	Power	131.23	0.50	0.819	Yes	Poor	57.06	0.91	0.356	Yes	Excellent
	ALF					Yes					Yes	
	WesTrack	Linear	40.59	0.49	0.878	Yes	Fair	44.25	0.39	0.957	Yes	Poor
FP (n) (Eq.1.16b)	MnRoad	Power	130.30	0.50	0.813	Yes	Poor	56.01	0.91	0.350	Yes	Excellent
	ALF					Yes					Yes	
	WesTrack	Log.	41.80	0.45	0.904	Yes	Fair	44.80	0.37	0.969	Yes	Poor
FP (log A) (Eq.1.16a)	MnRoad	Power	145.95	0.38	0.911	Yes	Very Poor	55.75	0.91	0.348	Yes	Excellent
	ALF					No					No	
	WesTrack	Linear	42.36	0.44	0.917	Yes	Fair	45.05	0.37	0.975	Yes	Poor
FP (log A) (Eq.1.17)	MnRoad	Power	182.35	0.03	1.138	Yes	Very Poor	166.70	0.19	1.040	Yes	Very Poor
	ALF					Yes					Yes	
	WesTrack	Linear	35.88	0.60	0.776	Yes	Fair	39.13	0.52	0.847	Yes	Fair
FP (n) (Eq.1.18a)	MnRoad	Power	129.80	0.51	0.810	Yes	Poor	60.38	0.89	0.377	Yes	Good
	ALF					Yes					Yes	
	WesTrack	Log.	40.57	0.49	0.878	Yes	Fair	44.18	0.39	0.956	Yes	Poor
FP (log A) (Eq.1.18b)	MnRoad	Power	176.80	0.09	1.103	Yes	Very Poor	100.67	0.70	0.628	Yes	Fair
	ALF					Yes					Yes	
	WesTrack	Linear	36.28	0.59	0.785	Yes	Fair	40.16	0.50	0.869	Yes	Fair
Elastic Strain (ϵ_e)	MnRoad	Power	180.76	0.05	1.128	Yes	Very Poor	152.52	0.32	0.952	Yes	Very Poor
	ALF					Yes					Yes	
	WesTrack	Linear	56.18	0.02	1.216	No	Very Poor	56.61	0.00	1.225	No	Very Poor
Plastic Strain (ϵ_p)	MnRoad	Power	181.02	0.04	1.130	No	Very Poor	103.96	0.68	0.650	Yes	Fair
	ALF					No					Yes	
	WesTrack	Linear	18.82	0.89	0.407	Yes	Good	55.02	0.06	1.190	No	Very Poor
Viscoelastic Strain (ϵ_{ve})	MnRoad	Power	185.10	0.00	1.160	Yes	Very Poor	107.55	0.66	0.670	Yes	Fair
	ALF					Yes					No	
	WesTrack	Linear	49.58	0.23	1.073	Yes	Poor	41.39	0.47	0.895	Yes	Fair
Viscoplastic Strain (ϵ_{vp})	MnRoad	Power	174.00	0.12	1.090	Yes	Very Poor	87.36	0.78	0.550	Yes	Good
	ALF					No					Yes	
	WesTrack	Linear	41.47	0.46	0.897	Yes	Fair	32.08	0.68	0.694	Yes	Fair
Permanent Strain (ϵ_{pn})	MnRoad	Power	174.22	0.11	1.090	Yes	Very Poor	86.58	0.78	0.540	Yes	Good
	ALF					No					Yes	
	WesTrack	Linear	41.42	0.46	0.896	Yes	Fair	32.46	0.67	0.702	Yes	Fair
Total Strain (ϵ_T)	MnRoad	Power	174.28	0.11	1.090	Yes	Very Poor	82.13	0.80	0.512	Yes	Good
	ALF					No					Yes	
	WesTrack	Linear	43.83	0.40	0.948	Yes	Fair	35.59	0.61	0.770	Yes	Fair

tensile strain at failure, fracture energy, and energy at failure. Table 40 summarizes the results from the graphical comparisons and statistical measures of the correlation between the individual response parameters and cracking. Overall, the individual response parameters have a poor-to-very poor correlation to cracking.

A brief comparison was completed using the indirect tensile strain at failure and modulus and the cracking data measured at each of the three projects. The indirect tensile strain at failure was determined in accordance with the procedure

documented in *NCHRP Report 338 (12)*. Two modulus values were used in the comparison: the triaxial dynamic modulus and the resilient modulus calculated from the repeated load indirect tensile fatigue test.

The rationality of the relationship and comparison was good—as the failure strain increased, cracking decreased. In addition, the relationship between modulus (either the dynamic modulus or resilient modulus) and tensile strain at failure discriminated between those mixtures susceptible to cracking and those that were not susceptible to cracking.

TABLE 43 Summary of the goodness-of-fit statistics, rationality and ratings of the models investigated for the creep compliance parameter

TEST	TEST CONDITION	EXPERIMENTAL SITE	MODEL TYPE	LOW STRESS LEVEL (55°F)			
				R ²	Se/Sy	Rational	Rating
IDT D(t)	1000 sec	MnRoad	Power	0.87	0.414	Yes	Good

TEST	TEST CONDITION	EXPERIMENTAL SITE	MODEL TYPE	LOW STRESS LEVEL (55°F - 70°F)			
				R ²	Se/Sy	Rational	Rating
IDT D(t)	1000 sec	ALF				Yes	
IDT D(t)	1000 sec	WesTrack	Linear	0.53	0.842	Yes	Fair

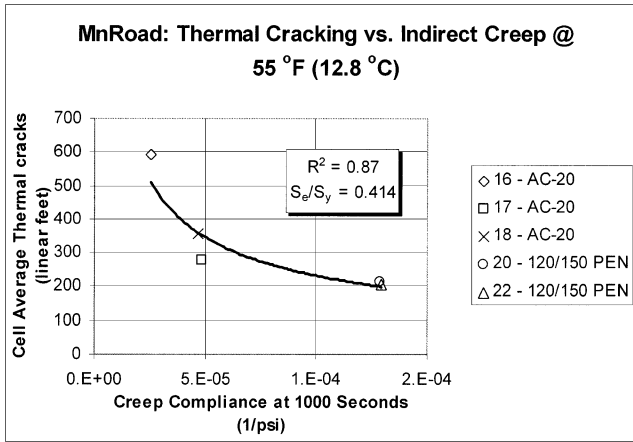


Figure 56. Thermal cracking versus indirect tensile creep compliance at 1,000 s for the MnRoad test sections.

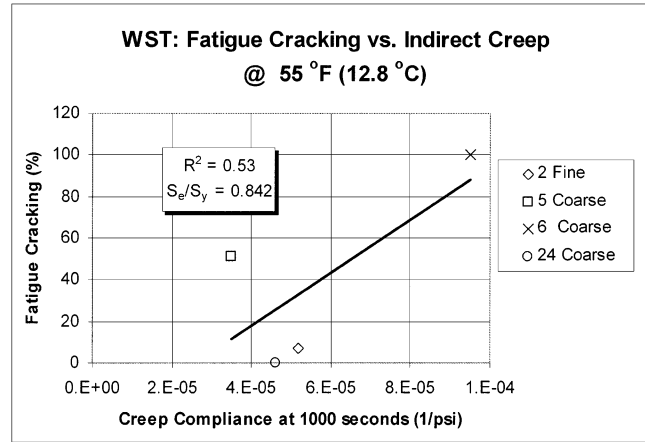


Figure 58. Fatigue cracking versus indirect tensile creep compliance at 1,000 s for the WesTrack test sections.

5.5 INDIRECT TENSILE FATIGUE PARAMETERS VERSUS CRACKING

All indirect tensile fatigue test data are presented in the individual test–experimental site reports (17, 28, and 38). The response parameters from the indirect tensile fatigue test included (1) the tensile stress intercept and the slope of the relationship between tensile stress and the number of loading cycles to total failure (i.e., cracking) and to a 50-percent reduction in resilient modulus; (2) the tensile strain intercept and slope of the relationship between tensile strain and the number of loading cycles to total failure and to a 50-percent reduction in resilient modulus; and (3) the resilient modulus and the stress-to-strength ratio.

Table 41 summarized the results from the graphical comparisons and statistical measures of the correlation between the response parameters and cracking. Overall, the correlation to cracking was site dependent. The stress-to-strength ratio gave the better statistical measures for the correlation.

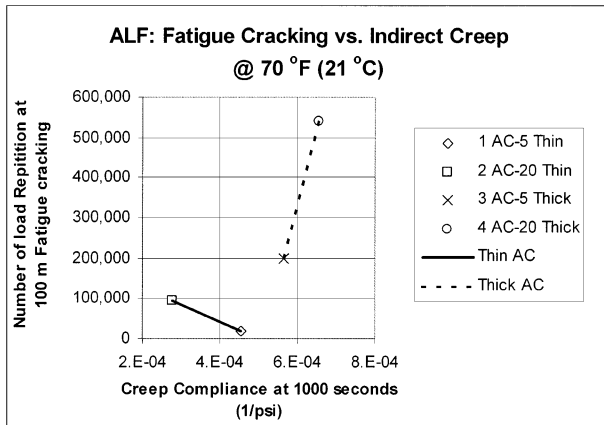


Figure 57. Fatigue cracking versus indirect tensile creep compliance at 1,000 s for the ALF test sections.

CHAPTER 6

SUMMARY OF FINDINGS

6.1 TEST METHODS APPLICABLE FOR THE SPT

Industry representatives were interviewed during the first part of Task C to determine which distress type was most important in support of the Superpave volumetric mix design procedure. Overwhelmingly, rutting (i.e., permanent deformation) was identified as the most important distress. As a result, most follow-up work regarding the SPT was devoted to developing correlations between HMA mixture response parameters and rutting. Fracture, however, also was considered an important distress in the long-term performance of HMA mixtures. As a result, the Superpave models team has continued to pursue the use of the SPT for analysis of fracture-related distresses, primarily load-related fatigue cracking.

There were specific requirements for developing the SPT:

- The SPT is to be used in support of the Superpave volumetric mix design procedure.
- The SPT must test HMA specimens compacted with SGC devices.
- The SPT must accurately measure true fundamental responses or properties of HMA mixtures, or both.
- The SPT must be based on existing technology and equipment (i.e., require no new test development).
- Responses measured with the SPT need not predict the entire performance history, but the test must identify inferior HMA mixtures (i.e., must determine a mix's relative susceptibility to excessive distortion and fracture under defined conditions).
- Properties determined from the SPT should be tied to the advanced mixture characterization methods being developed under other tasks of NCHRP Project 9-19, "Superpave Support and Performance Models Management."

Numerous test methods and mixture response parameters that satisfy the above requirements were used in the experimental test plan for determining the correspondence between the test results and the magnitude of rutting and cracking. Some of the test methods and equipment have been used for decades for evaluating the performance characteristics of HMA mixtures, while others have been recently developed. The following sections summarize the findings from the laboratory study and correlation to performance for the three

distresses considered (i.e., rutting, fatigue cracking, and thermal cracking).

6.1.1 SPT for Permanent Deformation—Rutting

Five laboratory tests consistently had parameters that resulted in an overall good-to-excellent correlation to the measured rut depths. These test methods and responses are the dynamic modulus as measured by the SST and triaxial compression tests at high temperatures, the flow time as measured by the triaxial creep test, the cumulative permanent strain measured at 1,000 loading cycles using the triaxial repeated load test, and the permanent shear strain measured at 1,000 loading cycles using the SST RSCH test.

6.1.1.1 Summary of Advantages and Disadvantages of Candidate Test Methods

Table 44 summarizes the advantages and disadvantages for each test method and response parameter found to be highly correlated to the amount of rutting. These advantages and disadvantages were the consensus of the project team and were based on the results of the testing program included in this study and previous test programs. As shown, each test method has advantages and disadvantages regarding its use for the SPT.

6.1.1.2 Ranking and Selection of Test Methods and Responses

The purpose of the statistical analysis of all test data was to find the best laboratory test method and parameter that satisfy the requirements of the SPT. The utility analysis summarized in Chapter 1 addressed several issues related to the selection process of the SPT. Some of these factors were as follows:

- Reliability of the test parameter to distinguish among the performance of a wide range of mixtures,
- Repeatability of the test and the sensitivity of the test parameter to different mixture variables,

TABLE 44 Advantages and disadvantages of the top-selected SPTs for permanent deformation

Test Type	Parameter	Test Condition	Model	R ²	S _e /S _y	Advantages	Disadvantages
Stiffness E* / sinφ	E* / sinφ	Sinusoidal, Linear, 130 °F, 5 Hz	Power	0.91	0.310	<ul style="list-style-type: none"> • May have direct tie to 1-37 (2002 Design Guide). • Provides necessary input for structural analysis. • Rational way to establish criteria (guidelines). • Not forced to do master curves; only evaluates at T_{eff}. • Can be linked to Witczak, et al. (5), regression; allows one to develop provisional starting parameter for mix criteria. 	<ul style="list-style-type: none"> • Coring and sawing. • At high temperature, complex test system (still need small deformations at high temperature). • Some possible minor problems due to stud, LVDT arrangement. • May need to further investigate accuracy of confined (linear) tests for gap-graded mixtures. • Confined gave poor results.
	E*	Sinusoidal, Linear, 130 °F, 5 Hz	Power	0.79	0.52		
Tertiary Flow (Static Creep)	F _T	Unconfined, 130 °F	Power	0.91	0.323	<ul style="list-style-type: none"> • Simple test (equipment). • Potentially inexpensive. • Best correlation of experimental sites to field rutting for confined conditions. 	<ul style="list-style-type: none"> • May have difficulty to develop guidelines. • Coring and sawing. • Confined testing may be required for open-graded (SMA) mixtures. • May not simulate field dynamic phenomena.
		Confined, 130 °F	Power	0.87	0.388		
Shear Repeated Load (γ _p -N)	γ _p @ N=1,000	Constant Height, 130 °F, τ =10–15 psi	Linear	0.75	0.550	<ul style="list-style-type: none"> • Ability to test field cores. • An original SPT. • Empirical guidelines currently exist (TAI, CLM). 	<ul style="list-style-type: none"> • Guidelines may be difficult. • Not fundamental to define from structural models such as 2002 Design Guide.
	γ _p @ N=3,000		Linear	0.88	0.392		
Stiffness G* / sinφ	G* (no difference G* / sinφ)	130 °F, 100 μstrain, 5 Hz	Power	0.79	0.52	<ul style="list-style-type: none"> • Ability to test field cores. 	<ul style="list-style-type: none"> • Cannot use G* in 2002 Design Guide. • Sawing required. • At 130 °F, system control problems may arise leading to low G* values. • Boundary conditions are problem for test property.

- Complexity of the test procedure,
- Cost of the equipment and testing preparation requirements,
- Testing time needed to complete the testing program, and
- Technical level or experience required from the operator.

Multiple members of the research team analyzed the statistical results, evaluated the potential test parameters, and outlined the advantages and disadvantages of the test procedures for permanent deformation. The research team ranked the tests and parameters based on the comprehensive evaluation conducted on a scale from 1 to 6, 1 having the high or top priority and 6 having the low or bottom. Results of the team’s evaluation and ranking procedure are shown in Table 45. The overall ranking for each test and parameter was obtained by totaling the entire individual team ranking. The tests and parameters then were ranked according to this sum. The lower the total score, the better the test.

As shown in Table 45, the top three parameters for permanent deformation were (1) the dynamic modulus term, (E*/sinφ), determined from the triaxial dynamic modulus test; (2) the flow time (F_T) from the triaxial static creep; and (3) the flow number (F_n) from the triaxial repeated load test. During the July 2000 NCHRP panel meeting, the top two parameters were recommended by the research team for the follow-up field validation work. The panel’s recommendation was to include the triaxial repeated load as a third alternative. Thus, the above three test methods were selected as the SPT candidates for evaluating an HMA mixture’s resistance to rutting.

6.1.2 SPT for Fracture—Fatigue and Thermal Cracking

Three laboratory tests had parameters that resulted in a fair correlation to the measured amount of cracking. These test

TABLE 45 Ranking summary of the high-priority SPT candidates for permanent deformation

Test	Individual Team Rankings*									Total Score
$E^*/\sin\phi$ Stiffness	1	1	1	3	2	2	2	6	2	20
Triaxial Flow Time (F_T)	5	3	2	2	1	1	1	3	4	22
Triaxial Reated Load (F_N)	2	2	4	1	4	4	3	2	1	23
Repeated Shear γ_p-N	3	6	3	5	3	3	5	4	3	35
Triaxial Repeated Load ϵ_p-N	4	5	5	4	5	5	4	1	5	38
G^* Stiffness	6	4	6	6	6	6	6	5	6	51

* 1 for high priority, 6 for low priority.

methods and the mixture response parameters were the dynamic modulus measured from the triaxial compression test at lower test temperatures, the compliance measured at 1,000 s from the indirect tensile creep test, and the tensile strain at failure adjusted by the modulus of the mixture. The tensile strain at failure is determined from the indirect tensile strength test, and the modulus from the triaxial dynamic modulus test.

The research team recommended two parameters for the follow-up field validation work. The dynamic modulus measured at low test temperatures was recommended because it is compatible with the fatigue cracking–prediction model from NCHRP Project 1-37A (“Development of the 2002 Guide for Design of New and Rehabilitated Pavement Structures: Phase II”) and because it provides some consistency in the tests between rutting and cracking. The compliance measured by the indirect tensile creep test at longer loading times and low temperatures was recommended because it is compatible with the thermal-cracking model from NCHRP Project 1-37A (10).

6.1.3 SPT Protocols

Draft test protocols for the candidate test methods are provided in Appendixes A through E. These draft test protocols were prepared in the standard AASHTO format for testing procedures. The final test and analysis protocol will guide and direct the user in the following three areas:

1. Provide the steps and procedures required for mixture and test specimen preparation,
2. Provide a procedure for determining or selecting the test temperature and stress state to be used for the climate and pavement structure at a specific site, and
3. Provide the criteria for determining the adequacy of the HMA mixture for site-specific conditions.

The first area has been completed as the initial part of Task C. The second part of Task C will finalize details of the test

protocol, including development of design or evaluation criteria, or both, and field validation of the SPT.

6.1.4 Time Estimates for SPT Test Methods

Table 46 summarizes the amount of time to perform the test methods recommended for the SPT for design and quality control (Appendixes A through E). As shown, most of the tests can be completed within 3 days in support of the Superpave volumetric mix design procedure and within 2 days for quality control with the exception of the dynamic modulus at five test temperatures. That time period is considered acceptable for mixture design, but unacceptable for quality-control operations. Reducing the time for quality-control operations will be a goal of future activities under Task C.

6.2 DEVELOPMENT OF SPT CRITERIA

Although the goal of the SPT is to identify inferior mixtures and not to predict the entire performance history of the mixture, a model will be needed to develop the criteria for different conditions. Many distress-prediction models are available for use. However, compatibility with structural design methods is important to minimize the confusion that might occur in industry if different models are used for mixture design and structural design. To integrate mixture and structural designs, the SPT criteria will be derived from the same models being enhanced for the 2002 Guide for the Design of New and Rehabilitated Pavement Structures as a part of NCHRP Project 1-37A (10). The following lists key issues related to developing the mix analysis criteria in support of volumetric mixture design.

1. The 2002 Guide for the Design of New and Rehabilitated Pavement Structures distress-prediction models will be used to determine the amount of rutting, fatigue cracking, and thermal cracking in the HMA mixture under

TABLE 46 Time estimate for the SPTs recommended for further study

	Laboratory Activity	Estimated Time for Lab Prepared Specimens	Estimated Time for QC/QA Mix Specimens
Sample Preparation	1. Dry Aggregates	Overnight	—
	2. Aggregate Stockpile Breakdown into Individual Sieve Sizes	1 Day	—
	3. Batching \approx 6,500 Samples	15 min	—
	4. Heat Batched Aggregates	Overnight	—
	5. Heat Binder	\approx 2 h	—
	6. Mixing	10 min	—
	7. Aging	4 h	Heat mix, 2 h
	8. Compaction	20 min	20 min
	9. Extraction from Mold	1 h	1 h
	10. Cooling to Room Temperature	Overnight	Overnight
	11. Sawing and Coring	30 min	30 min
	12. Get Wet and SSD Weights	5 min	5 min
	13. Dry Core	Overnight	Overnight
	14. Get Dry Weight	1 min	1 min
	Total Sample Preparation Time	2 Days	4 H
Testing Preparation	1. Glue Studs (Not Needed for RaTT Device)	30 min	30 min
	2. Mount LVDT Brackets (Not Needed for RaTT Device)	10 min	10 min
	3. Place in Environmental Chamber at Test Temperature	2–3 h	2–3 h
	4. Place LVDTs on Sample & Prepare for Test	10 min	10 min
	Total Testing Preparation Time	4 Hours	4 H
SPT Testing	1. Dynamic Modulus Test for One Temperature, All Frequencies	20 min	20 min
	2. Dynamic Modulus Test at Five Temperatures, All Frequencies	3 days	3 days
	3. Static Creep/Flow Time Test	10–60 min	10–60 min
	4. Repeated Load Permanent Deformation Test	30–180 min	30–180 min
	Total Testing Time	Variable	Variable

- specific conditions. These models will be used to determine the criteria to be used in identifying mixtures that are susceptible to permanent deformation and fracture. Calibration and validation of these distress-prediction models are being completed under NCHRP Project 1-37A for both new and rehabilitated pavements.
- The rutting model will be used to predict not only one-dimensional densification, but also the lateral displacement of the mix and tertiary flow. Both types of rutting will be considered in the criteria development. Accurate calibration of the rutting model is being completed under NCHRP Project 1-37A.
 - The amount of fatigue cracks that initiate at the top and propagate downward, as well as the traditional bottom-initiated cracks that propagate to the surface, will be predicted and considered in the criteria development.

- Accurate calibration of the fatigue-cracking model is being completed under NCHRP Project 1-37A.
- The thermal-cracking model is being revised under NCHRP Project 9-19. The revised thermal-cracking model is being recalibrated under NCHRP 9-19 to update the model parameters. This effort is substantiated by the significant improvements that will be made to the model, particularly in the interpretation of laboratory test data and in the development of the master creep compliance relationship for HMA mixtures. The recalibrated model will be used to develop the criteria for the SPT.
 - The pavement temperature regime (i.e., the environmental zone) is a major consideration for permanent deformation in HMA mixtures because it influences the viscoelastic and viscoplastic properties of the mixtures.

Temperature will be included as a key factor in developing the criteria for permanent deformation and fracture. The temperature-equivalency concept will be used to determine the test temperature for the SPT.

6. HMA layer thickness, insofar as it influences the magnitudes of stress and strain in the HMA layer, also has relevance to permanent deformation and fracture. The total HMA layer thickness not only influences strain and stress magnitude, but is also linked to the location where fatigue cracks initiate (i.e., at the bottom of the HMA layer or at the surface). Thus, total HMA thickness is considered a key factor in developing the evaluation criteria.
7. Similar to the HMA layer thickness noted above, pavement type and rehabilitation strategy are additional factors for checking the magnitudes of stress and strain in the HMA mixture and failure hypothesis.
8. Traffic will be considered in the design criteria and will be compatible with the Superpave mix design traffic categories.
9. The modulus and strength of the supporting pavement layers will be considered in the criteria development as they related to the occurrence of fatigue cracks and, to a lesser extent, rutting.

6.3 FIELD VALIDATION OF THE SPT

The first major element of Task C was to select the best test methods and responses for the SPT. The second major element of Task C is the field validation of the SPT and evalua-

tion criteria. The goal of most validation plans is to determine whether (1) the conceptual model or test protocol is a reasonable representation of the real-world system and (2) the desired accuracy exists between the laboratory (i.e., test protocol) and the real-world system. In fact, the validation of the SPT is considered by industry to be the most important product of NCHRP Project 9-19.

NCHRP and the project team recognize that the long-term field validation of the SPT protocol is critically important to its final acceptance and implementation in day-to-day Superpave mix design practice. Thus, a field validation effort is needed and planned for finalizing the test protocols and criteria. The goal of the field validation plan is to provide a reliable, fully evaluated test protocol that can be used in support of the Superpave volumetric design procedure.

One of the most time-consuming, expensive, and high-risk activities associated with validating pavement-performance models is the collection of field performance data on a substantial number of test sections. Field performance data is required for validating the SPT, Superpave mechanistic distress-prediction models, the new *2002 Guide for the Design of New and Rehabilitated Pavement Structures (10)* based on mechanistic-empirical principles, and other hypotheses formulated from the LTPP program.

Coordination of the data collection activities between projects can substantially reduce the number of test sections that will be required if each project is conducted independently. Thus, the field validation plan for the SPT protocol and evaluation criteria will use the LTPP SPS-9 experimental projects and as many of the test sections as possible that are being used on the other projects.

CHAPTER 7

RECOMMENDATIONS AND FUTURE ACTIVITIES

7.1 SUMMARY AND RECOMMENDATIONS

This report presents the initial results of a comprehensive research study to identify an SPT or a set of SPTs for use with the Superpave volumetric mix design method. It describes the selection of the best candidate simple performance test method–response parameter combinations through a detailed laboratory evaluation of actual HMA materials obtained from three major U.S. accelerated pavement testing (APT) projects: MnRoad, FHWA-ALF, and WesTrack.

The research assessed how well the measured results of 33 combinations of SPTs and associated laboratory response parameters correlated with the degree of distress observed within each experimental test section in the three APT projects. Three major distress types were evaluated in this study. Rutting (i.e., permanent deformation) within the HMA layer was present at all three field projects. Load-associated fatigue cracking was found at the ALF and WesTrack projects, although the fatigue experiment at the former project yielded limited results because of the small number of test sections used (i.e., two levels of thickness and two levels of asphalt concrete stiffness–modulus). Transverse thermal fracture-associated low-temperature cracking only occurred at the MnRoad project. The actual effort expended by the research team for each distress was in relative proportion to the distress’s generally acknowledged importance, that is, HMA rutting, load-associated fatigue fracture, and low-temperature cracking, in that order.

The initial recommendations of the research team were reviewed by the NCHRP project panel, and the following SPT method–response parameter combinations were selected for comprehensive field validation in the next phase of the project.

- **HMA Rutting** (testing conducted at 100 to 130°F):
 - The dynamic complex modulus term, $E^*/\sin\phi$, determined from the triaxial dynamic modulus test;
 - The flow time, F_t , determined from the triaxial static creep test; and
 - The flow number, F_n , determined from the triaxial repeated load test.
- **HMA Fatigue Cracking** (testing conducted at 40 to 60°F):
 - The dynamic complex modulus, E^* , determined from the triaxial dynamic modulus test.

- **HMA Low-Temperature Cracking** (testing conducted at 0, –10, and –20°C):
 - The indirect tensile creep compliance, $D(t)$, determined from the indirect tensile creep test.

Preliminary draft protocols for these SPTs are presented in the appendixes to this report.

7.2 FUTURE ACTIVITIES

In the next phase of the project, the SPT method–response parameter combinations shown in Section 7.1 will be further validated using HMA materials and performance data from 50 to 75 pavement sections in the FHWA LTPP Special Pavement Study and similar full-scale field performance experiments. Based on these results, a final recommendation will be made of SPT method–response parameter combinations to estimate the susceptibility of an HMA mix design to rutting, fatigue cracking, and low-temperature cracking. Recommendations will include proposed specification criteria developed with the HMA performance models in the *2002 Guide for the Design of New and Rehabilitated Pavement Structures (10)* and recommended test methods in AASHTO standard format for future review and possible adoption by state highway agencies.

In addition to the main field validation effort, four ancillary studies will be conducted toward the goals of simplifying the SPTs and making them as practical as possible. These studies are briefly described in the following sections.

7.2.1 Specimen Diameter Study: 4-in. (100-mm) Versus 6-in. (150-mm)

A major cost in testing time and equipment expense arises from the need to core and saw 4-in.-diameter SPT samples from 6-in.-diameter gyratory-compacted specimens routinely manufactured in the current Superpave mix design process.

This sample preparation was based on the conclusions of an extensive study on sample geometry and aggregate size conducted during NCHRP Project 9-19. It was found that (1) a minimum height-to-diameter ratio of 1.5 was required in order to ensure that the response of a sample evaluated in either the dynamic modulus or permanent deformation tests

represents a fundamental engineering property; (2) a minimum sample diameter of 4 in. (100 mm) would be satisfactory for all HMA mixtures up to a maximum aggregate size of 1.5 in. (37.5 mm); and (3) smooth, parallel specimen ends were needed to eliminate end friction and violation of the theoretical boundary effects of the specimen during the test. Another factor discouraging the use of the 6-in.-diameter specimens is that numerous studies have illustrated the large degree of nonhomogeneity of air voids within the larger gyratory-compacted specimens. This variability, and its subsequent impact upon the variability of the SPT results, is significantly larger than the variability found when the smaller 4-in.-diameter cored-and-sawn specimens are used.

This ancillary study will determine whether a constant multiplier can be found between SPT results obtained on 4-in.-diameter and 6-in.-diameter specimens. Although the utility of using the 4-in.-diameter specimen for the fundamental response cannot be argued, it is also apparent that if an accurate common-multiplying factor can be determined for SPTs at differing diameters, the significant decrease in sample test time and equipment cost over using the 4-in.-diameter cored-and-sawn specimens will be a major consideration in the eventual selection of the final SPT protocol.

7.2.2 Dynamic Complex Modulus Study: Flexural Versus Compressive Testing

All of the SPTs used for the rutting and load-associated fatigue cracking distress are based on the use of 4-in.-diameter by 6-in.-high specimens tested in a uniaxial or triaxial compressive mode. Although this specimen geometry is very compatible with the use of gyratory-compacted specimens in volumetric mix design, it does present problems if the SPTs are used for forensic investigations of existing pavements, either to prepare for the rehabilitation or to identify specific causes of premature distress. Generally, pavements do not incorporate single, 6-in.-high HMA layers, so obtaining a specimen with the appropriate height-to-diameter ratio for the SPT is nearly impossible.

This ancillary study will investigate whether the dynamic complex modulus measured in compression on 4-in.-diameter by 6-in.-high specimens can be correlated to the modulus values measured from flexural beam stiffness testing. If a true

equivalence between the two tests exists, beam testing can be used with the appropriate SPT specification criteria to estimate the performance characteristics of the existing HMA pavement.

7.2.3 Sensitivity Study: SPT Response Parameter and Magnitude

This ancillary study will investigate the sensitivity of candidate SPT response parameters to key HMA mixture properties. For example, if the SPT response parameter chosen to measure HMA rutting does not significantly change as a function of the amount of asphalt cement in the mix, the accuracy of the SPT as an indicator of performance and distress will be suspect.

The study will focus on the sensitivity of the SPT response parameter as a function of the air voids and asphalt binder contents (V_a and V_b) in both confined and unconfined testing. If time and resources allow, the sensitivity of the response parameters to other mix variables such as asphalt-binder type, aggregate gradation, and aggregate type will also be investigated.

7.2.4 Tertiary Flow Measurement Methods Study

The SPTs based on the triaxial repeated load and triaxial static creep tests use the point of initiation of tertiary flow in the HMA mixture to determine its flow number (F_n) and flow time (F_t), respectively. The tertiary phase is easily distinguishable from the secondary phase in both the repeated loading and static creep tests by comparing the first derivatives (i.e., rates of change) of the test-response parameters. These deformation measurements commonly use vertical-mounted LVDTs to measure the deformation of the test specimens under load. However, there is some evidence that identical flow numbers and times can be generated by assessing the rate response of radial-mounted LVDTs.

This ancillary study will investigate the feasibility of defining the flow time, flow number, or both, of an HMA mixture from measurements made with radial LVDTs and the load ram actuator as well as with vertical LVDTs. The purpose is to find the simplest practical way to determine the flow time and flow number with the respective SPTs.

REFERENCES

1. Leahy, R.B., E.T. Harrigan, and H. Von Quintus. *Validation of Relationships Between Specification Properties and Performance*. Report No. SHRP-A-409. Transportation Research Board, National Research Council, Washington, DC (1994).
2. *Mix Design Methods for Asphalt Concrete and Other Hot-Mix Types*. 6th edition. The Asphalt Institute, Lexington, KY (1997).
3. "Preliminary Recommendations for the Simple Performance Test," Interim Task C Report, FHWA Contract DTFH61-95-C-00100. University of Maryland, College Park, MD (1998).
4. Cominsky, R.J., B.M. Killingsworth, R.M. Anderson, D.A. Anderson, and W.M. Crockford. *NCHRP Report 409: Quality Control and Acceptance of Superpave-Designed Hot Mix Asphalt*. Transportation Research Board, National Research Council, Washington, DC (1998).
5. Witczak, M.W., D. Andrei, and W. Mirza. "Development of Revised Predictive Model for the Dynamic (Complex) Modulus of Asphalt Mixtures," Interteam Technical Report, NCHRP Project 1-37A, University of Maryland, March 1999.
6. Bonnaure, F., G. Gest, A. Garvois, and P. Uge. "A New Method of Predicting the Stiffness of Asphalt Paving Mixes," *Journal of the Association of Asphalt Paving Technologists*, Vol. 46 (1977).
7. Drucker, D.C. "Limit Analysis of Two- and Three-Dimensional Soil Mechanics Problems," *Journal of Mechanics and Physical Solids*, Vol. 1 (1953).
8. Hafez, I. "Development of a Simplified Asphalt Mix Stability Procedure for Use in Superpave Volumetric Mix Design." Ph.D. Dissertation, Civil Engineering Department, University of Maryland, College Park, MD (1997).
9. Witczak, M.W., M.W. Mirza, and K. Kaloush. "Compliance Model Development," NCHRP Project 1-37A Interim Report University of Maryland, College Park, MD (1997).
10. ERES Consultants, Inc. "Development of 2002 Guide for the Design of New and Rehabilitated Pavement Structures—Stage A Report," NCHRP Project 1-37A Interim Report (1999).
11. ERES Consultants, Inc. "LTPP Data Analysis Technical Assistance," FHWA Contract DTFH61-96-C-00003, Washington, DC (2002).
12. Von Quintus, H.L., J.A. Scherocman, C.S. Hughes, and T.W. Kennedy. *NCHRP Report 338: Asphalt-Aggregate Mixture Analysis System: AAMAS*. Transportation Research Board, National Research Council, Washington, DC (1991).
13. Witczak, M.W., and M.W. Mirza. "Development of Relationships to Predict Poisson's Ratio for Paving Materials," Interteam Technical Report for NCHRP 1-37A. University of Maryland, College Park, MD (1999).
14. Roque, R., R.L. Lytton, J. Uzan, E.G. Fernando, D. Hiltunen, and S.M. Stoffels. *Development and Validation of Performance Prediction Models and Specifications for Asphalt Binders and Paving Mixes*. Report No. SHRP-A-357, Transportation Research Board, National Research Council, Washington, DC (1993).
15. Witczak, M.W., M. El-Basyouny, and M.W. Mirza. "Indirect Tensile Strength Test," NCHRP Project 9-19, Task C. Team Report SPT-MN-2(A) (MnRoad Experiment), Arizona State University, Tempe, AZ (1999).
16. Witczak, M.W., M. El-Basyouny, and M.W. Mirza. "Indirect Creep Test," Team NCHRP Project 9-19, Task C. Report SPT-MN-2(B) (MnRoad Experiment), Arizona State University, Tempe, AZ (1999).
17. Witczak, M.W., M. El-Basyouny, and M.W. Mirza. "Indirect Fatigue Tests," NCHRP Project 9-19, Task C. Team Report SPT-MN-2(C) (MnRoad Experiment), Arizona State University, Tempe, AZ (1999).
18. Witczak, M.W., S.H. Cardoso, and K. Kaloush. "Triaxial Strength Test," NCHRP Project 9-19, Task C. Team Report SPT-MN-2(D) (MnRoad Experiment), Arizona State University, Tempe, AZ (1999).
19. Witczak, M.W., S.H. Cardoso, and T. Pellinen. "G*-Field Shear Test (FST)," NCHRP Project 9-19, Task C. Team Report SPT-MN-2(E) (MnRoad Experiment), Arizona State University, Tempe, AZ (1999).
20. Witczak, M.W., R. Bonaquist. "G*-Simple Shear Tests (SST)," NCHRP Project 9-19, Task C. Team Report SPT-MN-2(F) (MnRoad Experiment), Arizona State University, Tempe, AZ (1999).
21. Witczak, M.W., G. Huber, and X. Zhang. "Repeated Shear Permanent Deformation Tests," NCHRP Project 9-19, Task C. Team Report SPT-MN-2(G) (MnRoad Experiment), Arizona State University, Tempe, AZ (1999).
22. Witczak, M.W., and K. Kaloush. "Repeated Normal Permanent Deformation Tests," NCHRP Project 9-19, Task C. Team Report SPT-MN-2(H) (MnRoad Experiment), Arizona State University, Tempe, AZ (1999).
23. Witczak, M.W., and K. Kaloush. "Triaxial Static Creep Test (Flow and Compliance)," NCHRP Project 9-19, Task C. Team Report SPT-MN-2(I) (MnRoad Experiment), Arizona State University, Tempe, AZ (1999).
24. Witczak, M.W., and T. Pellinen. "E*-Dynamic Complex Modulus and Ed-Dynamic Pulse Wave Velocity Tests," NCHRP Project 9-19, Task C. Team Report SPT-MN-2(J-K) (MnRoad Experiment), Arizona State University, Tempe, AZ (1999).
25. Witczak, M.W., T. Pellinen, and D. Andrei. "E* and Sm Prediction Equation Methodology Results," NCHRP Project 9-19, Task C. Team Report SPT-MN-2(L) (MnRoad Experiment), Arizona State University, Tempe, AZ (1999).
26. Witczak, M.W., M. El-Basyouny, and M.W. Mirza. "Indirect Tensile Strength Test," NCHRP Project 9-19, Task C. Team Report SPT-ALF-2(A) (ALF Experiment), Arizona State University, Tempe, AZ (2000).
27. Witczak, M.W., M. El-Basyouny, and M.W. Mirza. "Indirect Creep Test," NCHRP Project 9-19, Task C. Team Report SPT-ALF-2(B) (ALF Experiment), Arizona State University, Tempe, AZ (2000).
28. Witczak, M.W., M. El-Basyouny, and M.W. Mirza. "Indirect Fatigue Tests," NCHRP Project 9-19, Task C. SPT-ALF-2(C) (ALF Experiment), Arizona State University, Tempe, AZ (2000).
29. Witczak, M.W., Cardoso, S.H., and K. Kaloush. "Triaxial Strength Test," NCHRP Project 9-19, Task C. Team Report SPT-ALF-2(D) (ALF Experiment), Arizona State University, Tempe, AZ (2000).

30. Witczak, M.W., and R. Bonaquist. "G*-Simple Shear Tests (SST)," NCHRP Project 9-19, Task C. Team Report SPT-ALF-2(F) (ALF Experiment), Arizona State University, Tempe, AZ (2000).
 31. Witczak, M.W., G. Huber, and X. Zhang. "Repeated Shear Permanent Deformation Tests," NCHRP Project 9-19, Task C. Team Report SPT-ALF-2(G) (ALF Experiment), Arizona State University, Tempe, AZ (2000).
 32. Witczak, M.W., and K. Kaloush. "Repeated Normal Permanent Deformation Tests," NCHRP Project 9-19, Task C. Team Report SPT-ALF-2(H) (ALF Experiment), Arizona State University, Tempe, AZ (2000).
 33. Witczak, M.W., and K. Kaloush. "Triaxial Static Creep Test (Flow and Compliance)," NCHRP Project 9-19, Task C. Team Report SPT-ALF-2(I) (ALF Experiment), Arizona State University, Tempe, AZ (2000).
 34. Witczak, M.W., and T. Pellinen. "E*-Dynamic Complex Modulus and Ed-Dynamic Pulse Wave Velocity Tests," NCHRP Project 9-19, Task C. Team Report SPT-ALF-2(J-K) (ALF Experiment), Arizona State University, Tempe, AZ (2000).
 35. Witczak, M.W., and T. Pellinen. "E* and Sm Prediction Equation Methodology Results," NCHRP Project 9-19, Task C. Team Report SPT-ALF-2(L) (ALF Experiment), Arizona State University, Tempe, AZ (2000).
 36. Witczak, M.W., M. El-Basyouny, and M.W. Mirza. "Indirect Tensile Strength Test," NCHRP Project 9-19, Task C. Team Report SPT-WST-2(A) (WesTrack Experiment), Arizona State University, Tempe, AZ (2000).
 37. Witczak, M.W., M. El-Basyouny, and M.W. Mirza. "Indirect Creep Test," NCHRP Project 9-19, Task C. Team Report SPT-WST-2(B) (WesTrack Experiment), Arizona State University, Tempe, AZ (2000).
 38. Witczak, M.W., M. El-Basyouny, and M.W. Mirza. "Indirect Fatigue Tests," NCHRP Project 9-19, Task C. Team Report SPT-WST-2(C) (WesTrack Experiment), Arizona State University, Tempe, AZ (2000).
 39. Witczak, M.W., S.H. Cardoso, and K. Kaloush. "Triaxial Strength Test," NCHRP Project 9-19, Task C. Team Report SPT-WST-2(D) (WesTrack Experiment), Arizona State University, Tempe, AZ (2000).
 40. Witczak, M.W., R. Bonaquist "G*-Simple Shear Tests (SST)," NCHRP Project 9-19, Task C. Team Report SPT-WST-2(F) (WesTrack Experiment), Arizona State University, Tempe, AZ (2000).
 41. Witczak M.W., G. Huber, and X. Zhang. "Repeated Shear Permanent Deformation Tests," NCHRP Project 9-19, Task C. Team Report SPT-WST-2(G) (WesTrack Experiment), Arizona State University, Tempe, AZ (2000).
 42. Witczak, M.W., and K. Kaloush. "Repeated Normal Permanent Deformation Tests," NCHRP Project 9-19, Task C. Team Report SPT-WST-2(H) (WesTrack Experiment), Arizona State University, Tempe, AZ (2000).
 43. Witczak, M.W., and K. Kaloush. "Triaxial Static Creep Test (Flow and Compliance)," NCHRP Project 9-19, Task C. Team Report SPT-WST-2(I) (WesTrack Experiment), Arizona State University, Tempe, AZ (2000).
 44. Witczak, M.W., and T. Pellinen. "E*-Dynamic Complex Modulus and Ed-Dynamic Pulse Wave Velocity Tests," NCHRP Project 9-19, Task C. Team Report SPT-WST-2(J-K) (WesTrack Experiment), Arizona State University, Tempe, AZ (2000).
 45. Witczak, M.W., and T. Pellinen. "E* and Sm Prediction Equation Methodology Results," NCHRP Project 9-19, Task C. Team Report SPT-MN-2(L) (WesTrack Experiment), Arizona State University, Tempe, AZ (2000).
 46. Method for Preparation of Triaxial Specimens (Test Protocol UMD 9808), "Superpave Models Team Inter-Laboratory Testing Manual." University of Maryland, College Park, MD (1998).
 47. Witczak, M.W., R. Bonaquist, H. Von Quintus, and K. Kaloush. "Specimen Geometry and Aggregate Size Lab Test Study," NCHRP Project 9-19, Task C. Team Report SLS-3, Arizona State University, Tempe, AZ (1999).
 48. Azari, H., M.W. Witczak, and W. Mirza. "Development of Predictive Model for Asphalt Concrete Phase Angle," Interteam Technical Report, NCHRP Project 1-37A, University of Maryland, April 1999.
-

GLOSSARY

ABBREVIATIONS

AC = asphalt concrete
 ALF = accelerated loading facility, Turner–Fairbanks
 APT = accelerated pavement testing
 F or FC = fatigue cracking
 FSCH = frequency sweep at constant height test
 FST = field shear tester
 HMA = hot mix asphalt
 IDT = indirect tensile
 LTPP = long-term pavement performance
 LVDT = linear variable differential transducer
 MESAL = million equivalent single axle load
 PG = performance grade
 QC = quality control
 R = rutting or rut depth
 RSCH = repeated shear at constant height test
 SGC = Superpave gyratory compactor
 SHRP = Strategic Highway Research Program
 SPT = simple performance test
 SSCH = simple shear at constant height test
 SSD = surface saturated dry test method
 SST = Superpave shear tester
 T or TC = thermal cracking

NOTATIONS

a = intercept
 a, b = mixture permanent deformation parameters, regression coefficients from the secondary portion of the cumulative permanent deformation curve
 a, m = materials regression coefficients from the viscoelastic compliance function
 a, b, d = integration constants for the indirect tensile test that are specimen geometry dependent
 b = slope
 c = cohesion or intercept parameter from a triaxial shear strength test
 d = diameter of the test specimen
 D = density
 D' = viscoelastic compliance component at any time
 D_o = instantaneous compliance
 $D(t)$ = total compliance at any time
 D_1, m_1 = mixture compliance parameters or regression coefficients from an indirect tensile creep test

E = modulus of elasticity or Young's modulus
 E^* = complex modulus
 $|E^*|$ = dynamic modulus
 E' = storage or elastic modulus
 E'' = loss or viscous modulus
 E_d = elastic modulus
 E_R = resilient modulus
 f = loading frequency
 F_n = flow number from a repeated load permanent deformation test
 F_t = flow time from a static creep test
 $g = 32.19 \text{ ft/s}^2$
 G^* = shear complex modulus
 $|G^*|$ = shear dynamic modulus
 G' = shear storage modulus
 G'' = shear loss or viscous modulus
 i = imaginary unit from the complex modulus test
 I_1 = first invariant stress tensor
 J_2 = second invariant deviatoric stress tensor
 k = intercept parameter of the Drucker–Prager failure envelope
 K_1, K_2 = regression coefficients or constants from a repeated load fatigue test
 L = distance between the transducers for an ultrasonic wave propagation test
 m = slope
 n = sample size or number of test specimens
 N = number of loading cycles
 N_f = number of loading cycles to failure, fracture life
 N_{50} = number of loading cycles to a 50 percent reduction in the modulus of a test specimen during a fatigue test
 P = applied load
 R^2 = coefficient of determination
 S_i = indirect tensile strength
 S_e = standard error
 S_y = standard deviation of the criterion variable
 S_b = binder modulus for the Shell Oil predictive equation

Sm = HMA mixture modulus from the Shell Oil predictive equation	ε_{ff} = horizontal tensile strain at failure from an indirect tensile test
t = thickness of the test specimen	Γ_{fr} = total fracture energy
t = time	Γ_{fa} = fracture energy to failure
t_i = time lag between a cycle of stress and strain	η = bitumen viscosity
t_p = time for a stress cycle	ρ = density
T = effective transit time for an ultrasonic wave propagation test	ρ_4 = cumulative percentage retained on 4.76-mm sieve
V = pulse velocity from an ultrasonic wave propagation test	ρ_{34} = cumulative percentage retained on 19-mm sieve
V_a = air void content in HMA mixtures, %	ρ_{38} = cumulative percentage retained on 9.5-mm sieve
V_b = volume of bitumen	ρ_{200} = percentage passing the 0.075-mm sieve
V_{beff} = effective bitumen content, % by volume	ϕ = slope of the failure envelope or the angle of internal friction from a triaxial shear strength test
V_g = volume of aggregate	ϕ = phase angle from the complex modulus test
α, μ = plastic or permanent deformation parameters from a repeated load test	γ = slope of the Drucker–Prager failure envelope
β_1 – β_4 = regression constants in the Shell Oil predictive equation	γ = shear strain
δ_{xx} = horizontal deformation across the test specimen from an indirect tensile test	γ_o = peak shear strain amplitude
ε = normal strain	γ_p = plastic shear strain
ε_e = elastic strain, recoverable and time-independent	γ_r = resilient or recoverable shear strain
ε_o = recoverable axial strain	σ_o = dynamic stress
ε_p = cumulative permanent or plastic strain, irrecoverable and time-independent	σ = normal stress
ε_r = resilient or recoverable axial strain	σ_{xx} = horizontal tensile stress in an indirect tensile test specimen
ε_T = total strain	τ = shear stress
ε_{ve} = viscoelastic strain, recoverable and time-dependent	τ_o = peak shear stress amplitude
ε_{vp} = viscoplastic strain, irrecoverable and time-dependent	μ = Poisson's ratio
ε_{xx} = horizontal tensile strain in an indirect tensile test specimen	v = number of regression coefficients
	v_{cl} = velocity of sound

APPENDIX A

TEST METHOD FOR DYNAMIC MODULUS OF ASPHALT CONCRETE MIXTURES FOR PERMANENT DEFORMATION

1. Scope

- 1.1 This test method covers procedures for preparing and testing asphalt concrete mixtures to determine the dynamic modulus and phase angle at a single effective temperature T_{eff} and design loading frequency.
- 1.2 This test method is a part of test protocols that include determination of the dynamic modulus of the asphalt mix for paving purposes. The other test methods are Standard Test Method for Simple Performance Test for Fatigue Cracking based Upon Dynamic Modulus of Asphalt Concrete Mixture and Standard Test Method for Dynamic Modulus of Asphalt Concrete Mixtures, which is for constructing a master curve for characterizing asphalt concrete for pavement thickness design and performance analysis.
- 1.3 This standard is applicable to laboratory-prepared specimens of mixtures with nominal maximum size aggregate less than or equal to 37.5 mm (1.5 in).
- 1.4 *This standard may involve hazardous material, operations, and equipment. This standard does not purport to address all safety problems associated with its use. It is the responsibility of the user of this procedure to establish appropriate safety and health practices and to determine the applicability of regulatory limitations prior to use.*

2. Referenced Documents

2.1 AASHTO Standards

- | | |
|------|---|
| TP4 | Method for Preparing and Determining the Density of Hot Mix Asphalt (HMA) Specimens by Means of the SHRP Gyratory Compactor |
| PP2 | Practice for Mixture Conditioning of Hot Mix Asphalt (HMA) |
| T67 | Standard Practices for Load Verification of Testing Machines (cross-listed with ASTM E4) |
| T269 | Percent Air Voids in Compacted Dense and Open Bituminous Paving Mixtures |

3. Definitions

- 3.1 *Dynamic Modulus*— $|E^*|$, the norm value of the complex modulus calculated by dividing the peak-to-peak

stress by the peak-to-peak strain for a material subjected to a sinusoidal loading.

- 3.2 *Complex Modulus*— E^* , a complex number that defines the relationship between stress and strain for a linear viscoelastic material.
- 3.3 *Phase angle*— δ , the angle in degrees between a sinusoidally applied stress and the resulting strain in a controlled-stress test.
- 3.4 *Linear viscoelastic*—within the context of this test, refers to behavior in which the dynamic modulus is independent of stress or strain amplitude.
- 3.5 *Effective Temperature* T_{eff} —Is a single test temperature at which an amount of permanent deformation would occur equivalent to that measured by considering each season separately throughout the year.

4. Summary of Method

- 4.1 A sinusoidal (haversine) axial compressive stress is applied to a specimen of asphalt concrete at a given temperature and loading frequency. The applied stress and the resulting recoverable axial strain response of the specimen is measured and used to calculate the dynamic modulus and phase angle.
- 4.2 Figure 1 presents a schematic of the dynamic modulus test device.

5. Significance and Use

- 5.1 Dynamic modulus values, measured at one effective temperature T_{eff} and one design frequency selected by the design engineer, are used as performance criteria for permanent deformation resistance of the asphalt concrete mixture to be used in conjunction with the Superpave Volumetric Mix Design Method.

Note 1—The effective temperature T_{eff} covers approximately the temperature range of 25 to 60°C (77 to 140°F).

Note 2—10 Hz frequency can be used for highway speed and 0.1 Hz for creep—intersection traffic.

- 5.2 Dynamic modulus values measured over a range of temperatures and frequencies of loading can be shifted

into a master curve for characterizing asphalt concrete for pavement thickness design and performance analysis.

- 5.3 This test method covers the determination of the dynamic modulus values measured unconfined within the linear viscoelastic range of the asphalt mixture.

Note 3—Future research may indicate the need for confined stress states and nonlinear material characterization. Confinement may be applied with various types of axisymmetric triaxial cells to address these needs.

6. Apparatus

- 6.1 Dynamic Modulus Test System—A dynamic modulus test system consisting of a testing machine, environmental chamber, measuring system, and specimen end fixtures.

- 6.1.1 *Testing Machine*—A materials testing machine capable of producing a controlled haversine compressive loading of paragraphs 9.7 and 9.8 is required.

Note 4—The testing machine shall have a capability of applying load over a range of frequencies from 0.1 to 30 Hz. Stress levels up to 2800 kPa (400 psi) may be required at certain temperatures and frequencies. However, for virtually all effective temperatures in the US, stress levels between 10 kPa and 690 kPa (1.5–100 psi) have been found to be sufficient. This latter range of stress levels converts to an approximate range of 0.08–5.5 kN (18–1218 lbf) on a 100 mm diameter specimen. If the machine is to be dedicated only to this test procedure with no requirement for additional strength testing or low temperature testing, it is recommended that the lowest capacity machine capable of applying the required waveforms be used. Alternatively, larger capacity machines may be used with low capacity load cells or signal amplifiers. It has been found that feedback controlled testing machines equipped with appropriate servovalves can be used for this test. As a general rule of thumb, the dynamic load capacity of a testing machine between 10 and 30 Hz will be approximately 65–75 percent of the monotonic (“static”) capacity, but this rule varies by manufacturer. A 25–50 kN capacity servohydraulic testing machine has been found to be adequate for virtually all of the tests in the suite of simple performance tests.

- 6.1.2 *Environmental Chamber*—A chamber for controlling the test specimen at the desired tempera-

ture is required. The environmental chamber shall be capable of controlling the temperature of the specimen over a temperature range from 25 to 60°C (77 to 140°F) to an accuracy of $\pm 0.5^\circ\text{C}$ (1°F). The chamber shall be large enough to accommodate the test specimen and a dummy specimen with temperature sensor mounted at the center for temperature verification.

Note 5—A chamber that will control temperatures down to -10°C (14°F) may be required for other tests mentioned in paragraph 1.2 of this method.

Note 6—If the chamber does not have sufficient room for a dummy specimen, it is permissible to have a second chamber controlling the temperature of the dummy. The separate dummy chamber must be operated similar to the operation of the main test specimen chamber so that the dummy will accurately register the time required to obtain temperature equilibrium on the test specimen.

- 6.1.3 *Measurement System*—The system shall include a data acquisition system comprising analog to digital conversion and/or digital input for storage and analysis on a computer. The system shall be capable of measuring and recording the time history of the applied load and the axial deformations for the cycles required by this test method. The system shall be capable of measuring the period of the applied sinusoidal load and resulting deformations with a resolution of 0.5 percent.

- 6.1.3.1 *Load*—The load shall be measured with an electronic load cell having adequate capacity for the anticipated load requirements. The load cell shall be calibrated in accordance with AASHTO T67. The load measuring transducer shall have an accuracy equal to or better than 0.25 percent of full scale.

Note 7—A 25 kN (5600 lbf) load cell has been found to be the approximate maximum capacity limit for this test method because of range versus resolution factors. It is recommended that if the selected load cell capacity is 25 kN or greater, the system should be equipped with either manual or automatic amplification selection capability so that it can be used to enhance control of the system at the minimum anticipated loads given in paragraph 9.7.

Axial Deformations—Axial deformations shall be measured with displacement transducers referenced to gauge points contacting the specimen as shown in Figure 2. The deformations shall be measured at a minimum of two locations 180°

apart (in planview); however, three locations located 120° apart is recommended to minimize the number of replicate specimens required for testing.

Note 8—Analog transducers such as linear variable differential transformers (LVDTs) having a range of ± 0.5 mm (0.02 in) and inherent nonlinearity equal to or better than ± 0.025 percent of full scale have been found adequate for this purpose. Software or firmware linearization techniques may be used to improve the inherent nonlinearity. Amplification and signal conditioning techniques may be used with the ± 0.5 mm range LVDTs to obtain resolutions down to 0.001 mm (0.00004 in) or better for small strain tests conditions. These techniques may be manual or automatic. In general, increasing the resolution by manual signal amplification will result in reduction of the overall range of the instrument by the same factor.

6.1.4 *Loading Platens*—Platens, with a diameter equal to or greater than that of the test specimen are required above and below the specimen to transfer the load from the testing machine to the specimen. Generally, these platens should be made of anodized high strength aluminum. Softer materials will require more frequent replacement. Materials that have linear elastic modulus properties and hardness properties lower than that of 6061-T6 aluminum shall not be used. Steel platens may cause too much seating load to the specimen at high temperature and are not recommended.

6.1.5 *End Treatment*—Friction reducing end treatments shall be placed between the specimen ends and the loading platens.

Note 9—End treatments consisting of two 0.5 mm (0.02 in) thick latex sheets separated with silicone grease have been found to be suitable friction reducing end treatments.

6.2 *Gyratory Compactor*—A gyratory compactor and associated equipment for preparing laboratory specimens in accordance with AASHTO TP4 shall be used. Field cores shall meet the requirements of paragraphs 7.4 through 7.6 of this test method and any reports on cores so tested will contain a detailed description of the location of any lift boundaries within the height of the specimen (e.g. lift order, thickness and material homogeneity).

6.3 *Saw*—A machine for cutting test specimens to the appropriate length is required. The saw or grinding machine shall be capable of cutting specimens to the

prescribed dimensions without excessive heating or shock.

Note 10—A double-bladed diamond masonry saw greatly facilitates the preparation of test specimens with smooth, parallel ends. Both single- and double-bladed diamond saws should have feed mechanisms and speed controls of sufficient precision to ensure compliance with paragraphs 7.5 and 7.6 of this method. Adequate blade stiffness is also important to control flexing of the blade during thin cuts.

6.4 *Core Drill*—A coring machine with cooling system and a diamond bit for cutting nominal 100 mm (4 in) diameter test specimens.

Note 11—A coring machine with adjustable vertical feed and rotational speed is recommended. The variable feeds and speeds may be controlled by various methods. A vertical feed rate of approximately 0.05 mm/rev (0.002 in/rev) and a rotational speed of approximately 455 RPM has been found to be satisfactory for several of the Superpave mixtures.

7. Test Specimens

7.1 *Size*—Dynamic modulus testing shall be performed on 100 mm (4 in) diameter by 150 mm (6 in) high test specimens cored from gyratory compacted mixtures.

7.2 *Aging*—Mixtures shall be aged in accordance with the short-term oven aging procedure in AASHTO PP2.

7.3 *Gyratory Specimens*—Prepare 165 mm (6.5 in) high specimens to the required air void content in accordance with AASHTO TP-4.

Note 12—Testing should be performed on test specimens meeting specific air void tolerances. The gyratory specimen air void content required to obtain a specified test specimen air void content must be determined by trial and error. Generally, the test specimen air void content is 1.5 to 2.5 percent lower than the air void content of the gyratory specimen when the test specimen is removed from the middle as specified in this test method.

7.4 *Coring*—Core the nominal 100 mm (4 in) diameter test specimens from the center of the gyratory specimens. Both the core drill and the gyratory specimen should be adequately supported to ensure that the resulting test specimen is cylindrical with sides that are smooth, parallel, and free from steps, ridges, and grooves.

7.5 *Diameter*—Measure the diameter of the test specimen at the mid-height and third points along axes that are

90 degrees apart. Record each of the six measurements to the nearest 1 mm (0.05 in). Calculate the average and the standard deviation of the six measurements. If the standard deviation is greater than 2.5 mm (0.01 in) discard the specimen. For acceptable specimens, the average diameter, reported to the nearest 1 mm, shall be used in the stress calculations.

7.6 *End Preparation*—The ends of all test specimens shall be smooth and perpendicular to the axis of the specimen. Prepare the ends of the specimen by sawing with a single- or double-bladed saw. The prepared specimen ends shall meet the tolerances described below. Reject test specimens not meeting these tolerances.

7.6.1 The specimen ends shall have a cut surface waviness height within a tolerance of ± 0.05 mm across any diameter. This requirement shall be checked in a minimum of three positions at approximately 120° intervals using a straight edge and feeler gauges approximately 8–12.5 mm (0.315–0.5 in) wide or an optical comparator.

7.6.2 The specimen end shall not depart from perpendicular to the axis of the specimen by more than 0.5 degrees (i.e. 0.87 mm or 0.03 in across the diameter of a 100 mm diameter specimen). This requirement shall be checked on each specimen using a machinists square and feeler gauges.

7.7 *Air Void Content*—Determine the air void content of the final test specimen in accordance with AASHTO T269. Reject specimens with air voids that differ by more than 0.5 percent from the target air voids.

7.8 *Number*—The number of test specimens required depends on the number of axial strain measurements made per specimen and the desired accuracy of the average dynamic modulus. Table 1 summarizes the replicate number of specimens that should be tested to obtain an accuracy limit of less than ± 15 percent.

7.9 *Sample Storage*—Wrap completed specimens in polyethylene and store in an environmentally protected storage area at temperatures between 5 and 25°C (40 and 75°F).

Note 13—To eliminate effects of aging on test results, it is recommended that specimens be stored no more than two weeks prior to testing.

8. Test Specimen Instrumentation

8.1 Attach mounting studs for the axial LVDTs to the sides of the specimen with epoxy cement. Figure 3

presents details of the mounting studs and LVDT mounting hardware.

Note 14—Quick setting epoxy such as Duro Master Mend Extra Strength Quick Set QM-50 has been found satisfactory for attaching studs. Under certain conditions when using the triaxial cell mentioned in Note 3, the mounting studs may not require gluing to the specimen. While the surface contact area of the mounting studs is normally minimized consistent with transducer support requirements, it is generally recommended that the area of the studs be sufficiently large to bridge any open void structure features evident on the cut face of the specimen. The minimum diameter mounting stud consistent with support requirements is normally set at 8 mm (0.315 in), maximum diameters have not been established. A circular stud contact surface shape is not required, rectangular or other shapes are acceptable.

8.2 The gauge length for measuring axial deformations shall be 100 mm ± 1 mm. An alignment and spacing fixture similar to that shown in Figure 3 can be used to facilitate mounting of the axial deformation measuring hardware. The gauge length is normally measured between the stud centers.

9. Procedure

9.1 The recommended test protocol for the Simple Performance Test for use in the Superpave volumetric mix design consists of testing the asphalt mix at one effective pavement temperature T_{eff} and one design frequency selected by the design engineer. The effective pavement temperature T_{eff} covers approximately the temperature range of 25 to 60°C (77 to 140°F). The design frequency covers the range between 0.1 to 10 Hz.

9.2 Place the test specimen in the environmental chamber and allow it to equilibrate to the specified testing temperature. A dummy specimen with a temperature sensor mounted at the center can be monitored to determine when the specimen reaches the specified test temperature. In the absence of the dummy specimen, Table 2 summarizes minimum recommended temperature equilibrium times from room temperature (i.e. 25°C).

9.3 Place one of the friction reducing end treatments on top of the platen at the bottom of the loading frame. Place the specimen on top of the lower end treatment, and mount the axial LVDTs to the hardware previously attached to the specimen. Adjust the LVDT to

near the end of its linear range to allow the full range to be available for the accumulation of compressive permanent deformation.

- 9.4 Place the upper friction reducing end treatment and platen on top of the specimen. Center the specimen with the load actuator visually in order to avoid eccentric loading.
- 9.5 Apply a contact load (P_{\min}) equal to 5 percent of the dynamic load that will be applied to the specimen.
- 9.6 Adjust and balance the electronic measuring system as necessary.
- 9.7 Apply haversine loading (P_{dynamic}) to the specimen without impact in a cyclic manner. The dynamic load should be adjusted to obtain axial strains between 50 and 150 microstrains.

Note 15—The dynamic load depends upon the specimen stiffness and generally ranges between 10 and 690 kPa (1.5 and 100 psi). Higher load is needed at colder temperatures. Table 3 presents target dynamic load levels based on temperature.

- 9.8 Test the specimens at selected temperature by first preconditioning the specimen with 200 cycles at 25 Hz using the target dynamic loads in Table 3 (interpolate if necessary). Then load the specimen using the selected frequency and number of cycles as specified in Table 4.
- 9.9 If excessive permanent deformation (greater than 1000 micro units of strain) occurs, reduce the maximum loading stress level to half. Discard the specimen and use a new specimen for testing under reduced load conditions.

10. Calculations

- 10.1 Capture and store the last 6 loading cycles of full waveform data for each transducer. Determine the average amplitude of the sinusoidal load and deformation from each axial displacement transducer over the first 5 cycles of the last 6 loading cycle group (since the displacement will lag behind the load, the computations may use data from the 6th cycle, but might not have enough of the waveform to fully determine the properties in the 6th cycle).
- 10.2 Average the signals from the displacement transducers. Determine the average time lag between the peak load and the peak deformation over the 5 loading cycles.

Note 16—Different approaches are available to determine these. The approach is highly dependent upon the number of data points collected per cycle. Approaches that have been used include peak search algorithms, various curve fitting techniques, and Fourier Transform. Curve fitting techniques and other numerical techniques have also been used to determine the phase angle from the more stable center portion of the waveform instead of the peaks. If any displacement transducer is out of range or otherwise obviously reading incorrectly during a cycle, discard the data for that cycle.

Note 17—For testing that will be used for statistical within-specimen variability and for establishing local precision and bias statements, paragraphs 10.3 through 10.7 must include computations from each individual displacement transducer in addition to the results from the averaged displacements. Therefore, it is a strict requirement that the data storage requirements of paragraph 10.1 be met.

- 10.3 Calculate the loading stress, σ_o , as follows (see Figure 4):

$$\sigma_o = \frac{\bar{P}}{A}$$

Where:

\bar{P} = average load amplitude
 A = area of specimen
 σ_o = stress.

- 10.4 Calculate the recoverable axial strain for each frequency, ϵ_o , as follows:

$$\epsilon_o = \frac{\bar{\Delta}}{GL}$$

Where:

$\bar{\Delta}$ = average deformation amplitude
 GL = gauge length
 ϵ_o = strain.

- 10.5 Calculate dynamic modulus, $|E^*|$ for each frequency as follows:

$$\text{Dynamic Modulus, } |E^*| = \frac{\sigma_o}{\epsilon_o}$$

- 10.6 Calculate the phase angle for each frequency:

$$\phi = \frac{t_i}{t_p} \times (360)$$

Where

t_i = average time lag between a cycle of stress and strain (sec)

t_p = average time for a stress cycle (sec.).

10.7 Calculate the dynamic modulus divided by sine of phase angle for each frequency:

$$\frac{|E^*|}{\sin \phi}$$

11. Report

11.1 Report the average stress and strain for each temperature-frequency combination tested.

11.2 Report the dynamic modulus and phase angle for each temperature-frequency combination tested.

11.3 Report the average dynamic modulus divided by sine of phase angle for the test specimen for each temperature-frequency tested.

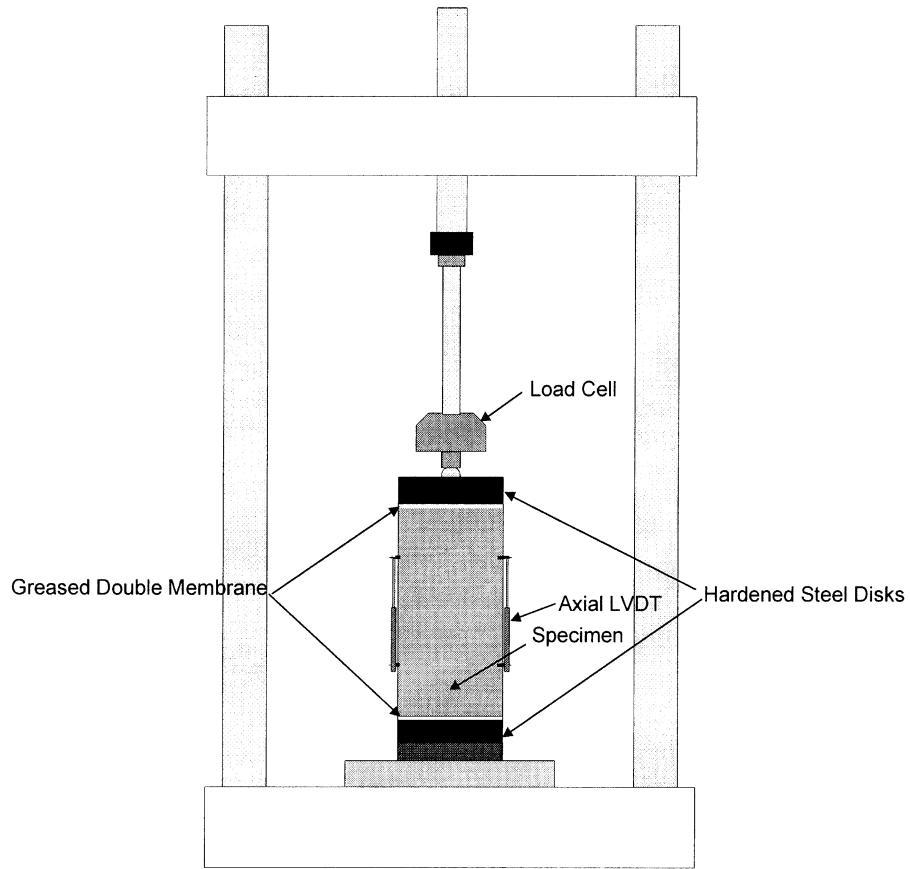
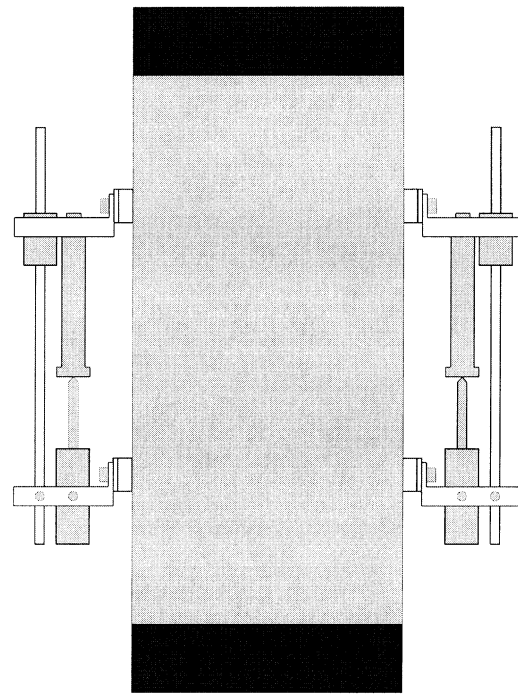


Figure 1. Schematic of dynamic modulus test device.



On-Sample Assembly

Figure 2. Schematic of gauge points.

TABLE 1 Recommended number of specimens

LVDTs per Specimen	Number of Specimens	Estimated Limit of Accuracy
2	4	13.4
3	2	13.1

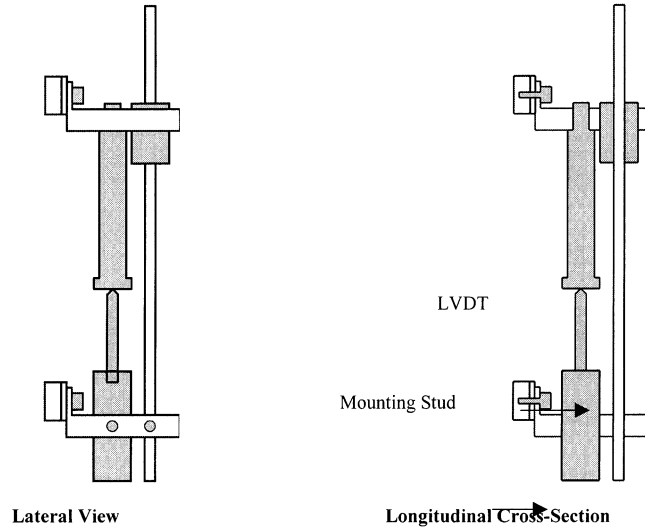


Figure 3. Mounting hardware details.

TABLE 2 Recommended equilibrium times

Specimen Test Temperature, °C (°F)	Time, hrs
30 (86)	TBD*
40 (104)	
50 (122)	
60 (140)	

* To be determined

TABLE 3 Target dynamic loads

Temperature, °C (°F)	Range, kPa	Range, psi
25 (77)	70 – 690	10 –100
38 (100)	40-200	6 –29
54 (130)	10 - 70	1.5 – 10

TABLE 4 Cycles for test sequence

Frequency	Number of Cycles
10	100
5	50
1	25
0.5	6
0.1	6

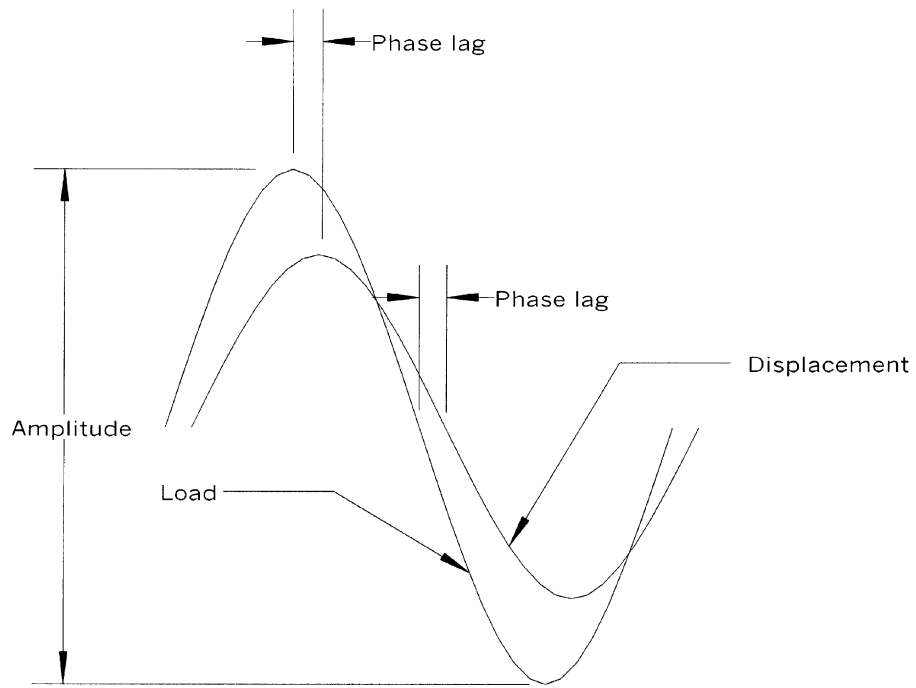


Figure 4. Ideal waveform schematic.

APPENDIX B

TEST METHOD FOR REPEATED LOAD TESTING OF ASPHALT CONCRETE MIXTURES IN UNIAXIAL COMPRESSION

1. Scope

- 1.1 This test method covers procedures for the preparation, testing and measurement of permanent deformation of cylindrical asphalt concrete specimens in a triaxial state of compressive loading.
- 1.2 The procedure uses a loading cycle of 1.0 second in duration, and consisting of applying 0.1-second haversine load followed by 0.9-second rest period. Permanent axial and/or radial strains are recorded throughout the test.
- 1.3 The test is conducted at a single effective temperature T_{eff} and design stress levels.
- 1.4 This standard is applicable to laboratory prepared specimens 100 mm in diameter and 150 mm in height for mixtures with nominal maximum size aggregate less than or equal to 37.5 mm (1.5 in).
- 1.5 *This standard may involve hazardous material, operations, and equipment. This standard does not purport to address all safety problems associated with its use. It is the responsibility of the user of this procedure to establish appropriate safety and health practices and to determine the applicability of regulatory limitations prior to use.*

2. Referenced Documents

2.1 AASHTO Standards

TP4	Method for Preparing and Determining the Density of Hot Mix Asphalt (HMA) Specimens by Means of the SHRP Gyrotory Compactor
PP2	Practice for Mixture Conditioning of Hot Mix Asphalt (HMA)
T67	Standard Practices for Load Verification of Testing Machines (cross-listed with ASTM E4)
T269	Percent Air Voids in Compacted Dense and Open Bituminous Paving Mixtures

3. Definitions

- 3.1 *Permanent Deformation*—is a manifestation of two different mechanisms and is a combination of densification (volume change) and repetitive shear deformation (plastic flow with no volume change).
- 3.2 *Flow Number*—is defined as the number of load repetitions at which shear deformation, under constant volume, starts.
- 3.3 *Effective Temperature T_{eff}* —Is a single test temperature at which an amount of permanent deformation would occur equivalent to that measured by considering each season separately throughout the year.

4. Summary of Method

- 4.1 A cylindrical sample of bituminous paving mixture is subjected to a haversine axial load. The load is applied for duration of 0.1-second with a rest period of 0.9-second. The rest period has a load equivalent to the seating load. The test can be performed either without confinement, or a confining pressure is applied to better simulate in situ stress conditions. Cumulative permanent axial and radial strains are recorded throughout the test. In addition, the number of repetitions at which shear deformation, under constant volume, starts is defined as the Flow Number.

5. Significance and Use

- 5.1 Current Superpave volumetric mix design procedure lacks a fundamental design criterion to evaluate fundamental engineering properties of the asphalt mixture that directly affect performance. In this test, the selection of the design binder content and aggregate structure is fundamentally enhanced by the evaluation of the mix resistance to shear flow (Flow Number of Repetitions).
- 5.2 This fundamental engineering property can be used as a performance criteria indicator for permanent deformation resistance of the asphalt concrete mixture, or can be simply used to compare the shear resistance properties of various bituminous paving mixtures.

6. Apparatus

- 6.1 *Load Test System*—A load test system consisting of a testing machine, environmental chamber, measuring system, and specimen end fixtures.

6.1.1 *Testing Machine*—The testing machine should be capable of applying haversine loads up to 25 kN (5,600 lbs). An electro-hydraulic machine is recommended but not necessarily required. The loading device should be calibrated as outlined in the “Equipment Calibration” Section of the testing manual.

6.1.2 *Confining Pressure Device*—A system capable of maintaining a constant confining pressure, up to 207 kPa (30 psi), such as an air pressure intensifier or a hydraulic pump. The device shall be equipped with a pressure relief valve and a system to pressurize and depressurize the cell with gas or fluid. The device should also have a high temperature control subsystem for testing up to 60°C (140°F) within an accuracy of $\pm 0.5^\circ\text{C}$ (1°F) at constant pressure.

Note 1—It has been found that feedback control of a servovalve to control the pressure is the preferred method of control. However, manual valves or proportional valves may be adequate for some applications. The axisymmetric triaxial cells of AASHTO T292 or T294 may be used for this purpose. Other types of triaxial cells may be permitted. In all cases, see-through cells are not recommended for use with gas confining media. Sight glass ports or reduced area windows are recommended with gas media for safety reasons. It is not required that the specimen be visible through the cell wall if specimen centering and proper instrumentation operation can be verified without a see-through pressure vessel. Certain simulations of pavement loads and extended material characterization desired for local conditions may suggest using confining pressures greater than 207 kPa. For pressures higher than 690 kPa (100 psi), fluid cells are recommended.

6.1.3 *Environmental Chamber*—A chamber for controlling the test specimen at the desired temperature is required. The environmental chamber shall be capable of controlling the temperature of the specimen over a temperature range from 25 to 60°C (77 to 140°F) to an accuracy of $\pm 0.5^\circ\text{C}$ (1°F). The chamber shall be large enough to accommodate the test specimen and a dummy specimen with temperature sensor mounted at the center for temperature verification.

Note 2—If the chamber does not have sufficient room for a dummy specimen, it is permissible to have a second chamber controlling the temperature of the dummy. The separate dummy chamber must be operated similar to the operation of the main test

specimen chamber so that the dummy will accurately register the time required to obtain temperature equilibrium on the test specimen.

6.1.4 *Measurement System*—The system shall include a data acquisition system comprising analog to digital conversion and/or digital input for storage and analysis on a computer. The system shall be capable of measuring and recording the time history of the applied load, axial and radial deformations for the time duration required by this test method. The system shall be capable of measuring the load and resulting deformations with a resolution of 0.5 percent.

6.1.4.1 *Load*—The load shall be measured with an electronic load cell having adequate capacity for the anticipated load requirements. The load cell shall be calibrated in accordance with AASHTO T67. The load measuring transducer shall have accuracy equal to or better than 0.25 percent of full scale.

Note 3—A 25 kN (5600 lbf) load cell has been found to be the approximate maximum capacity limit for this test method because of range versus resolution factors. It is recommended that if the selected load cell capacity is 25 kN or greater, the system should be equipped with either manual or automatic amplification selection capability so that it can be used to enhance control of the system at lower anticipated loads.

6.1.4.2 *Axial and Radial Deformations*—Axial and/or radial deformations shall be measured with displacement transducers referenced to gauge points contacting the specimen as shown in Figure 1. The axial deformations shall be measured at a minimum of two locations 180° apart (in plan view); radial deformations shall be measured at a minimum of four locations aligned, in planform, on diametral, perpendicular lines which intersect at the center of the specimen.

Note 4—Analog transducers such as linear variable differential transformers (LVDTs) having a range of ± 0.5 mm (0.02 in) and inherent nonlinearity equal to or better than ± 0.025 percent of full scale have been found adequate for this purpose. Software or firmware linearization techniques may be used to improve the inherent nonlinearity. Amplification and signal conditioning techniques may be used with the ± 0.5 mm range LVDTs to obtain resolutions down to 0.001mm (0.00004 in) or better for small strain test conditions. These

techniques may be manual or automatic. In general, increasing the resolution by manual signal amplification will result in reduction of the overall range of the instrument by the same factor.

6.1.5 *Loading Platens*—Platens, with a diameter equal to or greater than that of the test specimen are required above and below the specimen to transfer the load from the testing machine to the specimen. Generally, these platens should be made of hardened or plated steel, or anodized high strength aluminum. Softer materials will require more frequent replacement. Materials that have linear elastic modulus properties and hardness properties lower than that of 6061-T6 aluminum shall not be used.

6.1.6 *Flexible Membrane*—For the confined tests, the specimen should be enclosed in an impermeable flexible membrane. The membrane should be sufficiently long to extend well onto the platens and when slightly stretched be of the same diameter as the specimen. Typical membrane wall thickness ranges between 0.012 and 0.0625 inches (0.305–1.588 mm).

6.1.7 *End Treatment*—Friction reducing end treatments shall be placed between the specimen ends and the loading platens.

Note 5—End treatments consisting of two 0.5 mm (0.02 in) thick latex sheets separated with silicone grease have been found to be suitable friction reducing end treatments.

6.2 *Gyratory Compactor*—A gyratory compactor and associated equipment for preparing laboratory specimens in accordance with AASHTO TP4 shall be used. Field cores shall meet the requirements of paragraphs 7.4 through 7.6 of this test method and any reports on cores so tested will contain a detailed description of the location of any lift boundaries within the height of the specimen (e.g. lift order, thickness and material homogeneity).

6.3 *Saw*—A machine for sawing test specimen ends to the appropriate length is required. The saw machine shall be capable of cutting specimens to the prescribed dimensions without excessive heating or shock.

Note 6—A diamond masonry saw greatly facilitates the preparation of test specimens with smooth, parallel ends. Both single- or double-bladed diamond saws should have feed mechanisms and speed controls of sufficient precision to ensure compliance with paragraphs 7.5 and 7.6 of this method.

Adequate blade stiffness is also important to control flexing of the blade during thin cuts.

6.4 *Core Drill*—A coring machine with cooling system and a diamond bit for cutting nominal 100 mm (4 in) diameter test specimens.

Note 7—A coring machine with adjustable vertical feed and rotational speed is recommended. The variable feeds and speeds may be controlled by various methods. A vertical feed rate of approximately 0.05 mm/rev (0.002 in/rev) and a rotational speed of approximately 455 RPM has been found to be satisfactory for several of the Superpave mixtures.

7. Test Specimens

7.1 *Size*—Testing shall be performed on 100 mm (4 in) diameter by 150 mm (6 in) high test specimens cored from gyratory compacted mixtures.

7.2 *Aging*—Mixtures shall be aged in accordance with the short-term oven aging procedure in AASHTO PP2.

7.3 *Gyratory Specimens*—Prepare 165 mm (6.5 in) high specimens to the required air void content in accordance with AASHTO TP-4.

7.4 *Coring*—Core the nominal 100 mm (4 in) diameter test specimens from the center of the gyratory specimens. Both the core drill and the gyratory specimen should be adequately supported to ensure that the resulting test specimen is cylindrical with sides that are smooth, parallel, and free from steps, ridges, and grooves.

7.5 *Diameter*—Measure the diameter of the test specimen at the mid-height and third points along axes that are 90 degrees apart. Record each of the six measurements to the nearest 1 mm (0.05 in). Calculate the average and the standard deviation of the six measurements. If the standard deviation is greater than 2.5 mm (0.01 in) discard the specimen. For acceptable specimens, the average diameter, reported to the nearest 1 mm, shall be used in the stress calculations.

7.6 *End Preparation*—The ends of all test specimens shall be smooth and perpendicular to the axis of the specimen. Prepare the ends of the specimen by sawing with a single- or double-bladed saw. To ensure that the sawed samples have parallel ends, the prepared specimen ends shall meet the tolerances described below. Reject test specimens not meeting these tolerances.

7.6.1 The specimen ends shall have a cut surface waviness height within a tolerance of ± 0.05 mm across

any diameter. This requirement shall be checked in a minimum of three positions at approximately 120° intervals using a straight edge and feeler gauges approximately 8–12.5 mm (0.315–0.5 in) wide or an optical comparator.

7.6.2 The specimen end shall not depart from perpendicular to the axis of the specimen by more than 0.5 degrees (i.e. 0.87 mm or 0.03 in across the diameter of a 100 mm diameter specimen). This requirement shall be checked on each specimen using a machinists square and feeler gauges.

7.7 *Air Void Content*—Determine the air void content of the final test specimen in accordance with AASHTO T269. Reject specimens with air voids that differ by more than 0.5 percent from the target air voids.

7.8 *Replicates*—The number of test specimens required depends on the number of axial and/or radial strain measurements made per specimen and the desired accuracy of the average flow time values. Table 1 summarizes the LVDTs and replicate number of specimens needed to obtain a desired accuracy limit.

7.9 *Sample Storage*—Wrap completed specimens in polyethylene and store in an environmentally protected storage area at temperatures between 5 and 25°C (40 and 75°F).

Note 8—To eliminate effects of aging on test results, it is recommended that specimens be stored no more than two weeks prior to testing.

8. Test Specimen Instrumentation

8.1 Attach mounting studs for the axial LVDTs to the sides of the specimen with epoxy cement. Figure 2 presents details of the mounting studs and LVDT mounting hardware.

Note 9—Quick setting epoxy such as Duro Master Mend Extra Strength Quick Set QM-50 has been found satisfactory for attaching studs. Under certain conditions when using the triaxial cell with confining pressure, the mounting studs may not require gluing to the specimen. While the surface contact area of the mounting studs is normally minimized consistent with transducer support requirements, it is generally recommended that the area of the studs be sufficiently large to bridge any open void structure features evident on the cut face of the specimen. The minimum diameter mounting stud consistent with support requirements is normally set at 8 mm (0.315 in), maximum diameters have not been established. A circular stud contact

surface shape is not required, rectangular or other shapes are acceptable.

8.2 The gauge length for measuring axial deformations shall be 100 mm ±1 mm. Suitable alignment and spacing fixture shall be used to facilitate mounting of the axial deformation measuring hardware. The gauge length is normally measured between the stud centers.

9. Procedure

9.1 The recommended test protocol for the Simple Performance Test for use in the Superpave volumetric mix design consists of testing the asphalt mix at one effective pavement temperature T_{eff} and one design stress level selected by the design engineer. The effective pavement temperature T_{eff} covers approximately the temperature range of 25 to 60°C (77 to 140°F). The design stress level covers the range between 69 and 207 kPa (10–30 psi) for the unconfined tests, and 483 to 966 kPa for the confined tests. Typical confinement levels range between 35 and 207 kPa (5–30 psi).

9.2 Place the test specimen in the environmental chamber and allow it to equilibrate to the specified testing temperature. For the confined tests in a standard geotechnical cell, glue the gauge points to the specimen surface as necessary, fit the flexible membrane over the specimen and mount the axial hardware fixtures to the gauge points through the membrane. Place the test specimen with the flexible membrane on in the environmental chamber. A dummy specimen with a temperature sensor mounted at the center can be monitored to determine when the specimen reaches the specified test temperature. In the absence of the dummy specimen, Table 2 provides a summary of the minimum required temperature equilibrium times for samples starting from room temperature (i.e. 25°C).

Unconfined Tests

9.3 After temperature equilibrium is reached, place one of the friction reducing end treatments on top of the platen at the bottom of the loading frame. Place the specimen on top of the lower end treatment, and mount the axial LVDTs to the hardware previously attached to the specimen. Adjust the LVDT to near the end of its linear range to allow the full range to be available for the accumulation of compressive permanent deformation.

9.4 Place the upper friction reducing end treatment and platen on top of the specimen. Center the specimen with the load actuator visually in order to avoid eccentric loading.

- 9.5 Apply a contact load equal to 5 percent of the total load that will be applied to the specimen, while ensuring the proper response of the LVDTs (i.e., check for proper direction sensing for all LVDTs).
- 9.6 Place the radial LVDTs in contact with the specimen, adjust the LVDTs to near the end of their linear range to allow the full range to be available for the accumulation of radial permanent deformation. Adjust and balance the electronic measuring system as necessary.
- 9.7 Close the environmental chamber and allow sufficient time (normally 10 to 15 minutes) for the temperature to stabilize within the specimen and the chamber.
- 9.8 After the time required for the sample to reach the testing temperature, apply the haversine load, which yields the desired stress on the specimen. The maximum applied load (P_{max}) is the maximum total load applied to the sample, including the contact and cyclic load: $P_{max} = P_{contact} + P_{cyclic}$.
- 9.9 The contact load ($P_{contact}$) is the vertical load placed on the specimen to maintain a positive contact between loading strip and the specimen: $P_{contact} = 0.05 \times P_{max}$.
- 9.10 The cyclic load (P_{cyclic}) is the load applied to the test specimen which is used to calculate the permanent deformation parameters: $P_{cyclic} = P_{max} - P_{contact}$.
- 9.11 Apply the haversine loading (P_{cyclic}) and continue until 10,000 cycles (2.8 hours) or until the specimen fails and results in excessive tertiary deformation to the specimen, whichever comes first. The total number of cycles or the testing time will depend on the temperature and the stress levels applied.
- 9.12 During the load applications, record the load applied, the axial and radial deflection measured from all LVDTs through the data acquisition system. Signal-to-noise ratio should be at least 10. All data should be collected in real time and collected/processed so as to minimize phase errors due to sequential channel sampling. In order to save storage space during data acquisition for 10,000 cycles, it is recommended to use the data acquisition of the cycles shown in Table 3.
- Confined Tests**
- 9.13 After temperature equilibrium is reached, place one of the friction reducing end treatments on top of the platen at the bottom of the loading frame. Place the specimen on top of the lower end treatment, place the top platen and extend the flexible membrane over the top and bottom platens. Attach the O-rings to seal the specimen on top and bottom platens from the confining air/fluid. Center the specimen with the load actuator visually in order to avoid eccentric loading.
- 9.14 Mount the axial LVDTs to the hardware previously attached to the specimen. Adjust the LVDT to near the end of its linear range to allow the full range to be available for the accumulation of compressive permanent deformation.
- 9.15 Connect the appropriate hose through the upper or lower platen (or take other appropriate steps) to keep the specimen's internal void structure under atmospheric pressure while pressure greater than atmospheric is applied to the outside of the membrane during testing.
- 9.16 Assemble the triaxial cell over the specimen, ensure proper seal with the base and connect the fluid (or gas) pressure lines.
- 9.17 Apply a contact load equal to 5 percent of the load that will be applied to the specimen, while ensuring the proper response of the LVDTs (i.e., both decrease accordingly). Place the radial LVDTs in contact with the specimen, adjust the LVDTs to near the end of their linear range to allow the full range to be available for the accumulation of radial permanent deformation.
- 9.18 Record the initial LVDT readings and slowly increase the lateral pressure to the desired test level (e.g. 2 psi /sec). Adjust and balance the electronic measuring system as necessary. Close the environmental chamber and allow sufficient time (normally 10 to 15 minutes) for the temperature to stabilize within the specimen and the chamber.
- 9.19 After the time required for the sample to reach the testing temperature, apply the haversine load, which yields the desired stress on the specimen. Continue until 10,000 cycles (2.8 hours) or until the specimen fails and results in excessive tertiary deformation to the specimen, whichever comes first. The total number of cycles or the testing time will depend on the temperature and the stress levels applied.
- 9.20 During the load applications, record the load applied, confining pressure, the axial and radial deflection measured from all LVDTs through the data acquisition system. Signal-to-noise ratio should be at

least 10. All data should be collected in real time and collected/processed so as to minimize phase errors due to sequential channel sampling. In order to save storage space during data acquisition for 10,000 cycles, it is recommended to use the data acquisition of the cycles shown in Table 3.

10. Calculations

- 10.1 Calculate the average axial deformation for each specimen by averaging the readings from the two axial LVDTs. Convert the average deformation values to total axial strain (ϵ_{Ta}), in/in, by dividing by the gauge length, L [100mm (4-inches)]. Typical total axial strain versus time is shown in Figure 3.
- 10.2 Compute the cumulative axial permanent strain.
- 10.3 Plot the cumulative axial permanent strain versus number of loading cycles in log space. Determine the

permanent deformation parameters, intercept (a) and slope (b), from the linear portion of the permanent strain curve (see Figure 4).

- 10.4 The flow number of repetitions is viewed as the lowest point in the curve of rate of change in axial strain versus number of loading cycles (see Figure 5). The rate of change of axial strain versus number of loading cycles should be plotted and the flow number (F_N) is estimated where a minimum or zero slope is observed.

11. Report

- 11.1 Report all specimen information including mix identification, storage conditions, dates of manufacturing and testing, specimen diameter and length, volumetric properties, stress levels used, confining pressure, axial permanent deformation parameters (a, b) and flow number of repetitions.

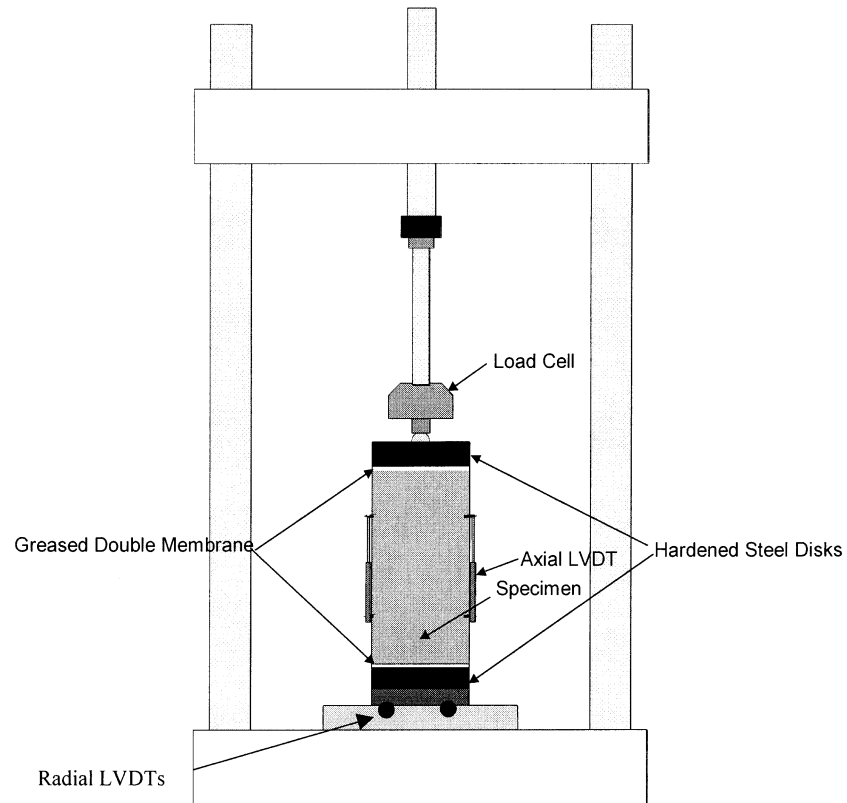


Figure 1. Schematic of repeated load permanent deformation test.

TABLE 1 Recommended number of specimens

LVDTs per Specimen (Total for either vertical or horizontal, not combined total)	Number of Specimens	Estimated Standard Error of the Mean, % Per Mixture's Nominal Aggregate Size		
		12.5mm	19mm	37.5mm
2	2	7.6	9.5	18.8
2	3	6.2	7.7	15.3
3	2	6.7	8.9	17.4
3	3	5.5	7.3	14.2
4	2	6.2	8.6	16.6
4	3	5.0	7.0	13.6

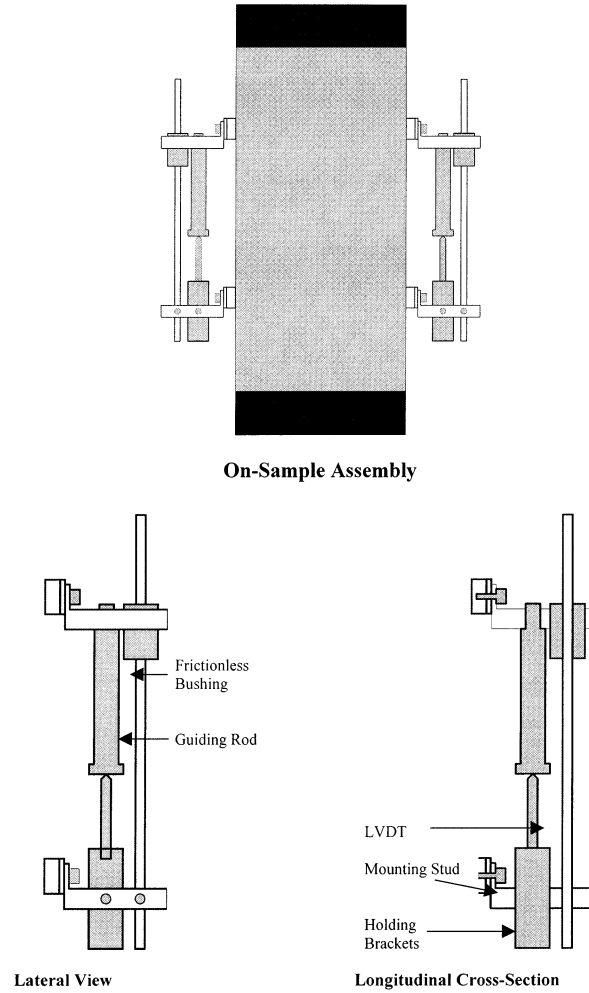


Figure 2. Axial LVDTs instrumentation.

TABLE 2 Recommended equilibrium times

Specimen Test Temperature, °C (°F)	Time, hrs
25 (77)	0.5
30 (86)	1.0
37.8 (100)	1.5
>54.4 (130)	2.0

TABLE 3 Suggested data collection for the repeated load permanent deformation test

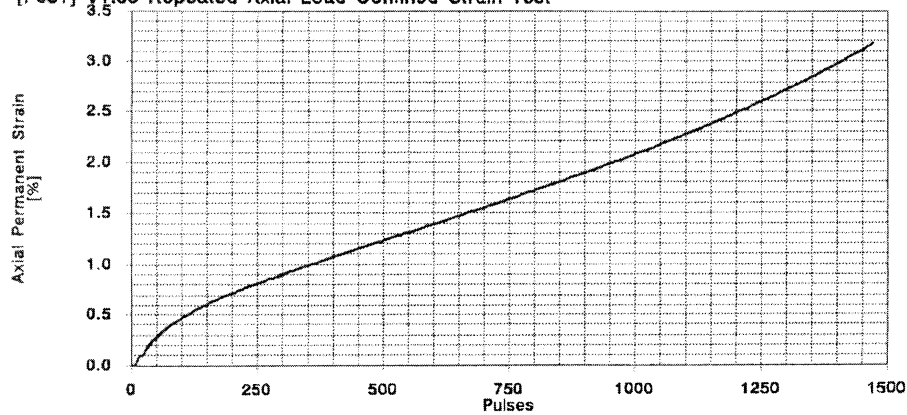
Data collected During Cycles	Data collected During Cycles	Data collected During Cycles
1 through 100	700	4,500
130	750	5,000
170	800	5,500
200	850	6,000
230	900	6,500
270	950	7,000
300	1,000	7,500
350	1,300	8,000
400	1,700	8,500
450	2,000	9,000
500	2,300	9,500
550	2,700	10,000
600	3,000	
650	4,000	

Arizona State University

INDUSTRIAL PROCESS CONTROLS Ltd.

[F051] V1.05 Repeated Axial Load Confined Strain Test

Universal Testing Machine (UTM V3.00B29)



```

final reading of measured parameters:
loading pulse count      1476
deviator stress (kPa)   134.44
seating stress (kPa)    17.096
axial permanent strain (%) 3.2537
axial resilient strain (%) 0.0234
axial resil modulus (MPa) 574.13
radial permanent strain (%) 3.9636
radial resilient strain (%) 0.0134
resilient Poisson ratio 0.5755
actuator perm strain (%) 3.182
actuator resil strain (%) 0.0693
actuator resil modulus (MPa) 193.87
min ax'l strn slope (um/m/p) 16.08
min axial slope pulse count 626
    
```

Figure 3. Cumulative permanent strain vs. loading cycles from a repeated load permanent deformation test.

Arizona State University
 [F051] V1.05 Repeated Axial Load Confined Strain Test

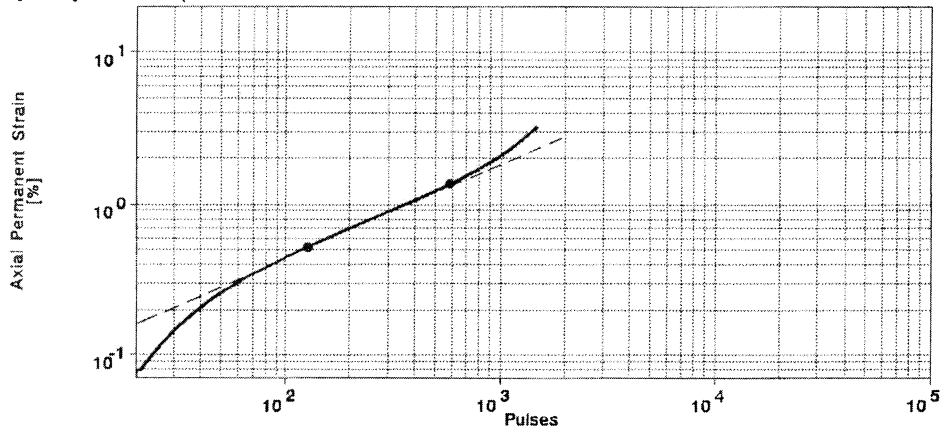


Figure 4. Regression constants “a” and “b” from log permanent strain—log number of loading cycles plot.

Arizona State University
 [F051] V1.05 Repeated Axial Load Confined Strain Test

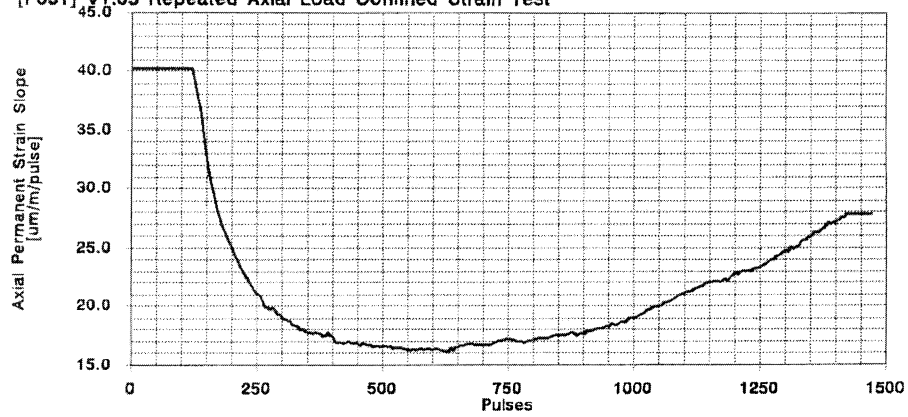


Figure 5. Typical plot of the rate of change in permanent strain vs. loading cycles.

APPENDIX C

TEST METHOD FOR STATIC CREEP/FLOW TIME OF ASPHALT CONCRETE MIXTURES IN COMPRESSION

1. Scope

- 1.1 This test method covers procedures for the preparation, testing and measurement of the resistance to tertiary flow of cylindrical asphalt concrete specimens in a triaxial state of compressive loading.
- 1.2 In this test, a cylindrical sample of bituminous paving mixture is subjected to a static axial load. Permanent axial and/or radial strains are recorded throughout the test.
- 1.3 The test is conducted at a single effective temperature T_{eff} and design stress levels.
- 1.4 This standard is applicable to laboratory prepared specimens 100 mm in diameter and 150 mm in height for mixtures with nominal maximum size aggregate less than or equal to 37.5 mm (1.5 in).
- 1.5 *This standard may involve hazardous material, operations, and equipment. This standard does not purport to address all safety problems associated with its use. It is the responsibility of the user of this procedure to establish appropriate safety and health practices and to determine the applicability of regulatory limitations prior to use.*

2. Referenced Documents

2.1 AASHTO Standards

- | | |
|------|---|
| TP4 | Method for Preparing and Determining the Density of Hot Mix Asphalt (HMA) Specimens by Means of the SHRP Gyratory Compactor |
| PP2 | Practice for Mixture Conditioning of Hot Mix Asphalt (HMA) |
| T67 | Standard Practices for Load Verification of Testing Machines (cross-listed with ASTM E4) |
| T269 | Percent Air Voids in Compacted Dense and Open Bituminous Paving Mixtures |

3. Definitions

- 3.1 *Flow Time*—is defined as the postulated time when shear deformation, under constant volume, starts.
 - 3.2 *Compliance*—is the reciprocal of the modulus and represents the ratio of strain to stress for a viscoelastic material.
 - 3.3 *Effective Temperature T_{eff}* —is a single test temperature at which an amount of permanent deformation would occur equivalent to that measured by considering each season separately throughout the year.
- #### 4. Summary of Method
- 4.1 A cylindrical sample of bituminous paving mixture is subjected to a static axial load. The test can be performed either without confinement, or a confining pressure is applied to better simulate in situ stress conditions. The flow time is defined as the postulated time when shear deformation, under constant volume, starts. The applied stress and the resulting permanent and/or axial strain response of the specimen is measured and used to calculate the flow time.
- #### 5. Significance and Use
- 5.1 Current Superpave volumetric mix design procedure lacks a basic design criterion to evaluate fundamental engineering properties of the asphalt mixture that directly affect performance. The selection of the design binder content and aggregate structure is enhanced by the evaluation of the mix resistance to shear flow (Flow Time) in this test.
 - 5.2 This fundamental engineering property can be used as a performance criteria indicator for permanent deformation resistance of the asphalt concrete mixture, or can be simply used to compare the shear resistance properties of various bituminous paving mixtures.
- #### 6. Apparatus
- 6.1 Load Test System—A load test system consisting of a testing machine, environmental chamber, measuring system, and specimen end fixtures.
 - 6.1.1 *Testing Machine*—The testing machine should be capable of applying static loads up to 25 kN (5,600 lbs). An electro-hydraulic machine is recommended but not necessarily required. The loading device should be calibrated as outlined in the

“Equipment Calibration” Section of the testing manual.

- 6.1.2 *Confining Pressure Device*—A system capable of maintaining a constant confining pressure, up to 207 kPa (30 psi), such as an air pressure intensifier or a hydraulic pump. The device shall be equipped with a pressure relief valve, and a system to pressurize and depressurize the cell with gas or fluid. The device should also have a high temperature control subsystem for testing up to 60°C (140°F) within an accuracy of $\pm 0.5^\circ\text{C}$ (1°F) at constant pressure.

Note 1—It has been found that feedback control of a servovalve to control the pressure is the preferred method of control. However, manual valves or proportional valves may be adequate for some applications. The axisymmetric triaxial cells of AASHTO T292 or T294 may be used for this purpose. Other types of triaxial cells may be permitted. In all cases, see-through cells are not recommended for use with gas confining media. Sight glass ports or reduced area windows are recommended with gas media for safety reasons. It is not required that the specimen be visible through the cell wall if specimen centering and proper instrumentation operation can be verified without a see-through pressure vessel. Certain simulations of pavement loads and extended material characterization desired for local conditions may suggest using confining pressures greater than 207 kPa. For pressures higher than 690 kPa (100 psi), fluid cells are recommended.

- 6.1.3 *Environmental Chamber*—A chamber for controlling the test specimen at the desired temperature is required. The environmental chamber shall be capable of controlling the temperature of the specimen over a temperature range from 25 to 60°C (77 to 140°F) to an accuracy of $\pm 0.5^\circ\text{C}$ (1°F). The chamber shall be large enough to accommodate the test specimen and a dummy specimen with temperature sensor mounted at the center for temperature verification.

Note 2—If the chamber does not have sufficient room for a dummy specimen, it is permissible to have a second chamber controlling the temperature of the dummy. The separate dummy chamber must be operated similar to the operation of the main test specimen chamber so that the dummy will accurately register the time required to obtain temperature equilibrium on the test specimen.

- 6.1.4 *Measurement System*—The system shall include a data acquisition system comprising analog to

digital conversion and/or digital input for storage and analysis on a computer. The system shall be capable of measuring and recording the time history of the applied load, axial and radial deformations for the time duration required by this test method. The system shall be capable of measuring the load and resulting deformations with a resolution of 0.5 percent.

- 6.1.4.1 *Load*—The load shall be measured with an electronic load cell having adequate capacity for the anticipated load requirements. The load cell shall be calibrated in accordance with AASHTO T67. The load measuring transducer shall have accuracy equal to or better than 0.25 percent of full scale.

Note 3—A 25 kN (5600 lbf) load cell has been found to be the approximate maximum capacity limit for this test method because of range versus resolution factors. It is recommended that if the selected load cell capacity is 25 kN or greater, the system should be equipped with either manual or automatic amplification selection capability so that it can be used to enhance control of the system at lower anticipated loads.

- 6.1.4.2 *Axial and Radial Deformations*—Axial and/or radial deformations shall be measured with displacement transducers referenced to gauge points contacting the specimen as shown in Figure 1. The axial deformations shall be measured at a minimum of two locations 180° apart (in plan view); radial deformations shall be measured at a minimum of four locations aligned, in planform, on diametral, perpendicular lines which intersect at the center of the specimen.

Note 4—Analog transducers such as linear variable differential transformers (LVDTs) having a range of ± 0.5 mm (0.02 in) and inherent nonlinearity equal to or better than ± 0.025 percent of full scale have been found adequate for this purpose. Software or firmware linearization techniques may be used to improve the inherent nonlinearity. Amplification and signal conditioning techniques may be used with the ± 0.5 mm range LVDTs to obtain resolutions down to 0.001 mm (0.00004 in) or better for small strain test conditions. These techniques may be manual or automatic. In general, increasing the resolution by manual signal amplification will result in reduction of the overall range of the instrument by the same factor.

- 6.1.5 *Loading Platens*—Platens, with a diameter equal to or greater than that of the test specimen are

required above and below the specimen to transfer the load from the testing machine to the specimen. Generally, these platens should be made of hardened or plated steel, or anodized high strength aluminum. Softer materials will require more frequent replacement. Materials that have linear elastic modulus properties and hardness properties lower than that of 6061-T6 aluminum shall not be used.

6.1.6 *Flexible Membrane*—For the confined tests, the specimen should be enclosed in an impermeable flexible membrane. The membrane should be sufficiently long to extend well onto the platens and when slightly stretched be of the same diameter as the specimen. Typical membrane wall thickness ranges between 0.012 and 0.0625 inches (0.305–1.588 mm).

6.1.7 *End Treatment*—Friction reducing end treatments shall be placed between the specimen ends and the loading platens.

Note 5—End treatments consisting of two 0.5 mm (0.02 in) thick latex sheets separated with silicone grease have been found to be suitable friction reducing end treatments.

6.2 *Gyratory Compactor*—A gyratory compactor and associated equipment for preparing laboratory specimens in accordance with AASHTO TP4 shall be used. Field cores shall meet the requirements of paragraphs 7.4 through 7.6 of this test method and any reports on cores so tested will contain a detailed description of the location of any lift boundaries within the height of the specimen (e.g. lift order, thickness and material homogeneity).

6.3 *Saw*—A machine for sawing test specimen ends to the appropriate length is required. The saw machine shall be capable of cutting specimens to the prescribed dimensions without excessive heating or shock.

Note 6—A double-bladed diamond masonry saw greatly facilitates the preparation of test specimens with smooth, parallel ends. Both single- or double-bladed diamond saws should have feed mechanisms and speed controls of sufficient precision to ensure compliance with paragraphs 7.5 and 7.6 of this method. Adequate blade stiffness is also important to control flexing of the blade during thin cuts.

6.4 *Core Drill*—A coring machine with cooling system and a diamond bit for cutting nominal 100 mm (4 in) diameter test specimens.

Note 7—A coring machine with adjustable vertical feed and rotational speed is recommended. The variable feeds and speeds may be controlled by various methods. A vertical feed rate of approximately 0.05 mm/rev (0.002 in/rev) and a rotational speed of approximately 455 RPM has been found to be satisfactory for several of the Superpave mixtures.

7. Test Specimens

7.1 *Size*—Testing shall be performed on 100 mm (4 in) diameter by 150 mm (6 in) high test specimens cored from gyratory compacted mixtures.

7.2 *Aging*—Mixtures shall be aged in accordance with the short-term oven aging procedure in AASHTO PP2.

7.3 *Gyratory Specimens*—Prepare 165 mm (6.5 in) high specimens to the required air void content in accordance with AASHTO TP-4.

7.4 *Coring*—Core the nominal 100 mm (4 in) diameter test specimens from the center of the gyratory specimens. Both the core drill and the gyratory specimen should be adequately supported to ensure that the resulting test specimen is cylindrical with sides that are smooth, parallel, and free from steps, ridges, and grooves.

7.5 *Diameter*—Measure the diameter of the test specimen at the mid-height and third points along axes that are 90 degrees apart. Record each of the six measurements to the nearest 1 mm (0.05 in). Calculate the average and the standard deviation of the six measurements. If the standard deviation is greater than 2.5 mm (0.01 in) discard the specimen. For acceptable specimens, the average diameter, reported to the nearest 1 mm, shall be used in the stress calculations.

7.6 *End Preparation*—The ends of all test specimens shall be smooth and perpendicular to the axis of the specimen. Prepare the ends of the specimen by sawing with a single- or double-bladed saw. To ensure that the sawed samples have parallel ends, the prepared specimen ends shall meet the tolerances described below. Reject test specimens not meeting these tolerances.

7.6.1 The specimen ends shall have a cut surface waviness height within a tolerance of ± 0.05 mm across any diameter. This requirement shall be checked in a minimum of three positions at approximately 120° intervals using a straight edge and feeler gauges approximately 8–12.5 mm (0.315–0.5 in) wide or an optical comparator.

7.6.2 The specimen end shall not depart from perpendicular to the axis of the specimen by more than 0.5 degrees (i.e. 0.87 mm or 0.03 in across the diameter of a 100 mm diameter specimen). This requirement shall be checked on each specimen using a machinists square and feeler gauges.

7.7 *Air Void Content*—Determine the air void content of the final test specimen in accordance with AASHTO T269. Reject specimens with air voids that differ by more than 0.5 percent from the target air voids.

7.8 *Replicates*—The number of test specimens required depends on the number of axial and/or radial strain measurements made per specimen and the desired accuracy of the average flow time values. Table 1 summarizes the LVDTs and replicate number of specimens needed to obtain a desired accuracy limit.

7.9 *Sample Storage*—Wrap completed specimens in polyethylene and store in an environmentally protected storage area at temperatures between 5 and 25°C (40 and 75°F).

Note 8—To eliminate effects of aging on test results, it is recommended that specimens be stored no more than two weeks prior to testing.

8. Test Specimen Instrumentation

8.1 Attach mounting studs for the axial LVDTs to the sides of the specimen with epoxy cement. Figure 2 presents details of the mounting studs and LVDT mounting hardware.

Note 9—Quick setting epoxy such as Duro Master Mend Extra Strength Quick Set QM-50 has been found satisfactory for attaching studs. Under certain conditions when using the triaxial cell with confining pressure, the mounting studs may not require gluing to the specimen. While the surface contact area of the mounting studs is normally minimized consistent with transducer support requirements, it is generally recommended that the area of the studs be sufficiently large to bridge any open void structure features evident on the cut face of the specimen. The minimum diameter mounting stud consistent with support requirements is normally set at 8 mm (0.315 in), maximum diameters have not been established. A circular stud contact surface shape is not required, rectangular or other shapes are acceptable.

8.2 The gauge length for measuring axial deformations shall be 100 mm \pm 1 mm. Suitable alignment and spacing fixture shall be used to facilitate mounting of the

axial deformation measuring hardware. The gauge length is normally measured between the stud centers.

9. Procedure

9.1 The recommended test protocol for the Simple Performance Test for use in the Superpave volumetric mix design consists of testing the asphalt mix at one effective pavement temperature T_{eff} and one design stress level selected by the design engineer. The effective pavement temperature T_{eff} covers approximately the temperature range of 25 to 60°C (77 to 140°F). The design stress level covers the range between 69 and 207 kPa (10–30 psi) for the unconfined tests, and 483 to 966 kPa for the confined tests. Typical confinement levels range between 35 and 207 kPa (5–30 psi).

9.2 Place the test specimen in the environmental chamber and allow it to equilibrate to the specified testing temperature. For the confined tests, in a standard geotechnical cell, glue the gauge points to the specimen surface as necessary, fit the flexible membrane over the specimen and mount the axial hardware fixtures to the gauge points through the membranes. Place the test specimen with the flexible membrane on in the environmental chamber. A dummy specimen with a temperature sensor mounted at the center can be monitored to determine when the specimen reaches the specified test temperature. In the absence of the dummy specimen, Table 2 provides a summary of the minimum required temperature equilibrium times for samples starting from room temperature (i.e. 25°C).

Unconfined Tests

9.3 After temperature equilibrium is reached, place one of the friction reducing end treatments on top of the platen at the bottom of the loading frame. Place the specimen on top of the lower end treatment, and mount the axial LVDTs to the hardware previously attached to the specimen. Adjust the LVDT to near the end of its linear range to allow the full range to be available for the accumulation of compressive permanent deformation.

9.4 Place the upper friction reducing end treatment and platen on top of the specimen. Center the specimen with the load actuator visually in order to avoid eccentric loading.

9.5 Apply a contact load equal to 5 percent of the static load that will be applied to the specimen, while ensuring the proper response of the LVDTs (i.e., check for proper direction sensing for all LVDTs).

- 9.6 Place the radial LVDTs in contact with the specimen, adjust the LVDTs to near the end of their linear range to allow the full range to be available for the accumulation of radial permanent deformation. Adjust and balance the electronic measuring system as necessary.
- 9.7 Close the environmental chamber and allow sufficient time (normally 10 to 15 minutes) for the temperature to stabilize within the specimen and the chamber.
- 9.8 After the time required for the sample to reach the testing temperature, apply a rapid axial static load at approximately 15 MPa/sec to obtain the desired stress on the specimen.
- 9.9 Hold the load constant until tertiary flow occurs or the total axial strain reaches approximately 2%. The test time will depend on the temperature and the stress levels applied.
- 9.10 During the load application, record the load applied, the axial and radial deflection measured from all LVDTs through the data acquisition system.

Confined Tests

- 9.11 After temperature equilibrium is reached, place one of the friction reducing end treatments on top of the platen at the bottom of the loading frame. Place the specimen on top of the lower end treatment, place the top platen and extend the flexible membrane over the top and bottom platens. Attach the O-rings to seal the specimen on top and bottom platens from the confining air/fluid. Center the specimen with the load actuator visually in order to avoid eccentric loading.
- 9.12 Mount the axial LVDTs to the hardware previously attached to the specimen. Adjust the LVDT to near the end of its linear range to allow the full range to be available for the accumulation of compressive permanent deformation.
- 9.13 Connect the appropriate hose through the upper or lower platen (or take other appropriate steps) to keep the specimen's internal void structure under atmospheric pressure while pressure greater than atmospheric is applied to the outside of the membrane during testing.
- 9.14 Assemble the triaxial cell over the specimen, ensure proper seal with the base and connect the fluid (or gas) pressure lines.
- 9.15 Apply a contact load equal to 5 percent of the static load that will be applied to the specimen, while ensuring the proper response of the LVDTs (i.e., both decrease accordingly). Place the radial LVDTs in contact with the specimen, adjust the LVDTs to near the end of their linear range to allow the full range to be available for the accumulation of radial permanent deformation.
- 9.16 Record the initial LVDT readings and slowly increase the lateral pressure to the desired test level (e.g. 2 psi /sec). Adjust and balance the electronic measuring system as necessary. Close the environmental chamber and allow sufficient time (normally 10 to 15 minutes) for the temperature to stabilize within the specimen and the chamber
- 9.17 After the time required for the sample to reach the testing temperature, apply a rapid axial static load at approximately 15 MPa/sec to obtain the desired deviatoric stress on the specimen. Hold the load constant until the tertiary flow occurs or the total axial strain reaches 4–5%. The test time will depend on the temperature and the stress levels applied.
- 9.18 During the load application, record the load, confining pressure, the axial and radial deflection measured from all LVDTs through the data acquisition system.

10. Calculations

- 10.1 Calculate the average axial deformation for each specimen by averaging the readings from the two axial LVDTs. Convert the average deformation values to total axial strain (ϵ_{Ta}), in/in, by dividing by the gauge length, L [100mm (4-inches)]. Typical total axial strain versus time is shown in Figure 3.
- 10.2 Compute the total axial compliance $D(t) = \epsilon_T / \sigma_d$, where σ_d is the deviator stress applied during testing in psi. ($\sigma_d = \text{applied constant load [lb]} / \text{divided by the cross sectional area of the specimen [in}^2\text{]}$).
- 10.3 Plot the total axial compliance versus time in log space.
- 10.4 Using the data generated between the total axial compliance and time, determine the axial creep compliance parameters (D_0 , D_1 , M_1) from the linear portion of the creep compliance data between a time of ten seconds until the end of the linear curve (see Figure 4). The creep compliance parameters are estimated as follows:
- D_0 : is the instantaneous compliance, and can be assumed to be the value of the total compliance at

a time equal to 100 ms (if the load is applied rapidly at 50 ms).

D_1 : is the intercept of the creep compliance–time relationship, which is the estimated value of the total compliance at a time of one second.

M_1 : is the slope of the creep compliance–time relationship.

- 10.5 The flow point is viewed as the lowest point in the curve of rate of change in axial compliance versus loading time (see Figure 5). The rate of change of creep compliance $D'(t)$ versus loading time should be plotted and the flow time (F_1) is estimated using the following mathematical procedure:

Ten data points are taken from every log scale unit of time at approximately equal intervals. Then, at a specific time t_1 , a polynomial equation is fitted using five points (two points forward and two points backward from the time t_1). The form of this equation is:

$$D(t)_1 = a + bt + ct^2$$

Where

$D(t)_1$ = compliance at time t for t_1 point evaluated

t = time of loading

a, b, c = regression coefficients

By taking the derivative of the above equation, one obtains the following:

$$\frac{d(D(t)_1)}{dt} = b + 2ct$$

Therefore, the rate of change in compliance at time t_1 is equal to $b + 2ct_1$. For each data point selected one can obtain the rate of change in compliance by repeating the above procedure. Once all the rates of change in compliance are calculated, one can find the zero value of rate of change in compliance, i.e., the flow point. This is accomplished by another polynomial curve fit, using equal data points on both sides of the minimum value. Theoretically the “flow point” is the time corresponding to a rate of compliance change equal to zero.

11. Report

- 11.1 Report all specimen information including mix identification, storage conditions, dates of manufacturing and testing, specimen diameter and length, volumetric properties, stress levels used, confining pressure, creep compliance parameters (D_0 , D_1 , M_1) and flow time.

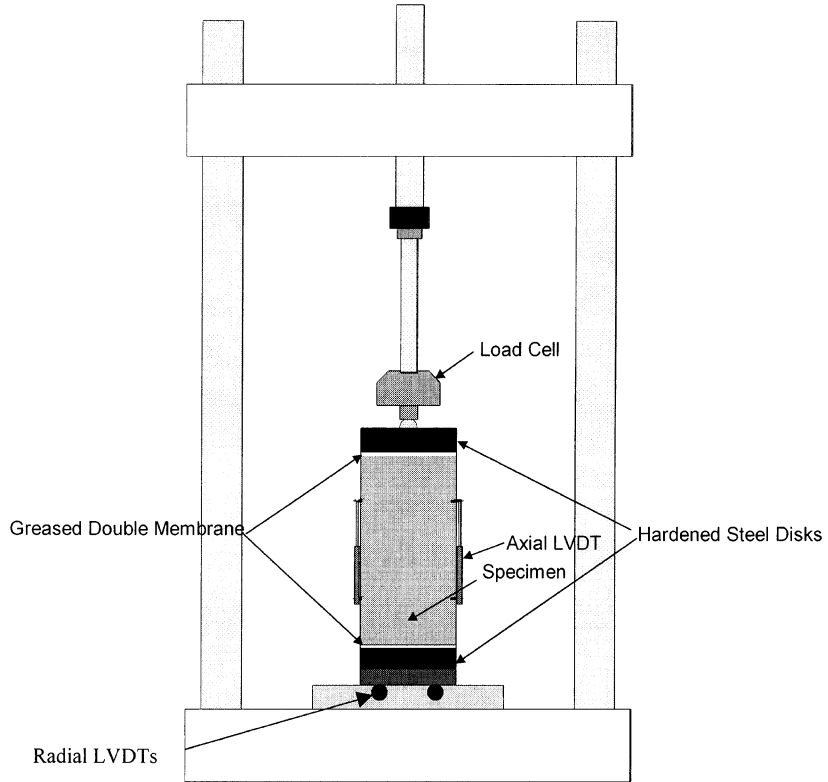


Figure 1. Schematic of static creep/flow time test.

TABLE 1 Recommended number of specimens

LVDTs per Specimen (Total for either vertical or horizontal, not combined total)	Number of Specimens	Estimated Standard Error of the Mean, % Per Mixture's Nominal Aggregate Size		
		12.5mm	19mm	37.5mm
2	2	7.6	9.5	18.8
2	3	6.2	7.7	15.3
3	2	6.7	8.9	17.4
3	3	5.5	7.3	14.2
4	2	6.2	8.6	16.6
4	3	5.0	7.0	13.6

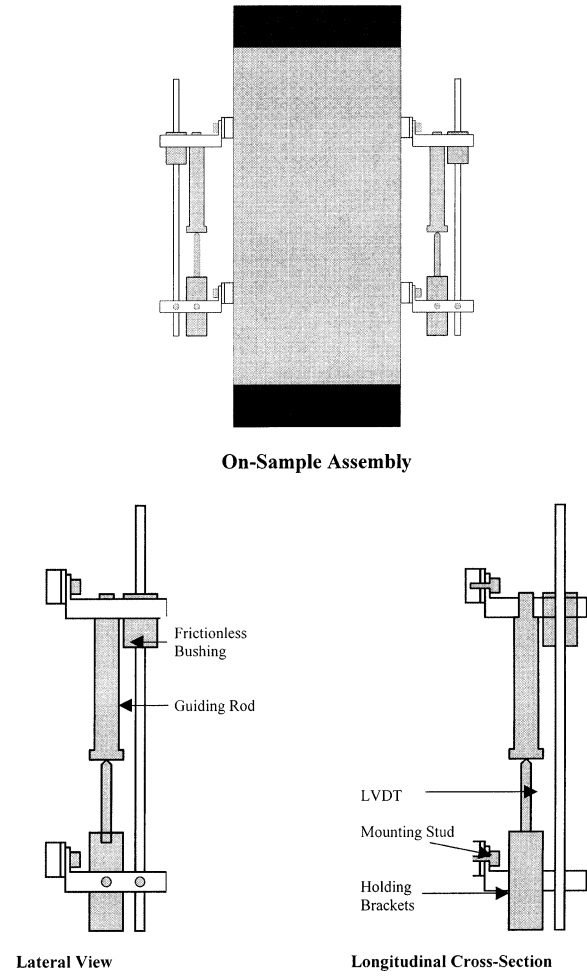


Figure 2. Axial LVDTs instrumentation.

TABLE 2 Recommended equilibrium times

Specimen Test Temperature, °C (°F)	Time, hrs
25 (77)	0.5
30 (86)	1.0
37.8 (100)	1.5
>54.4 (130)	2.0

Arizona State University

[F052] V1.09 Static Creep/Flow Time Strength Test

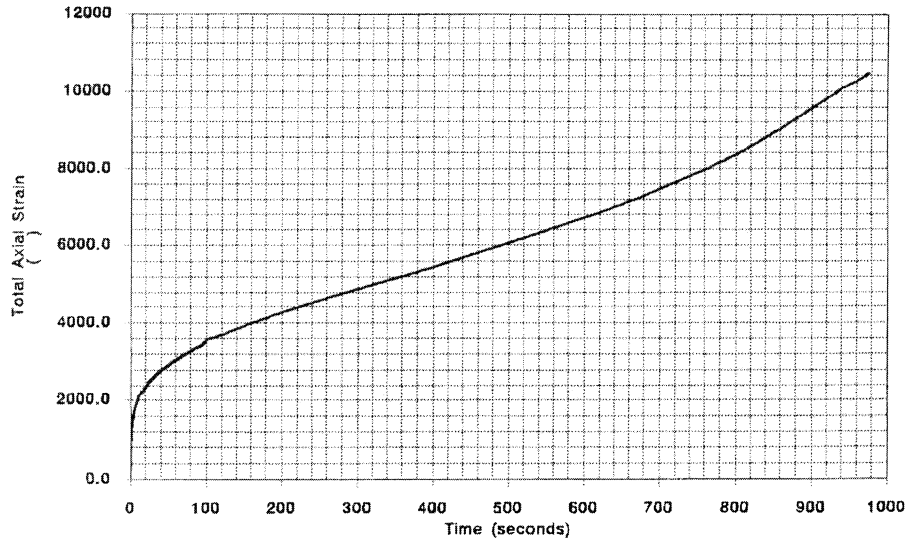


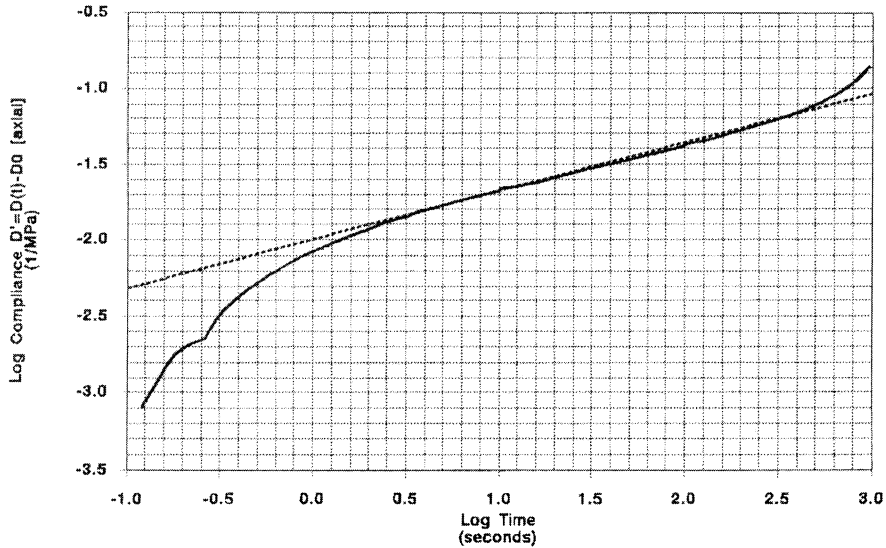
Figure 3. Total axial strain vs. time from a static creep/flow time test.

Arizona State University

[F052] V1.09 Static Creep/Flow Time Strength Test

INDUSTRIAL PROCESS CONTROLS Ltd.

Universal Testing Machine (UTM V3.00B29)



test date and time: Thursday February 3, 2000 9:56 PM

specimen identification: A0943

Data analysis results:

```

-----
minimum regression time (s)      1.0  average deviator stress (kPa) 69.2
maximum regression time (s)     300.0 average confining stress (kPa) 1.4
      time at D0 (s)             0.1
[averaged]  axial based D0 0.008744
            axial based D1 0.009997
            axial based m1 0.321279
            axial based flow time (s) 303.3023
    
```

Figure 4. Regression constants “D₁” and “M₁” from log compliance—log time plot.

Arizona State University
[F052] V1.09 Static Creep/Flow Time Strength Test

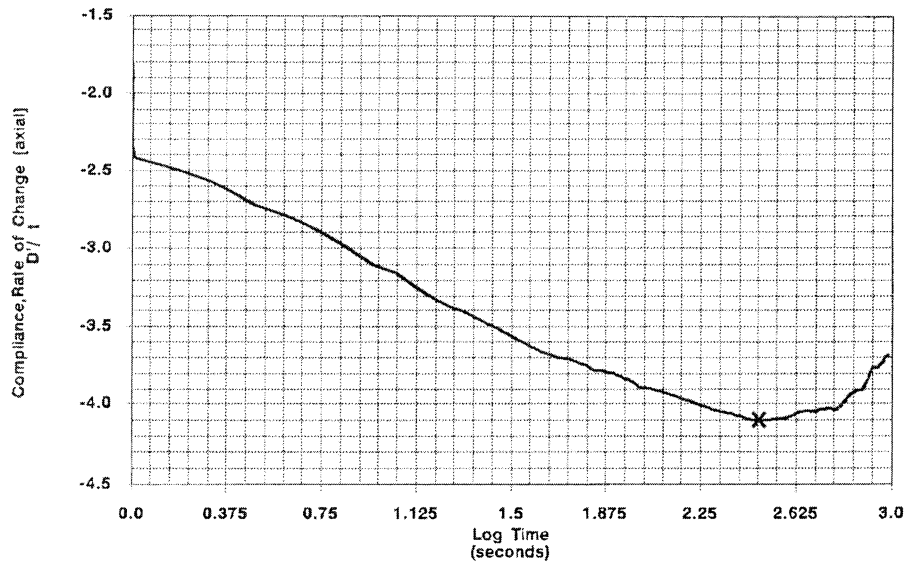


Figure 5. Typical plot of the rate of change in compliance vs. loading time on a log-log scale.

APPENDIX D

TEST METHOD FOR DYNAMIC MODULUS OF ASPHALT CONCRETE MIXTURES FOR FATIGUE CRACKING

1. Scope

- 1.1 This test method covers procedures for preparing and testing asphalt concrete mixtures to determine the dynamic modulus and phase angle at a single effective temperature T_{eff} and design loading frequency.
- 1.2 This test method is a part of test protocols that include determination of the dynamic modulus of the asphalt mix for paving purposes. The other test methods are Standard Test Method for Simple Performance Test for Permanent Deformation Based Upon Dynamic Modulus of Asphalt Concrete Mixture and Standard Test Method for Dynamic Modulus of Asphalt Concrete Mixtures, which is for constructing a master curve for characterizing asphalt concrete for pavement thickness design and performance analysis.
- 1.3 This standard is applicable to laboratory prepared specimens of mixtures with nominal maximum size aggregate less than or equal to 37.5 mm (1.5 in).
- 1.4 *This standard may involve hazardous material, operations, and equipment. This standard does not purport to address all safety problems associated with its use. It is the responsibility of the user of this procedure to establish appropriate safety and health practices and to determine the applicability of regulatory limitations prior to use.*

2. Referenced Documents

2.1 AASHTO Standards

- | | |
|------|---|
| TP4 | Method for Preparing and Determining the Density of Hot Mix Asphalt (HMA) Specimens by Means of the SHRP Gyratory Compactor |
| PP2 | Practice for Mixture Conditioning of Hot Mix Asphalt (HMA) |
| T67 | Standard Practices for Load Verification of Testing Machines (cross-listed with ASTM E4) |
| T269 | Percent Air Voids in Compacted Dense and Open Bituminous Paving Mixtures |

3. Definitions

- 3.1 *Dynamic Modulus*— $|E^*|$, the norm value of the complex modulus calculated by dividing the peak-to-peak stress by the peak-to-peak strain for a material subjected to a sinusoidal loading.
- 3.2 *Complex Modulus*— E^* , a complex number that defines the relationship between stress and strain for a linear viscoelastic material.
- 3.3 *Phase angle*— δ , the angle in degrees between a sinusoidally applied stress and the resulting strain in a controlled-stress test.
- 3.4 *Linear viscoelastic*—within the context of this test, refers to behavior in which the dynamic modulus is independent of stress or strain amplitude.
- 3.5 *Effective Temperature* T_{eff} —Is a single test temperature at which an amount of fatigue cracking would occur equivalent to that measured by considering each season separately throughout the year.

4. Summary of Method

- 4.1 A sinusoidal (haversine) axial compressive stress is applied to a specimen of asphalt concrete at a given temperature and loading frequency. The applied stress and the resulting recoverable axial strain response of the specimen is measured and used to calculate the dynamic modulus and phase angle.
- 4.2 Figure 1 presents a schematic of the dynamic modulus test device.

5. Significance and Use

- 5.1 Dynamic modulus values, measured at one effective temperature T_{eff} and one design frequency selected by the design engineer, are used as performance criteria for fatigue cracking resistance of the asphalt concrete mixture to be used in conjunction with the Superpave Volumetric Mix Design Method.

Note 1—The effective temperature T_{eff} covers approximately the temperature range of 4 to 20°C (39 to 68°F).

- 5.2 Dynamic modulus values measured over a range of temperatures and frequencies of loading can be shifted into a master curve for characterizing asphalt concrete for pavement thickness design and performance analysis.
- 5.3 This test method covers the determination of the dynamic modulus values measured unconfined within the linear viscoelastic range of the asphalt mixture.

Note 2—Future research may indicate the need for confined stress states and nonlinear material characterization. Confinement may be applied with various types of axisymmetric triaxial cells to address these needs.

6. Apparatus

- 6.1 Dynamic Modulus Test System—A dynamic modulus test system consisting of a testing machine, environmental chamber, measuring system, and specimen end fixtures.

- 6.1.1 *Testing Machine*—A materials testing machine capable of producing a controlled haversine compressive loading of paragraphs 9.7 and 9.8 is required.

Note 3—The testing machine shall have a capability of applying load over a range of frequencies from 1 to 30 Hz. Stress levels up to 2800 kPa (400 psi) may be required at certain temperatures and frequencies. However, for virtually all effective temperatures in the US, stress levels between 100 kPa and 1500 kPa (14–280 psi) have been found to be sufficient. This latter range of stress levels converts to an approximate range of 0.8–11.8 kN (170–2656 lbf) on a 100 mm diameter specimen. If the machine is to be dedicated only to this test procedure with no requirement for additional strength testing or low temperature testing, it is recommended that the lowest capacity machine capable of applying the required waveforms be used. Alternatively, larger capacity machines may be used with low capacity load cells or signal amplifiers. It has been found that feedback controlled testing machines equipped with appropriate servovalves can be used for this test. As a general rule of thumb, the dynamic load capacity of a testing machine between 10 and 30 Hz will be approximately 65–75 percent of the monotonic (“static”) capacity, but this rule varies by manufacturer. A 25–50 kN capacity servohydraulic testing machine has been found to be adequate for virtually all of the tests in the suite of simple performance tests.

- 6.1.2 *Environmental Chamber*—A chamber for controlling the test specimen at the desired tempera-

ture is required. The environmental chamber shall be capable of controlling the temperature of the specimen over a temperature range from 15 to 60°C (60 to 140°F) to an accuracy of $\pm 0.5^\circ\text{C}$ (1°F). The chamber shall be large enough to accommodate the test specimen and a dummy specimen with temperature sensor mounted at the center for temperature verification.

Note 4—A chamber that will control temperatures down to -10°C (14°F) may be required for other tests mentioned in paragraph 1.2 of this method.

Note 5—If the chamber does not have sufficient room for a dummy specimen, it is permissible to have a second chamber controlling the temperature of the dummy. The separate dummy chamber must be operated similar to the operation of the main test specimen chamber so that the dummy will accurately register the time required to obtain temperature equilibrium on the test specimen.

- 6.1.3 *Measurement System*—The system shall include a data acquisition system comprising analog to digital conversion and/or digital input for storage and analysis on a computer. The system shall be capable of measuring and recording the time history of the applied load and the axial deformations for the cycles required by this test method. The system shall be capable of measuring the period of the applied sinusoidal load and resulting deformations with a resolution of 0.5 percent.

- 6.1.3.1 *Load*—The load shall be measured with an electronic load cell having adequate capacity for the anticipated load requirements. The load cell shall be calibrated in accordance with AASHTO T67. The load measuring transducer shall have an accuracy equal to or better than 0.25 percent of full scale.

Note 6—A 25 kN (5600 lbf) load cell has been found to be the approximate maximum capacity limit for this test method because of range versus resolution factors. It is recommended that if the selected load cell capacity is 25 kN or greater, the system should be equipped with either manual or automatic amplification selection capability so that it can be used to enhance control of the system at the minimum anticipated loads given in paragraph 9.7.

Axial Deformations—Axial deformations shall be measured with displacement transducers referenced to gauge points contacting the specimen as shown in Figure 2. The deformations shall be measured at a minimum of two locations 180° apart (in planview); however, three locations located 120°

apart is recommended to minimize the number of replicate specimens required for testing.

Note 7—Analog transducers such as linear variable differential transformers (LVDTs) having a range of ± 0.5 mm (0.02 in) and inherent nonlinearity equal to or better than ± 0.025 percent of full scale have been found adequate for this purpose. Software or firmware linearization techniques may be used to improve the inherent nonlinearity. Amplification and signal conditioning techniques may be used with the ± 0.5 mm range LVDTs to obtain resolutions down to 0.001mm (0.00004 in) or better for small strain test conditions. These techniques may be manual or automatic. In general, increasing the resolution by manual signal amplification will result in reduction of the overall range of the instrument by the same factor.

6.1.4 *Loading Platens*—Platens, with a diameter equal to or greater than that of the test specimen are required above and below the specimen to transfer the load from the testing machine to the specimen. Generally, these platens should be made of anodized high strength aluminum. Softer materials will require more frequent replacement. Materials that have linear elastic modulus properties and hardness properties lower than that of 6061-T6 aluminum shall not be used. Steel platens may cause too much seating load to the specimen at high temperature and are not recommended.

6.1.5 *End Treatment*—Friction reducing end treatments shall be placed between the specimen ends and the loading platens.

Note 8—End treatments consisting of two 0.5 mm (0.02 in) thick latex sheets separated with silicone grease have been found to be suitable friction reducing end treatments.

6.2 *Gyratory Compactor*—A gyratory compactor and associated equipment for preparing laboratory specimens in accordance with AASHTO TP4 shall be used. Field cores shall meet the requirements of paragraphs 7.4 through 7.6 of this test method and any reports on cores so tested will contain a detailed description of the location of any lift boundaries within the height of the specimen (e.g. lift order, thickness and material homogeneity).

6.3 *Saw*—A machine for cutting test specimens to the appropriate length is required. The saw or grinding machine shall be capable of cutting specimens to the prescribed dimensions without excessive heating or shock.

Note 9—A double-bladed diamond masonry saw greatly facilitates the preparation of test specimens with smooth, parallel ends. Both single- and double-bladed diamond saws should have feed mechanisms and speed controls of sufficient precision to ensure compliance with paragraphs 7.5 and 7.6 of this method. Adequate blade stiffness is also important to control flexing of the blade during thin cuts.

6.4 *Core Drill*—A coring machine with cooling system and a diamond bit for cutting nominal 100 mm (4 in) diameter test specimens.

Note 10—A coring machine with adjustable vertical feed and rotational speed is recommended. The variable feeds and speeds may be controlled by various methods. A vertical feed rate of approximately 0.05 mm/rev (0.002 in/rev) and a rotational speed of approximately 455 RPM has been found to be satisfactory for several of the Superpave mixtures.

7. Test Specimens

7.1 *Size*—Dynamic modulus testing shall be performed on 100 mm (4 in) diameter by 150 mm (6 in) high test specimens cored from gyratory compacted mixtures.

7.2 *Aging*—Mixtures shall be aged in accordance with the short-term oven aging procedure in AASHTO PP2.

7.3 *Gyratory Specimens*—Prepare 165 mm (6.5 in) high specimens to the required air void content in accordance with AASHTO TP-4.

Note 11—Testing should be performed on test specimens meeting specific air void tolerances. The gyratory specimen air void content required to obtain a specified test specimen air void content must be determined by trial and error. Generally, the test specimen air void content is 1.5 to 2.5 percent lower than the air void content of the gyratory specimen when the test specimen is removed from the middle as specified in this test method.

7.4 *Coring*—Core the nominal 100 mm (4 in) diameter test specimens from the center of the gyratory specimens. Both the core drill and the gyratory specimen should be adequately supported to ensure that the resulting test specimen is cylindrical with sides that are smooth, parallel, and free from steps, ridges, and grooves.

Diameter—Measure the diameter of the test specimen at the mid-height and third points along axes that are 90 degrees apart. Record each of the six measurements to the nearest 1 mm (0.05 in). Calculate the average and the standard deviation.

tion of the six measurements. If the standard deviation is greater than 2.5 mm (0.01 in) discard the specimen. For acceptable specimens, the average diameter, reported to the nearest 1 mm, shall be used in the stress calculations.

7.5 End Preparation—The ends of all test specimens shall be smooth and perpendicular to the axis of the specimen. Prepare the ends of the specimen by sawing with a single- or double-bladed saw. The prepared specimen ends shall meet the tolerances described below. Reject test specimens not meeting these tolerances.

7.5.1 The specimen ends shall have a cut surface waviness height within a tolerance of ± 0.05 mm across any diameter. This requirement shall be checked in a minimum of three positions at approximately 120° intervals using a straight edge and feeler gauges approximately 8–12.5 mm (0.315–0.5 in) wide or an optical comparator.

7.5.2 The specimen end shall not depart from perpendicular to the axis of the specimen by more than 0.5 degrees (i.e. 0.87 mm or 0.03 in across the diameter of a 100 mm diameter specimen). This requirement shall be checked on each specimen using a machinists square and feeler gauges.

7.6 Air Void Content—Determine the air void content of the final test specimen in accordance with AASHTO T269. Reject specimens with air voids that differ by more than 0.5 percent from the target air voids.

7.7 Number—The number of test specimens required depends on the number of axial strain measurements made per specimen and the desired accuracy of the average dynamic modulus. Table 1 summarizes the replicate number of specimens that should be tested to obtain an accuracy limit of less than ± 15 percent.

7.8 Sample Storage—Wrap completed specimens in polyethylene and store in an environmentally protected storage area at temperatures between 5 and 25°C (40 and 75°F).

Note 12—To eliminate effects of aging on test results, it is recommended that specimens be stored no more than two weeks prior to testing.

8. Test Specimen Instrumentation

8.1 Attach mounting studs for the axial LVDTs to the sides of the specimen with epoxy cement. Figure 3 presents details of the mounting studs and LVDT mounting hardware.

Note 13—Quick setting epoxy such as Duro Master Mend Extra Strength Quick Set QM-50 has been found satisfactory for attaching studs. Under certain conditions when using the triaxial cell mentioned in Note 2, the mounting studs may not require gluing to the specimen. While the surface contact area of the mounting studs is normally minimized consistent with transducer support requirements, it is generally recommended that the area of the studs be sufficiently large to bridge any open void structure features evident on the cut face of the specimen. The minimum diameter mounting stud consistent with support requirements is normally set at 8 mm (0.315 in), maximum diameters have not been established. A circular stud contact surface shape is not required, rectangular or other shapes are acceptable.

8.2 The gauge length for measuring axial deformations shall be 100 mm ± 1 mm. An alignment and spacing fixture similar to that shown in Figure 3 can be used to facilitate mounting of the axial deformation measuring hardware. The gauge length is normally measured between the stud centers.

9. Procedure

9.1 The recommended test protocol for the Simple Performance Test for use in the Superpave volumetric mix design consists of testing the asphalt mix at one effective pavement temperature T_{eff} and one design frequency selected by the design engineer. The effective pavement temperature T_{eff} covers approximately the temperature range of 4 to 20°C (39 to 69°F). The design frequency covers the range between 5 to 20 Hz.

9.2 Place the test specimen in the environmental chamber and allow it to equilibrate to the specified testing temperature. A dummy specimen with a temperature sensor mounted at the center can be monitored to determine when the specimen reaches the specified test temperature. In the absence of the dummy specimen, Table 2 summarizes minimum recommended temperature equilibrium times from room temperature (i.e. 25°C).

9.3 Place one of the friction reducing end treatments on top of the platen at the bottom of the loading frame. Place the specimen on top of the lower end treatment, and mount the axial LVDTs to the hardware previously attached to the specimen. Adjust the LVDT to near the end of its linear range to allow the full range to be available for the accumulation of compressive permanent deformation.

- 9.4 Place the upper friction reducing end treatment and platen on top of the specimen. Center the specimen with the load actuator visually in order to avoid eccentric loading.
- 9.5 Apply a contact load (P_{\min}) equal to 5 percent of the dynamic load that will be applied to the specimen.
- 9.6 Adjust and balance the electronic measuring system as necessary.
- 9.7 Apply haversine loading (P_{dynamic}) to the specimen without impact in a cyclic manner. The dynamic load should be adjusted to obtain axial strains between 50 and 150 microstrains.

Note 14—The dynamic load depends upon the specimen stiffness and generally ranges between 100 and 1500 kPa (14 and 218 psi). Higher load is needed at colder temperatures. Table 3 presents target dynamic load levels based on temperature.

- 9.8 Test the specimens at selected temperature by first preconditioning the specimen with 200 cycles at 25 Hz using the target dynamic loads in Table 3 (interpolate if necessary). Then load the specimen using the selected frequency and number of cycles as specified in Table 4.

10. Calculations

- 10.1 Capture and store the last 6 loading cycles of full waveform data for each transducer. Determine the average amplitude of the sinusoidal load and deformation from each axial displacement transducer over the first 5 cycles of the last 6 loading cycle group (since the displacement will lag behind the load, the computations may use data from the 6th cycle, but might not have enough of the waveform to fully determine the properties in the 6th cycle).
- 10.2 Average the signals from the displacement transducers. Determine the average time lag between the peak load and the peak deformation over the 5 loading cycles.

Note 15—Different approaches are available to determine these. The approach is highly dependent upon the number of data points collected per cycle. Approaches that have been used include peak search algorithms, various curve fitting techniques, and Fourier Transform. Curve fitting techniques and other numerical techniques have also been used to determine the phase angle from the more stable center portion of the waveform instead of the peaks. If any displacement transducer is out of range or otherwise obviously reading incorrectly during a cycle, discard the data for that cycle.

Note 16—For testing that will be used for statistical within-specimen variability and for establishing local precision and bias statements, paragraphs 10.3 through 10.7 must include computations from each individual displacement transducer in addition to the results from the averaged displacements. Therefore, it is a strict requirement that the data storage requirements of paragraph 10.1 be met.

- 10.3 Calculate the loading stress, σ_o , as follows (see Figure 4):

$$\sigma_o = \frac{\bar{P}}{A}$$

Where:

\bar{P} = average load amplitude
 A = area of specimen
 σ_o = stress.

- 10.4 Calculate the recoverable axial strain for each frequency, ϵ_o , as follows:

$$\epsilon_o = \frac{\bar{\Delta}}{GL}$$

Where:

$\bar{\Delta}$ = average deformation amplitude
 GL = gauge length
 ϵ_o = strain.

- 10.5 Calculate dynamic modulus, $|E^*|$ for each frequency as follows:

$$\text{Dynamic Modulus, } |E^*| = \frac{\sigma_o}{\epsilon_o}$$

- 10.6 Calculate the phase angle for each frequency:

$$\phi = \frac{t_i}{t_p} \times (360)$$

Where

t_i = average time lag between a cycle of stress and strain (sec)
 t_p = average time for a stress cycle (sec.).

11. Report

- 11.1 Report the average stress and strain for each temperature-frequency combination tested.
- 11.2 Report the dynamic modulus and phase angle for each temperature-frequency combination tested.

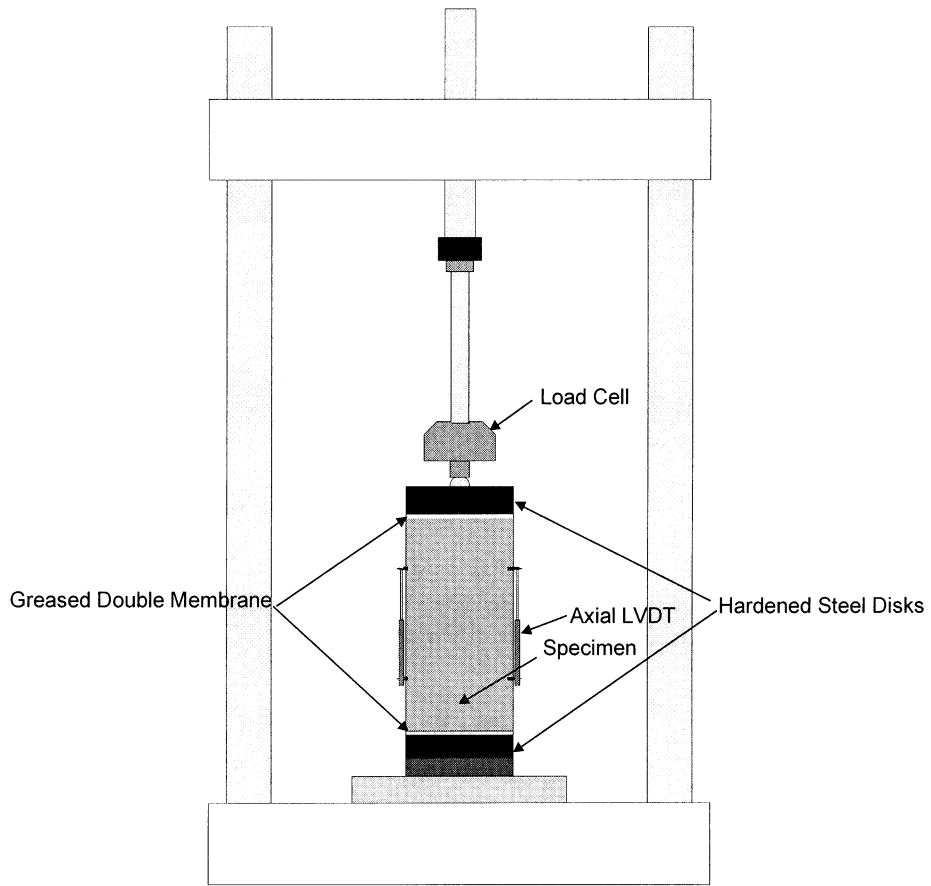
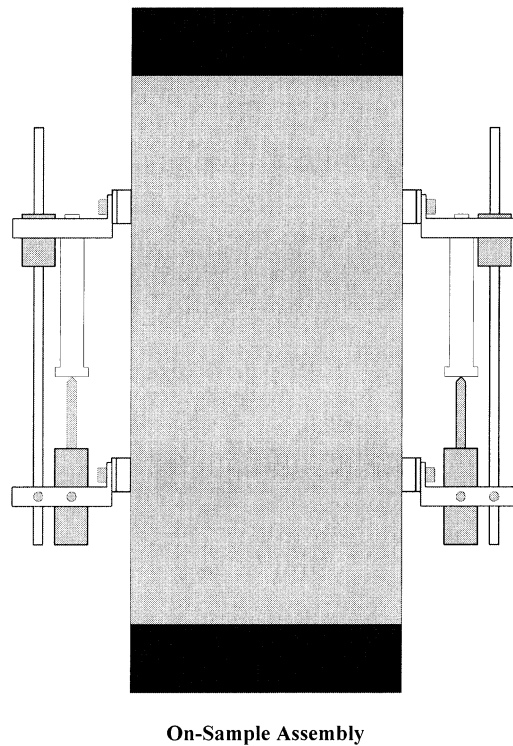


Figure 1. Schematic of dynamic modulus test device.



On-Sample Assembly

Figure 2. Schematic of gauge points.

TABLE 1 Recommended number of specimens

LVDTs per Specimen	Number of Specimens	Estimated Limit of Accuracy
2	4	13.4
3	2	13.1

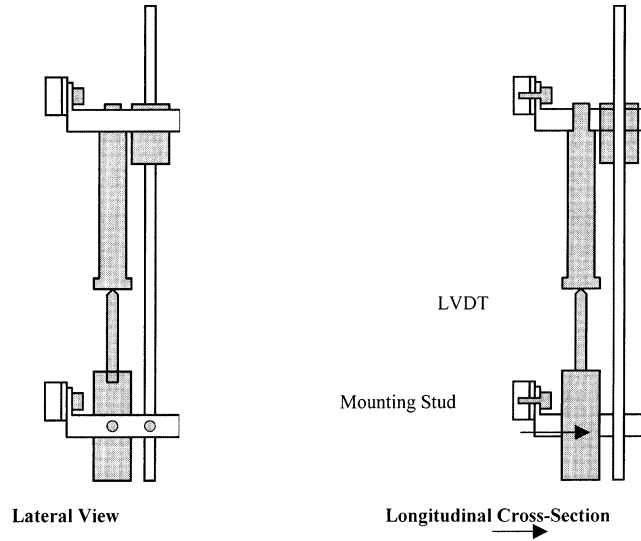


Figure 3. Mounting hardware details.

TABLE 2 Recommended equilibrium times

Specimen Test Temperature °C (°F)	Time, hrs
4 (39)	TBD*
10 (50)	
20 (69)	

*To be determined

TABLE 3 Target dynamic loads

Temperature, °C (°F)	Range, kPa	Range, psi
4 (40)	400 – 1500	58 – 218
10 (50)	200-500	29 – 73
20 (69)	100 -690	14 – 100

TABLE 4 Cycles for test sequence

Frequency	Number of Cycles
20	150
10	100
5	50

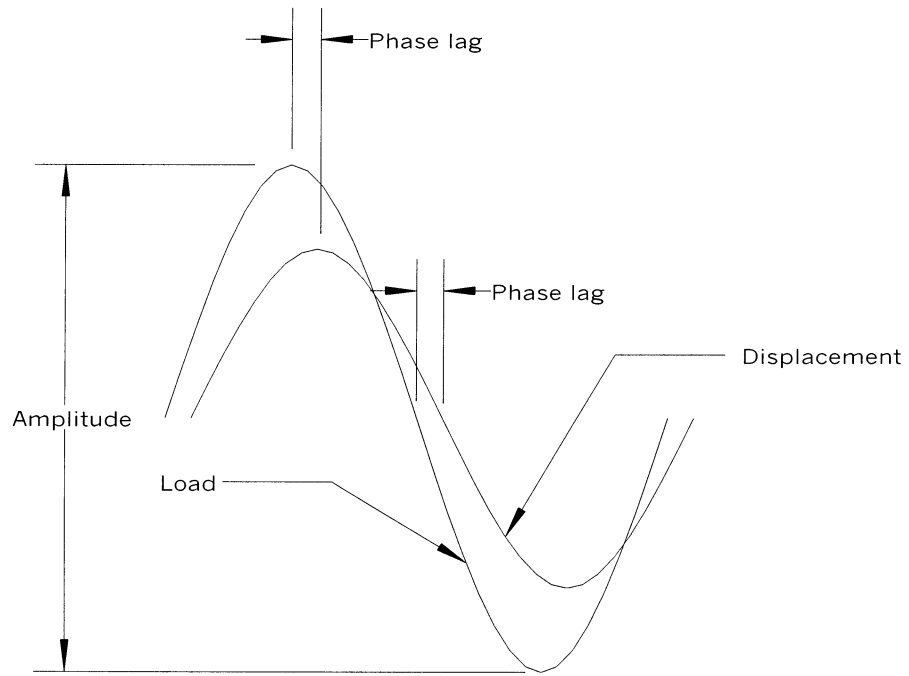


Figure 4. Ideal waveform schematic.

APPENDIX E

TEST METHOD FOR INDIRECT TENSILE CREEP TESTING OF ASPHALT MIXTURES FOR THERMAL CRACKING

1. Scope

- 1.1 This test method covers procedures for preparing and testing asphalt concrete mixtures to determine the creep compliance at a given temperature and stress level.
- 1.2 In this test, a disc sample of bituminous paving mixture is subjected to a diametral static creep load. Horizontal and vertical deformations are recorded throughout the test (vertical deformations are required only if Poisson's ratio is to be calculated from the test results).
- 1.3 This standard is applicable to laboratory prepared specimens of mixtures with nominal maximum size aggregate less than or equal to 19.0 mm (0.75 in).
- 1.4 *This standard may involve hazardous material, operations, and equipment. This standard does not purport to address all safety problems associated with its use. It is the responsibility of the user of this procedure to establish appropriate safety and health practices and to determine the applicability of regulatory limitations prior to use.*

2. Referenced Documents

2.1 AASHTO Standards

TP4	Method for Preparing and Determining the Density of Hot Mix Asphalt (HMA) Specimens by Means of the SHRP Gyration Compactor
PP2	Practice for Mixture Conditioning of Hot Mix Asphalt (HMA)
T269	Percent Air Voids in Compacted Dense and Open Bituminous Paving Mixtures
TP9-94	Standard Test Method for Determining the Creep Compliance and Strength of Hot Mix Asphalt (HMA) Using the Indirect Tensile Test Device

3. Definitions

- 3.1 *Creep*—The time-dependent part of strain resulting from stress.
- 3.2 *Tensile Strength*— S_t , the strength shown by a specimen subjected to tension.
- 3.3 *Creep Compliance*— $D(t)$, the time-dependent strain divided by the applied stress.

4. Summary of Method

- 4.1 This standard describes two procedures, the tensile strength and the tensile creep. Both testings are determined for thermal cracking analyses.
- 4.2 Tensile strength is determined by applying a constant rate of vertical deformation (ram movement) to failure.
- 4.3 The tensile creep is determined by applying a static load of fixed magnitude (percentage of the tensile strength) along the diametral axis of a specimen. The horizontal and vertical deformations measured near the center of the specimen are used to calculate tensile creep compliance as a function of time (vertical deformations are required only if Poisson's ratio is to be calculated from the test results). By measuring deformations in regions with relatively constant stresses and away from the localized non-linear effects induced by the steel loading strips, Poisson's ratio can be more accurately determined.

5. Significance and Use

- 5.1 Tensile strength and tensile creep test data are required to determine the master relaxation modulus curve and fracture parameters used for the thermal fracture analysis.
- 5.2 The values of creep compliance and tensile strength can be used in linear visco-elastic analysis to calculate the fatigue cracking potential of asphalt concrete.

6. Apparatus

- 6.1 Indirect Tensile Test System—The indirect tensile test system consists of an axial loading testing machine, environmental chamber, and measuring system. The indirect tensile test system is shown in Figure 1.
 - 6.1.1 *Testing Machine*—A servo-hydraulic testing machine capable of producing a controlled fixed or constant compressive loading and constant rate of ram displacement between 12 and 75 mm/minute.

6.1.2 *Environmental Chamber*—A chamber for controlling the test specimen at the desired temperature. The environmental chamber shall be capable of controlling the temperature of the specimen over a temperature range from -10 to 21.1°C (14 to 70°F) to an accuracy of $\pm 0.5^{\circ}\text{C}$ (1°F). The chamber shall be large enough to accommodate the test specimen and a dummy specimen with thermocouple mounted at the center for temperature verification.

6.1.3 *Measurement System*—The system shall be fully computer controlled capable of measuring and recording the time history of the applied load and the deformations. The system shall be capable of measuring the period of the applied load and resulting deformations with a resolution of 0.5 percent.

6.1.3.1 *Load*—The load shall be measured with an electronic load cell in contact with one of the specimen caps. The load measuring system shall have a range of 0 to 22 kN (0 to 5000 lb) with a resolution of 5 N (1 lb).

6.1.3.2 *Horizontal and Vertical Deformations*—Vertical and horizontal deformations shall be measured with linear variable differential transformers (LVDT) mounted between brass gauge points glued to the specimen as shown in Figure 2. The deformations shall be measured at both sides of the specimen. The LVDTs shall have a range of ± 0.5 mm (0.02 in). The deformation measuring system shall have auto zero.

Note 1—Amplification and signal conditioning techniques may be used to obtain resolutions down to 0.001 mm (0.00004 in) or better for small strain test conditions. These techniques may be manual or automatic.

Note 2—Vertical deformations are required only if Poisson's ratio is to be calculated from the test results.

6.1.4 *Mounting Template*—A mounting template for placing and mounting the brass gauge points to each side of the specimen as shown in Figure 3.

6.1.5 *Loading Guide Device*—A steel frame is used to apply the load diametrically to the specimen as shown in Figure 1.

6.2 *Gyratory Compactor*—A gyratory compactor and associated equipment for preparing laboratory specimens in accordance with AASHTO TP4 shall be used.

6.3 *Saw*—Diamond masonry saw for cutting test specimens to the appropriate thicknesses. The saw shall have a diamond cutting edge and shall be capable of cutting specimens to the prescribed dimensions without excessive heating or shock.

Note 3—A double-bladed saw greatly facilitates the preparation of test specimens with smooth, parallel ends.

7. Test Specimens

7.1 *Size*—Indirect tensile testing shall be performed on 150 mm (6 in) diameter by 38 mm (1.5 in) thick test specimens sawed from gyratory compacted mixtures.

7.2 *Aging*—Mixtures shall be aged in accordance with the short-term oven aging procedure in AASHTO PP2.

7.3 *Gyratory Specimens*—Prepare 128 mm (5 in) high specimens to the required air void content in accordance with AASHTO TP-4.

Note 4—Testing should be performed on test specimens meeting specific air void tolerances. The gyratory specimen air void content required to obtain a specified test specimen air void content must be determined by trial and error.

7.4 *Sawing*—Saw at least 6 mm from both sides of each test specimen to provide smooth, parallel surfaces for mounting the measurement gauges. Then saw the testing specimen to the required thickness (two specimens out of each compacted plug).

7.5 *Thickness*—Measure the thickness of the test specimen at four different locations. Record each of the four measurements to the nearest 1 mm (0.05 in). Calculate the average and the standard deviation of the four measurements. If the standard deviation is greater than 2.5 mm (0.01 in) discard the specimen. For acceptable specimens, the average thickness, reported to the nearest 1 mm, shall be used in the stress calculations.

7.6 *Mounting LVDTs*—Epoxy four brass gauge points to each flat face of the specimen. Two gauge points will be placed along the vertical and two along the horizontal axes. The placement and location of the gauge points on each face shall produce a mirror of each other. Mount the LVDTs on the gauge points (Figure 2).

7.7 *Air Void Content*—Determine the air void content of the final test specimen in accordance with AASHTO

T269. Reject specimens with air voids that differ by more than 0.5 percent from the target air voids.

7.8 *Replicates*—The number of test specimens required depends on the number of the desired stress levels. At least two replicates will be used for each test condition.

7.9 *Sample Storage*—Wrap completed specimens in polyethylene and store in an environmentally protected storage area at temperatures between 5 and 25°C (40 and 75°F).

Note 5—To eliminate effects of aging on test results, it is recommended that specimens be stored no more than two weeks prior to testing.

8. Test Specimen Instrumentation

8.1 Attach mounting studs for the LVDTs to the sides of the specimen with epoxy cement. Only the horizontal LVDTs are used for the indirect tensile strength test. For the indirect tensile creep test, both vertical and horizontal LVDTs are used if Poisson's ratio is to be calculated from the test results. However, if Poisson's ratio is calculated using the model provided in Section 11.3.4, only horizontal LVDTs will be used.

Note 6—Quick setting epoxy such as Duro Master Mend Extra Strength Quick Set QM-50 has been found satisfactory for attaching studs.

8.2 The gauge length for measuring deformations shall be 76 mm \pm 1 mm (3 in). An alignment and spacing fixture similar to that shown in Figure 3 can be used to facilitate mounting of the deformation measuring hardware.

9. Preliminary Determinations

9.1 *Determining Specimen Thickness and Diameter*—Determine specimen thickness and diameter to the nearest 1 mm.

9.2 *Determining the Bulk Specific Gravity*—Determine the bulk specific gravity of each specimen in accordance with T166.

9.3 *Specimen Drying*—If the specimens were immersed directly into water, after determining the bulk specific gravity allow each specimen to dry at room temperature to a constant mass.

10. Procedure

10.1 The recommended test protocol for the Simple Performance Test for use in the Superpave volumetric

mix design consists of testing the asphalt mix at one temperature and one design stress level. The test temperature selected for this test for the low temperature thermal fracture analysis is 12.8°C (55°F). A stress level of 2% of the indirect tensile strength is recommended for the test.

Indirect Tensile Strength Test

10.2 Set the temperature of the environmental chamber to the test temperature and, once the test temperature \pm 0.2°C is achieved, place the test specimen in the environmental chamber and allow it to equilibrate to the specified testing temperature. A dummy specimen with a thermocouple mounted at the center can be monitored to determine when the specimen reaches the specified test temperature. In the absence of the dummy specimen, allow each specimen to remain at the test temperature from 3 \pm 1-hour prior to testing.

10.3 Center the specimen with the hydraulic load actuator visually in order to avoid eccentric loading.

10.4 Apply a contact load (P_{\min}) equal to 5 percent of the expected load that will be applied to the specimen.

10.5 Zero the load cell reading. Set the LVDTs at the lower limit to be able to benefit from the whole range of the LVDT.

10.6 The tensile strength is determined by applying a load to the specimen at a rate of 50 mm of ram (vertical) movement per minute (2 in/minute). Record the horizontal deformations on both sides of the specimen and the load, until the load starts to decrease.

Indirect Tensile Creep Test

10.7 On a new specimen, repeat steps 10.2 to 10.5 similar to the indirect tensile strength test.

10.8 Calculate the load (P) to be applied on the specimen that would yield a stress equaled 2% of the tensile strength of the material.

10.9 Apply the static load (P) to the specimen without impact. The load should be applied for a time period of 1000 \pm 10 seconds. Unload the specimen, allow a recovery time of 1000 \pm 10 seconds. Horizontal and vertical deformations will be recorded during the both the load application and recovery time.

Note 7—The loading head should not be in contact with the specimen during the unloading time.

Note 8—Vertical deformations are required only if Poisson's ratio is to be calculated from the test results.

11. Calculations

11.1 Determine the air voids for each specimen.

11.2 Tensile Strength Calculations.

11.2.1 Determine the average thickness, diameter for each replicate.

11.2.2 Obtain the maximum load recorded for each replicate.

11.2.3 Calculate the horizontal tensile strength for each replicate, as follows:

$$\text{Horizontal Tensile Stress} = S_t = \frac{2P_{\max}}{\pi T d}$$

Where:

P_{\max} = maximum load on the load–deformation plot

d = diameter of specimen

T = thickness of specimen.

11.2.4 Calculate the average horizontal tensile strength of the two replicates. The two values should be within 15% of each other.

11.3 Creep Compliance Calculations.

11.3.1 Determine the average thickness, diameter for each replicate.

11.3.2 Determine the average horizontal (δ_{xx}) and vertical (δ_{yy}) deformations from both sides of the specimen as a function of time (t).

11.3.3 Calculate Poisson's ratio, μ , using the vertical and horizontal deformations, as follows:

$$\mu = \frac{(1.0695 * \delta_{xx} / \delta_{yy} - 0.2339)}{(0.7801 - 0.3074 * \delta_{xx} / \delta_{yy})}$$

11.3.4 Or Poisson's ratio, μ , can be determined from a regression equation developed by (Mirza &

Witczak) if only horizontal LVDTs are used. The equation is:

$$\mu = 0.15 + \frac{0.35}{1 + \exp(3.1849 - 0.04233 \times \text{Temp})}$$

Temperature is expressed in degree Fahrenheit.

11.3.5 Calculate the Modulus, $E(t)$, as follows:

$$\text{Modulus} = E(t) = \frac{P}{T \delta_{xx}} (0.2339 + 0.7801 \mu)$$

11.3.6 Calculate Creep Compliance, $D(t)$, as a function of time as follows:

$$D(t) = E(t)^{-1} = D t^m$$

Where:

D = the intercept of the creep compliance–time curve

m = the slope of the creep compliance–time curve.

11.3.7 Fit a power model for the creep compliance versus time to obtain the slope (m) and the intercept (D). Using the slope and the intercept values calculate the creep compliance at a time of 1000 seconds from the equation given in Section 11.3.6. Figure 4 shows a creep compliance versus log time plot.

11.3.8 Calculate the average values for the creep compliance parameters (D and m) and the creep compliance at 1000 seconds from both replicates.

12. Report

12.1 Report all specimen information including mix identification, storage conditions, dates of manufacturing and testing, specimen diameter and thickness, volumetric properties, and stress level used.

12.2 Report the average horizontal tensile strength for the specimen.

12.3 Report the average creep compliance parameters (D and m) and the creep compliance at the end of the loading cycle (1000 seconds) by averaging the indirect tensile creep test results from each replicate.

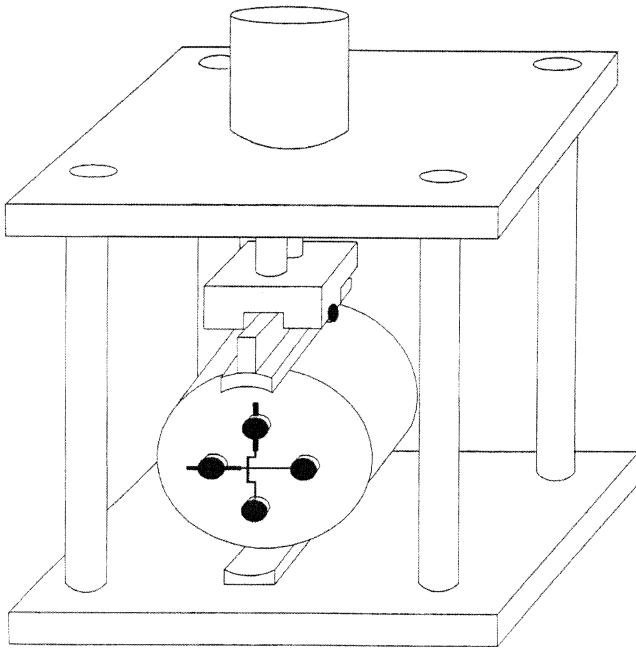


Figure 1. Schematic of indirect tensile test loading frame.

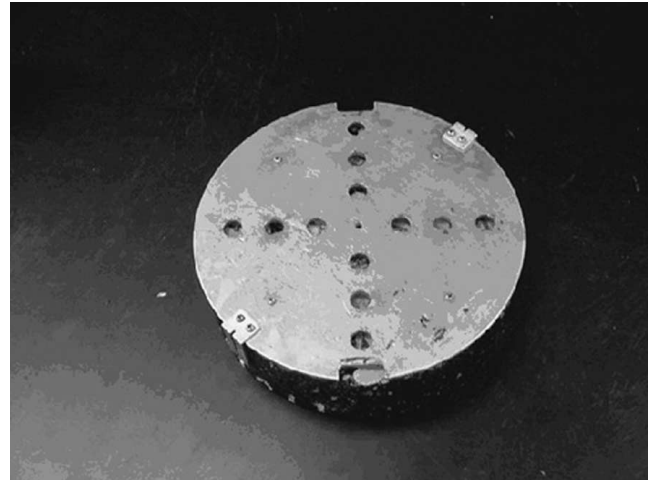


Figure 3. Mounting hardware details.



Figure 2. Gauge points.

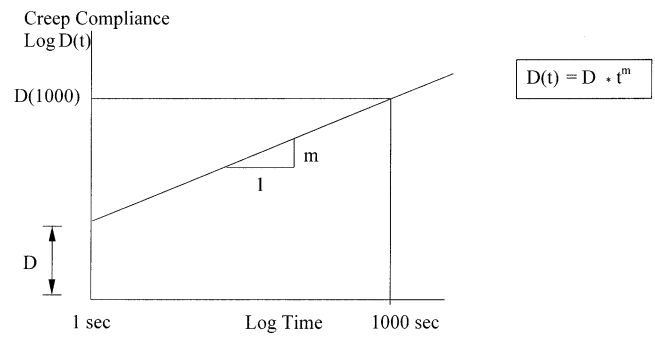


Figure 4. Creep compliance vs. log time.

The **Transportation Research Board** is a unit of the National Research Council, which serves the National Academy of Sciences and the National Academy of Engineering. The Board's mission is to promote innovation and progress in transportation by stimulating and conducting research, facilitating the dissemination of information, and encouraging the implementation of research results. The Board's varied activities annually draw on approximately 4,000 engineers, scientists, and other transportation researchers and practitioners from the public and private sectors and academia, all of whom contribute their expertise in the public interest. The program is supported by state transportation departments, federal agencies including the component administrations of the U.S. Department of Transportation, and other organizations and individuals interested in the development of transportation.

The National Academy of Sciences is a private, nonprofit, self-perpetuating society of distinguished scholars engaged in scientific and engineering research, dedicated to the furtherance of science and technology and to their use for the general welfare. Upon the authority of the charter granted to it by the Congress in 1863, the Academy has a mandate that requires it to advise the federal government on scientific and technical matters. Dr. Bruce M. Alberts is president of the National Academy of Sciences.

The National Academy of Engineering was established in 1964, under the charter of the National Academy of Sciences, as a parallel organization of outstanding engineers. It is autonomous in its administration and in the selection of its members, sharing with the National Academy of Sciences the responsibility for advising the federal government. The National Academy of Engineering also sponsors engineering programs aimed at meeting national needs, encourages education and research, and recognizes the superior achievements of engineers. Dr. William A. Wulf is president of the National Academy of Engineering.

The Institute of Medicine was established in 1970 by the National Academy of Sciences to secure the services of eminent members of appropriate professions in the examination of policy matters pertaining to the health of the public. The Institute acts under the responsibility given to the National Academy of Sciences by its congressional charter to be an adviser to the federal government and, upon its own initiative, to identify issues of medical care, research, and education. Dr. Kenneth I. Shine is president of the Institute of Medicine.

The National Research Council was organized by the National Academy of Sciences in 1916 to associate the broad community of science and technology with the Academy's purpose of furthering knowledge and advising the federal government. Functioning in accordance with general policies determined by the Academy, the Council has become the principal operating agency of both the National Academy of Sciences and the National Academy of Engineering in providing services to the government, the public, and the scientific and engineering communities. The Council is administered jointly by both the Academies and the Institute of Medicine. Dr. Bruce M. Alberts and Dr. William A. Wulf are chairman and vice chairman, respectively, of the National Research Council.

Abbreviations used without definitions in TRB publications:

AASHO	American Association of State Highway Officials
AASHTO	American Association of State Highway and Transportation Officials
ASCE	American Society of Civil Engineers
ASME	American Society of Mechanical Engineers
ASTM	American Society for Testing and Materials
FAA	Federal Aviation Administration
FHWA	Federal Highway Administration
FRA	Federal Railroad Administration
FTA	Federal Transit Administration
IEEE	Institute of Electrical and Electronics Engineers
ITE	Institute of Transportation Engineers
NCHRP	National Cooperative Highway Research Program
NCTRP	National Cooperative Transit Research and Development Program
NHTSA	National Highway Traffic Safety Administration
SAE	Society of Automotive Engineers
TCRP	Transit Cooperative Research Program
TRB	Transportation Research Board
U.S.DOT	United States Department of Transportation

THE NATIONAL ACADEMIES

Advisers to the Nation on Science, Engineering, and Medicine

National Academy of Sciences
National Academy of Engineering
Institute of Medicine
National Research Council